TÉCNICO LISBOA

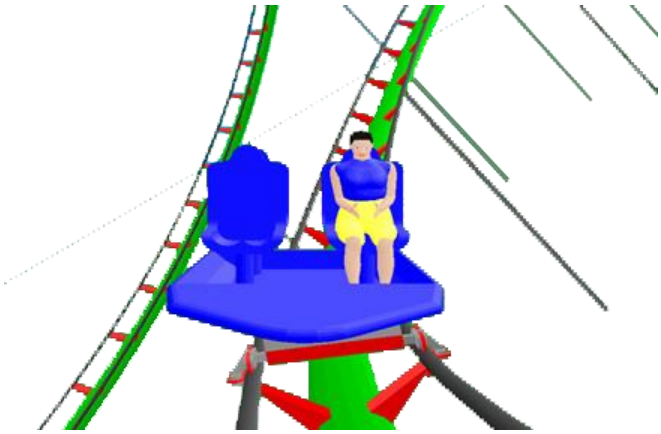

Development of Computational Models of Roller Coaster Vehicles and Occupants for Injury Analysis

Mário Rui Dias Viegas

Thesis to obtain the Master of Science Degree in

Mechanical Engineering

Supervisor: Prof. Jorge Alberto Cadete Ambrósio

Examination Committee

Chairperson: Prof. João Orlando Marques Gameiro Folgado

Supervisor: Prof. Jorge Alberto Cadete Ambrósio

Member of the Committee: Prof. Miguel Pedro Tavares da Silva

May 2016

Acknowledgments

Ao meu orientador, Professor Jorge Ambrósio, quero agradecer a oportunidade e a ajuda no desenvolvimento desta dissertação. Agradecer a notável dedicação e interesse que me transmitiu ao longo deste trabalho, que foram marcantes, não só para a minha formação académica como para a minha formação como pessoa.

Aos meus colegas, Hugo Magalhães e Pedro Antunes, por toda a ajuda, partilha de informação e feedback durante a realização deste trabalho.

A todos os meus amigos, que me apoiaram no desenrolar deste trabalho. Um especial agradecimento, à Soraia Ribeiro, Nuno Rodrigues e Mariana Freitas, que me aturaram nos momentos mais difíceis, obrigado pela companhia e paciência no desenrolar deste trabalho.

Por fim, um agradecimento muito especial aos meus pais e irmã, pelo apoio incondicional, especialmente nos momentos mais atarefados. Sem eles, a realização deste curso não seria possível. São um exemplo de trabalho e humildade. Obrigado!

Resumo

Uma viagem de montanha russa consiste num veículo a percorrer uma trajectória caracterizada por uma sequência de curvas com geometrias diferentes. Durante esse percurso, o passageiro é sujeito a acelerações que dependem, não só da variação de velocidade do veículo, mas também da curvatura da pista. Estas acelerações são sentidas pelo corpo humano, em direcções diferentes, com a intenção de provocar entusiasmo aos passageiros, com o mínimo risco de lesão. O projecto de geometrias de montanhas russas requer ferramentas computacionais para simular o percurso da pista. Um dos aspectos mais importantes para uma simulação realista das solicitações sobre o passageiro é a modelação da interação entre o veículo e a pista. Estes estudos permitem analisar o risco de lesão a que os passageiros estão sujeitos. Nesta dissertação, é proposto um modelo de interação entre o veículo e a pista, que é demonstrado com a implementação de dois novos constrangimentos de percurso prescrito. Estes constrangimentos permitem assegurar que cada roda tem a sua trajectória inscrita no percurso da montanha russa. Com base na geometria da pista da montanha russa, são criadas duas trajectórias, uma para cada carril. Neste trabalho, são criados modelos de multicorpo para representar tanto o veículo como o passageiro, que servem para simular e analisar duas montanhas russas específicas que servem como exemplo de aplicação deste trabalho. Para analisar o risco de lesão a que o passageiro está sujeito, foi criado um pos-processador para determinar as forças-g e verificar se estas estão dentro dos limites da tolerância humana, representados pelos critérios de lesão mais comuns, como o Head Injury Criteria (HIC) e o Result Head Accelerations (3ms). A ferramenta computacional, desenvolvida neste trabalho, é finalmente usada para analisar o risco de lesão de um passageiro de um veículo em duas montanhas russas diferentes.

Palavras-Chave

Montanha Russa

Dinâmica Multicorpo

Constrangimento de Movimento Prescrito

Modelo Biomecânico

Critério de Lesão

Abstract

A roller coaster ride consists of a vehicle negotiating a track characterized by a sequence of curves with different geometries. During the track negotiation, the occupants are subjected to accelerations that depend, not only on the car speed variation, but also on the instantaneous curvature of the track. These accelerations are experienced by the human body, in different directions, and intend to provide excitement to the occupants with a minimum risk of injury. The design of the roller coaster geometry requires reliable computational tools to simulate the roller coaster rides. An important ingredient to simulate realistically the exposure of the occupant to accelerations is the modelling of the vehicle-track interaction. Such simulations allows to analyse the risk of injury of the occupants. In this thesis, an approach to model the car-track interaction is proposed, being two new path motion constraints implemented for the purpose. These constraints allow to prescribe the path of each wheelset along each one of the track rails. Two paths are generated based on the roller coaster geometry, representing the geometry of the rails of the track. Not only multibody models to represent the roller coaster vehicle are developed, but also a biomechanical model to represent the roller coaster passenger is implemented. In this work, two roller coasters models are simulated and analysed, serving as application examples of the tools developed in this work. To analyse the risk of injury of the occupant, a post-processor is implemented to evaluate the g-forces acting on the passenger and to confer if they are within the human tolerance thresholds represented by regular injury criteria, such as the Head Injury Criteria (HIC) and the Result Head Acceleration (3ms). The computational tools developed in this work are then used to analyse the risk of injury of an occupant in two roller coasters, which correspond to an existing commercial coaster and to a new potential roller coaster, not existing yet.

Keywords

Roller Coaster

Multibody Dynamics

Path Motion Constraint

Biomechanical Model

Injury Criteria

Contents

List of Figures

List of Tables

List of Symbols

Convention

a, A, α	Scalar;
$\mathbf{a}$	Vector;
$\mathbf{A}$	Matrix;

Overscript

$\dot{\mathbf{a}}$	First time derivative;
$\ddot{\mathbf{a}}$	Second time derivative;

Superscript

$\mathbf{a}^{\mathbf{T}}$	Matrix or vector transpose;
$\mathbf{a}^{-1}$	Second time derivative;
$\mathbf{a}'$	Vector expressed in the body-fixed reference frame;
a^{i}	Referred to body *i;*

Subscript

$\mathbf{a}_{i}$	Referred to body *i*,
$\mathbf{a}^{-1}$	Second time derivative;
$\mathbf{a}'$	Vector expressed in the body-fixed reference frame;
a_{t}	Referred to the tangent component;
a_{n}	Referred to the normal component;
a_{b}	Referred to the binormal component;

Latin Symbols

$\mathbf{A}$	Generic transformation matrix;
$\mathbf{a}$	Acceleration vector;
$\mathbf{b}$	Binormal vector;
$\mathbf{d}$	Distance vector;
D	Distance between the rails geometric centre;
c	Damping coefficient;
f	Vector of generic forces;
$\mathbf{g}$	Vector of generalized forces;
h_{t}	Cant;

I	Area moment of inertia;
$\mathbf{J}$	Inertia tensor;
J'	Inertia;
J	Polar moment of inertia;
k	Stiffness;
l	Generic length;
m	Mass;
$\mathbf{M}$	Global mass matrix; Generic moment;
nb	Total number of bodies in the system;
$\mathbf{n}$	Normal vector;
$\mathbf{N}$	Diagonal matrix of masses;
P	Generic point on body *i;*
$\mathbf{q}, \dot{\mathbf{q}}, \ddot{\mathbf{q}}$	Vector of generalized coordinates, velocities and accelerations;
$\mathbf{r}$	Cartesian coordinates of generic point;
$\mathbf{t}$	Tangential Vector
t	Time;
$\mathbf{v}$	Velocity vector;
x, y, z	Global coordinates;
$\mathbf{y}, \dot{\mathbf{y}}$	Auxiliary vectors used in the integration process;

Greek Symbols

β	Rail inclination;
$\boldsymbol{\gamma}$	Right-hand-side vector of acceleration equation;
θ	Orientation of the track;
$\boldsymbol{\lambda}$	Vector of Lagrange multipliers;
$\boldsymbol{\nu}$	Right-hand-side vector of velocity equation;
ξ, η, ζ	Body fixed reference frame;
$\boldsymbol{\Phi}$	Vector of kinematic position constraints;
$\boldsymbol{\Phi}_{\mathbf{q}}$	Jacobian matrix of kinematic constraints;
φ	Cant angle.

Abbreviations

DAE	Differential Algebric Equations
ODE	Ordinary Differential Equations
NCA	Non-Compensated Acceleration
GLOC	G-force induced loss of conscious
HIC	Head Injury Criteria
DOF	Degree of Freedom

1 Introduction

1.1 Motivation

Roller coaster/amusement parks are popular worldwide. The roller coaster rides attract and entertain a substantial numbers of visitors to these parks. Some guests particularly enjoy rides in vehicle traveling along a track, such as roller coasters, in which, one or more vehicles run along a complex track geometry.

Injuries of occupants in roller coaster rides are periodically reported for normal operation conditions. Contrary to common individuals that have occasional rides in fighter jets, roller coaster riders are not screened beforehand to ensure that they can withstand high g-forces nor they are trained to endure them. Amidst controversy in which evidence of fatal or serious injury in roller coasters [1] is opposed by data showing that high g-force roller coasters still lead to head accelerations far below the minimum thresholds [2, 3].

Roller coasters seem to be relatively simple mechanical systems when compared to modern railways or cars, but due to high nonlinearity their kinematics, standard design techniques for dynamic systems have limitations. Moreover, since most of the roller coasters represent unique designs, extensive testing and design of real world prototypes is not possible from an economical point of view. To avoid expensive testing before the final installation of the roller coaster track, reliable computer aided design tools are required. In order to support the engineering design of safe roller coaster rides this work presents the development of a computational tool for the dynamic analysis of roller coasters with the ability to evaluate the biomechanical injury thresholds [4-7] including those associated to g-forces.

The development proposed in this work address; the design, for creating a geometric model of the track and vehicle; and the simulation, for evaluating the system behaviour in general, and the occupant in particular.

In order to understand the behaviour of the roller coaster using numerical simulations, a detailed model of the roller coaster is required. The design of the system requires the knowledge of the human tolerances to injury [4-7]. In a way, the roller coaster cannot be boring, it must be exciting and stimulating, but on the other hand, the roller coaster passenger should not be injured by riding it. The physiological excitement of the passenger is achieved through the roller coaster track, which assures the human body is subjected to accelerations in different directions, within the human tolerance thresholds [4, 5], but not any further.

The objectives of this work are the development of a proper roller coaster vehicle for use in roller coaster simulations, in the multibody dynamic analysis program DAP-3D and the development of a biomechanical model to evaluate the risk of injuries in different roller coasters.

1.2 Literature Review

1.2.1 Multibody Formulation

The dynamic analysis of a multibody system involves the study absolute and relative motion between the bodies that compose the system, over a period of time. This study is function of their initial conditions, positions, orientations and velocities, external forces and/or prescribed motions [8]. The mechanical system is characterized by a group of rigid bodies interconnected by joints and/or force elements. The bodies structural deformation is neglected because only the large rigid body motions have impact on the vehicle dynamic analysis [9]. The joints, also known as kinematic constraints, define the relative motions between bodies. Basically, there are two types of force elements, passive and active. In this work, it will only be used passive force elements, such as springs and dampers as no active elements, such as actuators or muscle activation forces, are considered.

The multibody formulation results in a set of equations composed by Differential Algebric Equations (DAE), which may lead to numerical instabilities and other numerical problems, such as existence and uniqueness of solution. The alternative is to transform the DAE into a set of Ordinary Differential Equations (ODE), which solution can be obtained, by integrating the ODE in time, using direct integration methods. This transformation is known to introduce instabilities and drift problems in integration process. Such problems can be attenuated by using Baumgarte method [10] or any other suitable method [11].

1.2.2 Roller Coaster Modelling

Pombo and Ambrósio [12-15] proposed a methodology for the accurate description of the track centreline, in the general case of a fully three-dimensional track geometry with roller coaster applications. Spatial geometric curve constraints are incorporated into multibody systems by Nikravesh [16]. Pombo [8] presented a methodology for representing a spatial curve constraint in multibody systems, using a Lagrange formulation of multibody dynamics.

The geometric description of the curve for a roller coaster analysis must allow the definition of a moving frame, in which the tangent, normal and binormal vectors define an orthogonal frame. Both Frenet and Dabroux frames are candidates to play the role of the required moving frame [17, 18]. Both have singularities in general spatial curve geometries, as discussed by Tandl and Kecskemethy [19, 20]. The work of Pombo uses the fundamental theory of differential geometry and kinematics of motion along spatial curves. For the differential-geometric analysis of spatial curves Frenet [17] introduced the moving frame and the formulas for derivative axis unit vectors, which were also found by Serret [21].

The design and simulation of roller coasters uses curve guided motion, to design tracks, based on numerical integration of equations of spatial point. The roller coaster position coordinates, the Frenet

frame vectors and their respective derivatives are required for the definition of path motion kinematic constraints. These calculations are made by a pre-processor, before the simulation, and provided to it in the form of a database. For general roller coaster features, cubic splines are used when describing the spatial trajectory [22]. The Dynamic Analysis Program (DAP-3D), described by Nikravesh [16], is used to simulate the roller coaster, imposing path kinematic constraints, using a Frenet moving frame, between the roller coaster vehicle and the track. During the roller coaster dynamic analysis, the quantities involved in the general spatial curve constraint are obtained by interpolation of the tabulated values.

A roller coaster [23] can be roughly divided into rails, the vehicle that moves along the rails, and devices such as lifts, drives and brakes. In this work, only the track and the vehicle were modelled, leaving the rest of the vehicle system to future developments. The vehicle is joined to the rail via a suspension mechanism and can either be a single car or a train consisting of many connected cars.

1.2.3 Biomechanical Model of the Occupant

Biomechanics supports the development of reliable mathematical models of the human body, to simulate the different human actions. These models provide a representation , with sufficient accuracy of the mechanical behaviour of the human body in various conditions of its activity [24]. In a biomechanical multibody system, the “gross-motion” simulators also represent the different segments of the human body by a set of rigid bodies interconnected by different types of kinematic constraints and force elements, with a varying degree of complexity, depending on the type of study[25].

The biomechanical systems are distinguished in two essential categories, detailed partial models, for particular anatomical segments with high level of detail, and whole body responses models [25], for the general characteristics. In this work, the whole body response model is used, since, right now, the objective is to simulate the general responses of the human body, rather than obtaining highly detailed information on particular components. The body response biomechanical model has a structure of sixteen anatomical segments, based on the anthropometric data provided in the computer code SOM-LA [26, 27]. The anthropometric model has the mass distribution and body size of the 50^{th} anthropomorphic dummy [28].

Numerical methods and models are important tools since they allow to assess the human biomechanical response in a large range of scenarios. Injury biomechanics uses the description of the human body, via its mechanical principles, kinematics and dynamics, to provide relations that can be associated to observed human physical trauma [29]. Common effects on the human body such as blackout or loss of consciousness are associated to g-forces [6, 30-32]. When discussing the effects of g-forces on the body, time emerges as one of the most critical factors. Commonly, in roller coaster tracks, exposure to high g-forces lasts only a fraction of a second. Blackouts and other health problems

associated with g's require exposure to g-forces that are either greater in magnitude or of much longer duration than those achieved by roller coasters. High g-forces are well tolerated during many activities and, therefore, are a poor measure for the risk of brain injury [1]. Smith an Meaney [2] suggest using rotational head accelerations, that can be caused by g-forces, to analyse potential for injury. Even for their conservative worst-case scenario, estimated head rotational accelerations experienced by roller coaster riders are nowhere near the range of established injury thresholds for severe forms of brain injury.

In this work, in order to analyse the risk of brain injury, injury criterions, such as the Head Injury Criteria (HIC), well known from the automotive industry and others, is used. HIC can be defined as a biomechanical response index of exposure that quantifies the magnitude of a determined injury caused by impact or large accelerations [7, 33, 34]. These qualifications can be regarded as a quantification of human response to a given level of injury, resulting from external actions. The understanding of the injury mechanisms is of great importance for passive safety improvement.

In the literature review, no computational tool for the simulation of roller coaster occupants was identified. Therefore, no specific computational procedures for the calculation of the sustained g-forces of the biomechanical model of the occupant based on its passive or active dynamic response are available prior to this work.

1.3 Thesis Organization

Chapter 2 presents the multibody formulation that supports program DAP-3D, including the two new kinematic path motion constraints, developed in this work, that are used as the basis for the definition of the vehicle-track interaction. In Chapter 3, first, the track geometry is presented, being its structure and database that support its geometry explained. Next, the roller coaster vehicle is developed, being its suspension mechanisms described and discussed in function of the operation all requirements of the system. In Chapter 4, the biomechanical model of the roller coaster occupant is presented, as well as the relevant injury criteria and the human tolerance thresholds. Chapter 5 presents two case scenarios of different roller coasters. One of the roller coaster is a current operating equipment, and the other is a conceptual design. In both scenarios the dynamic response is shown by the velocities and accelerations evaluated in the simulations, being depicted the impact that riding those roller coasters have in the human body and its risk of injury. The conclusions of this work and discussion of future developments are presented in Chapter 6.

2 Roller Coaster Dynamics

This chapter presents an introduction to the multibody formulation used to support the methodologies implemented in this work. The dynamic analysis of a multibody system involves the study of its motions and forces, transmitted during a given time period, as a function of the initial conditions, external applied forces and/or prescribed motions. The emphasis of this overview is put on the features required for the models developed hereafter.

Due to the application requirements of this work, a roller coaster model, the trajectory of the wheelsets is based on the general spatial curve kinematic constraint, developed by Pombo [14]. However, to avoid over constrained wheels, two new path motion constraints are developed here. The original motion constraint forces a body to follow a given trajectory and to rotate with respect to a Frenet moving frame. The first new constraint, deemed as Prescribed Cylindrical Joint, frees the roll rotation, while the second new constraint, the Prescribed Point Joint, frees all rotations maintaining only the prescribed translation. The basis of the vehicle-track interaction in the roller coaster multibody system is the prescribed point motion joint. All approaches are implemented in the computer program DAP-3D[16].

2.1 Multibody Systems Dynamics

A multibody system can be defined by a collection of rigid and/or flexible bodies linked by kinematic constraints and/or force elements. The kinematic joints restrain the relative motion between the bodies, while the force elements represent the internal forces that develop between bodies due to their relative motion. The external forces may be applied to the system components as a consequence of their surrounding environment. A generic multibody system is represented in Figure 2.1.

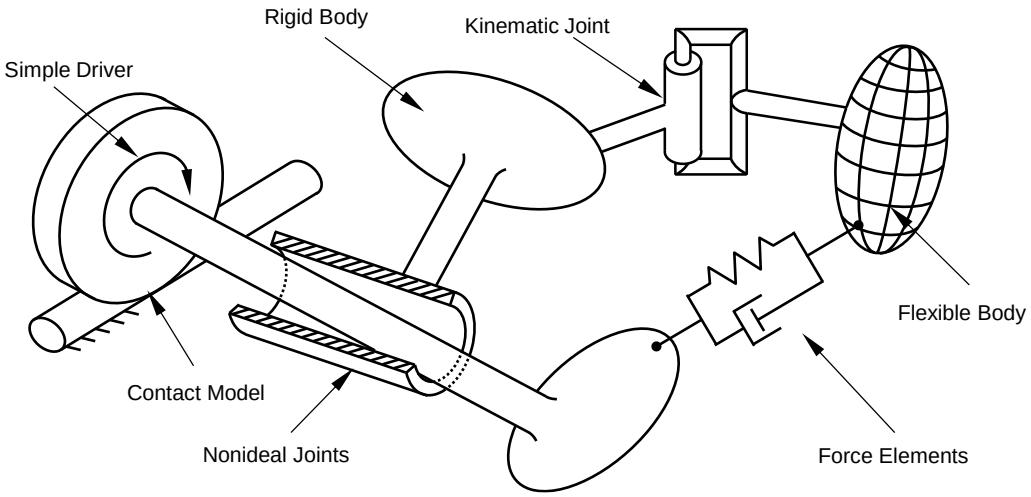

Figure 2.1: Generic multibody system

2.1.1 Kinematic Analysis

Kinematics is the study of the motion of rigid bodies. It allows to study the motion of a mechanical system without considering the forces that cause it. Kinematic and driving constraints are the only restrictions that affect the relative motion of the bodies. Drivers are required in order to control the degrees of freedom, making the system fully constrained and possible to be solved, kinematically.

The coordinates associated to a general rigid body i, Figure 2.2, are expressed [16]

$$\mathbf{q}_i = \left\{\mathbf{r}_i^T, \mathbf{q}_i^T\right\} = \left\{x, y, z, e_0, e_1, e_2, e_3\right\}_i^T \tag{2.1}$$

The vector $\mathbf{r}_i = \left\{x, y, z\right\}_i^T$ defines the position of the origin of the local reference frame $\left(\xi, \eta, \zeta\right)_i$ in a global reference frame $\left(x, y, z\right)$. The vector $\mathbf{p}_i = \left\{e_0, e_1, e_2, e_3\right\}_i^T$ define the body orientations, as Euler Parameters [16].

For a general multibody system with nb bodies, the vector $\mathbf{q}$ that represents the coordinates of all bodies is:

$$\mathbf{q} = \left\{\mathbf{q}_1^T, \mathbf{q}_2^T, \mathbf{q}_3^T, ..., \mathbf{q}_{nb}^T\right\}^T \tag{2.2}$$

Let a point P be defined on a body i, as shown in Figure 2.2. The vector $\mathbf{s}_i^{'P} = \left\{\xi_i^P, \eta_i^P, \zeta_i^P\right\}$ defines the location of point P with respect to the local reference frame origin of body i. Therefore, the position of point P with respect to the global reference frame is given by the vector $\mathbf{r}_i^P$, expressed as:

$$\mathbf{r}_i^P = \mathbf{r}_i + \mathbf{s}_i^P = \mathbf{r}_i + \mathbf{A}_i \mathbf{s}_i^{'P} \tag{2.3}$$

where $\mathbf{A_i}$ is the transformation matrix from local to global coordinates, and is given by [16]:

$$\mathbf{A} = \left(2e_0^2 - 1\right)\mathbf{I} + 2\left(\mathbf{e}\mathbf{e}^T + e_0\tilde{\mathbf{e}}\right) \tag{2.4}$$

with $\mathbf{e} = \left\{e_1, e_2, e_3\right\}^T$ and $\tilde{\mathbf{e}}$ is the skew-symmetric matrix, which is used to define the vector product.

The kinematic analysis consists of the study of the motion of a system, which involves the existing kinematic joints interconnecting the different bodies, leading to the constraint equations. These equations are grouped in a global position constraint vector, $\mathbf{\Phi}$, written as:

$$\mathbf{\Phi}\left(\mathbf{q}, t\right) = \mathbf{0} \tag{2.5}$$

where $\mathbf{q}$ is the generalized coordinates vector, defined in equation (2.2), and t represents time, which is generally associated to driving constraints, used to control the system DOF. The solution of this set of nonlinear equations is obtained using the Newton-Raphson method [16].

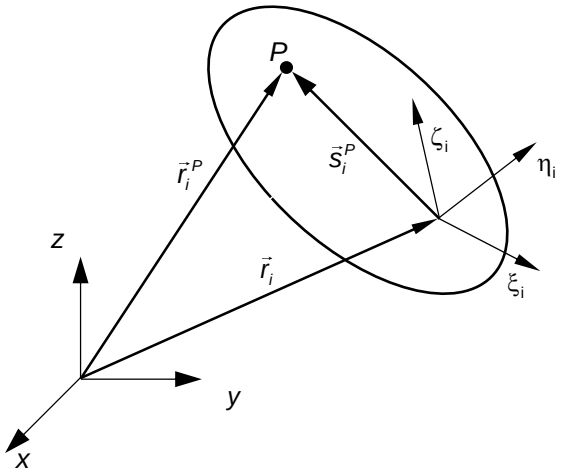

Figure 2.2: Rigid Body in Cartesian Coordinates

The first time derivative of the system of equations, equation (2.5), provides the velocities equation written as:

$$\dot{\mathbf{\Phi}}\left(\mathbf{q},\dot{\mathbf{q}},t\right)=\mathbf{0}\ \equiv\ \mathbf{\Phi}_{\mathbf{q}}\dot{\mathbf{q}}=\boldsymbol{\nu} \tag{2.6}$$

where $\mathbf{\Phi}_q$ is the Jacobian matrix of the constraints, $\dot{\mathbf{q}}$ is the generalized velocity vector and $\boldsymbol{\nu}$ is the vector containing partial derivatives of the constraints with respect to time:

$$\boldsymbol{\nu}=-\frac{\partial\mathbf{\Phi}}{\partial t} \tag{2.7}$$

The vector of the generalized accelerations, $\ddot{\mathbf{q}}$, is obtained by solving the second time derivative of the systems equations, equation (2.5), given by:

$$\ddot{\mathbf{\Phi}}\left(\mathbf{q},\dot{\mathbf{q}},\ddot{\mathbf{q}},t\right)=\mathbf{0}\ \equiv\ \mathbf{\Phi}_q\ddot{\mathbf{q}}=\boldsymbol{\gamma} \tag{2.8}$$

where $\boldsymbol{\gamma}$ is the vector that contains all terms in the equations that are not dependent on the accelerations, written as:

$$\boldsymbol{\gamma}=-\frac{\partial^2\mathbf{\Phi}}{\partial t^2}-\frac{\partial}{\partial t}\left(\mathbf{\Phi}_{\mathbf{q}}\right)\dot{\mathbf{q}} \tag{2.9}$$

The results of the kinematic analysis are obtained performing the following steps, using a solver for linear systems of equations:

i. Setup the initial conditions for the positions and initialize the time counter;
ii. Construct the position constraint equations (2.5) and solve them to obtain $\mathbf{q}$;
iii. Construct the velocity constraint equations (2.6) and solve them to obtain $\dot{\mathbf{q}}$;
iv. Construct the acceleration constraint equation (2.8) and solve them to obtain $\ddot{\mathbf{q}}$;
v. Increment the time counter and: a) If time is smaller than final time, go to step ii); b) If time exceeds the final time, stop the analysis.

It should be noted that in dynamics only the acceleration constraint equations are explicitly used. Furthermore, time dependent constraints such as driving constraints are used generally in the framework of control problems. However, a complete kinematic analysis may be required to establish initial positions and velocities that are consistent with the kinematic constraints when the dynamic analysis starts.

2.1.2 Dynamic Analysis

The dynamic analysis of a multibody systems already involves the forces and moments applied on the respective bodies of the system, as well as their motion. The system of differential algebraic equations (DAE) that describe the system constrained motion is written as [16]:

$$\begin{bmatrix} \mathbf{M} & \mathbf{\Phi}_\mathbf{q}^\mathbf{T} \\ \mathbf{\Phi}_\mathbf{q} & \mathbf{0} \end{bmatrix} \begin{bmatrix} \ddot{\mathbf{q}} \\ -\boldsymbol{\lambda} \end{bmatrix} = \begin{bmatrix} \mathbf{g} \\ \boldsymbol{\gamma} \end{bmatrix} \tag{2.10}$$

where $\mathbf{M}$ is the mass matrix, $\boldsymbol{\lambda}$ is the vector of the Lagrange multipliers and $\mathbf{g}$ is the vector of the external forces and moments applied on the bodies. The mass matrix is written as:

$$\mathbf{M} = \begin{bmatrix} \mathbf{M}_1 & & \\ & \ddots & \\ & & \mathbf{M}_{nb} \end{bmatrix} ; \ \mathbf{M_i} = \begin{bmatrix} \mathbf{N}_i & \\ & \mathbf{J}_i^{'} \end{bmatrix} \tag{2.11}$$

$$\mathbf{N}_i = \begin{bmatrix} m_i & & \\ & m_i & \\ & & m_i \end{bmatrix} ; \ \mathbf{J}_i^{'} = \begin{bmatrix} J_{\xi\xi_i}^{'} & & \\ & J_{\eta\eta_i}^{'} & \\ & & J_{\zeta\zeta_i}^{'} \end{bmatrix} \tag{2.12}$$

where, nb is the number of bodies of the system, m is the mass of body i, and $J_{\xi\xi}^{'}$, $J_{\eta\eta}^{'}$ and $J_{\zeta\zeta}^{'}$ are the moments of inertia with respect to the principal axis of inertia (ξ,η,ζ). The vector $\mathbf{g}$ comprises the sum of the external forces acting on the system. The internal forces associated to the kinematic constraints are calculated using the Lagrange multipliers method

$$\mathbf{g}^{(c)} = \mathbf{\Phi}_\mathbf{q}^T \boldsymbol{\lambda} \tag{2.13}$$

Note that the equations of motion for a rigid body, defined by equation (2.10), are for centroidal fixed body reference frames. Furthermore, they assume that the orientation of the frame axis is along the main inertia directions of the rigid body.

2.1.2.1 Integration of the Equations of Motion

The system of equations of motion, expressed at equation (2.10) has to be solved, and the resultant velocities and accelerations integrated in time. This dynamic analysis is performed on the computer program DAP-3D [16], where the new kinematic constraints are implemented. Its algorithm is depicted schematically in Figure 2.3.and can be summarized by the following steps:

i. Start, at time t_0, with initial conditions for coordinates, $\mathbf{q}_{t_0}$, and velocities, $\dot{\mathbf{q}}_{t_0}$;

ii. Check the consistency of the initial conditions and correct the positions and velocities, if necessary;

iii. Assemble the global mass matrix, $\mathbf{M}$, compute the Jacobian of the constraints equations, $\mathbf{\Phi}_\mathbf{q}$ and compute vectors $\mathbf{g}$ and $\boldsymbol{\gamma}$;

iv. Solve the system of equations (2.10) to obtain the acceleration vector, $\ddot{\mathbf{q}}$;

v. Numerically integrate the vector $\dot{\mathbf{y}} = \begin{bmatrix} \dot{\mathbf{q}}^T & \ddot{\mathbf{q}}^T \end{bmatrix}^T$, composed by the accelerations and velocities, to obtain the coordinates and velocities for the time step $t + \Delta t$;

vi. Update the time variable and check condition $t + \Delta t > t_{end}$; if the condition is satisfied, stop; otherwise go to step ii).

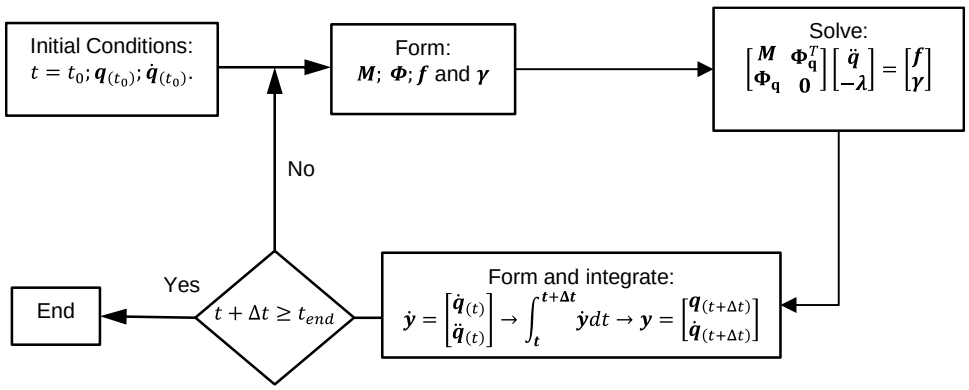

Figure 2.3: dynamic analysis program algorithm

The Baumgarte constraint stabilization method [10] is applied in the solution of the equations of motion (2.10) in order to obtain a more stable integration process and control the constraint violations. The solution of the second derivative of the constraints equation, $\ddot{\mathbf{\Phi}} = \mathbf{0}$, is known to be numerical unstable. This constitutes a problem when the system of equations (2.10) is solved, for long periods of time in particular, not only because small perturbations, due to numerical errors, have tendency to increase but also because the position and velocity constraint equations are not explicitly used. Therefore, the result of this numerical procedure provides positions and velocities that no longer satisfy exactly the kinematic constraints equations (2.5). To control this problem, the Baumgarte stabilization method is applied, which replaces the kinematic accelerations equation (2.8) by:

$$\ddot{\mathbf{\Phi}} + 2\alpha\dot{\mathbf{\Phi}} + \beta^2\mathbf{\Phi} = \mathbf{0} \tag{2.14}$$

where $\dot{\mathbf{\Phi}}$ and $\mathbf{\Phi}$ are the velocities and positions constraints equations, respectively, and α and β are parameters whose values are constants, in this case, both are equal to 5. Therefore, the equation (2.10) becomes [16]:

$$\begin{bmatrix} \mathbf{M} & \mathbf{\Phi}_\mathbf{q}^\mathbf{T} \\ \mathbf{\Phi}_\mathbf{q} & \mathbf{0} \end{bmatrix} \begin{bmatrix} \ddot{\mathbf{q}} \\ -\boldsymbol{\lambda} \end{bmatrix} = \begin{bmatrix} \mathbf{g} \\ \boldsymbol{\gamma} - 2\alpha\dot{\mathbf{\Phi}} - \beta^2\mathbf{\Phi} \end{bmatrix} \tag{2.15}$$

Note that although the Baumgarte stabilization controls the constraint violations, it does not ensure that they are completely fulfilled. In case of these violations to grow above a required threshold, only by using a coordinate partition method it is possible to eliminate such constraint violations [16]. As, in all applications pursued here, the constraint violations have always been kept under the speciefied thresholds, the coordinate partition method is not used.

2.2 Path Motion Constraints

To define a path motion constraint, in which a rigid body has to follow a prescribed curve, as shown in Figure 2.4, the geometric description of the curve must allow the definition of a moving frame in which the tangent, normal and binormal vectors, defining an orthogonal frame, are obtained. In this work, the Frenet Frame [22] is used for any curved part of the track, being the straight segments handled with the procedure described by Pombo and Ambrósio [14].

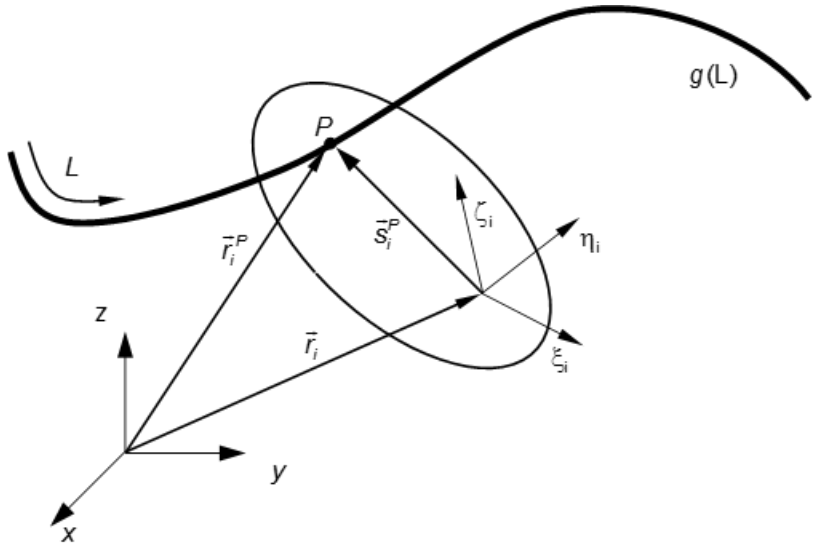

Figure 2.4: Path Motion Constraint

Using the moving frame definition selected for this work, a proper formulation for a path motion kinematic constraint was obtained by Ambrósio et all [22]. A kinematic constraint that imposes a point of a rigid body to follow a given curve, being its rotations with respect to the curve moving frame also prescribed.

In this work, two new path motion constraints are proposed. A prescribed cylindrical constraint, which allows the free roll of the body about the track tangent, and a prescribed point constraint allowing all three rotations, i.e, only enforcing the body translation. This prescribed point constraint is proposed to be used as the basis for the modelling of the vehicle-track interaction in the roller coaster multibody system. The roller coaster track coordinates, the Frenet frame vectors and their respective derivatives are required for the definition of the kinematic constraints.

2.2.1 Curve Parameterization

Let a curve be described using an n^{th} order spline segments, interpolating a set of control points, be defined as [35]:

$$\mathbf{g}(u) = \begin{Bmatrix} x(u) \\ y(u) \\ z(u) \end{Bmatrix} = a_0 + a_1 u + a_2 u^2 + a_3 u^3 + \ldots + a_n u^n \tag{2.16}$$

where $\mathbf{g}(u)$ is the vector locating a point on the curve, u is the local parametric variable and a_i are unknown algebraic coefficients that must be calculated using points with known coordinates. Although Eq. (2.16) is generic for any polynomial interpolation, in this work only cubic polynomials are considered.

2.2.1.1 Curve Moving Frame

There are different available frames definitions that can be used to represent general curves, being the Frenet frame used here, since provides an appropriate curve referential at every point. The definition of the Frenet frame starts with the identification of the osculating plane, at a given point P on a curve, which is the plane of closest contact to the curve in the neighborhood of P, as depicted in Figure 2.5.

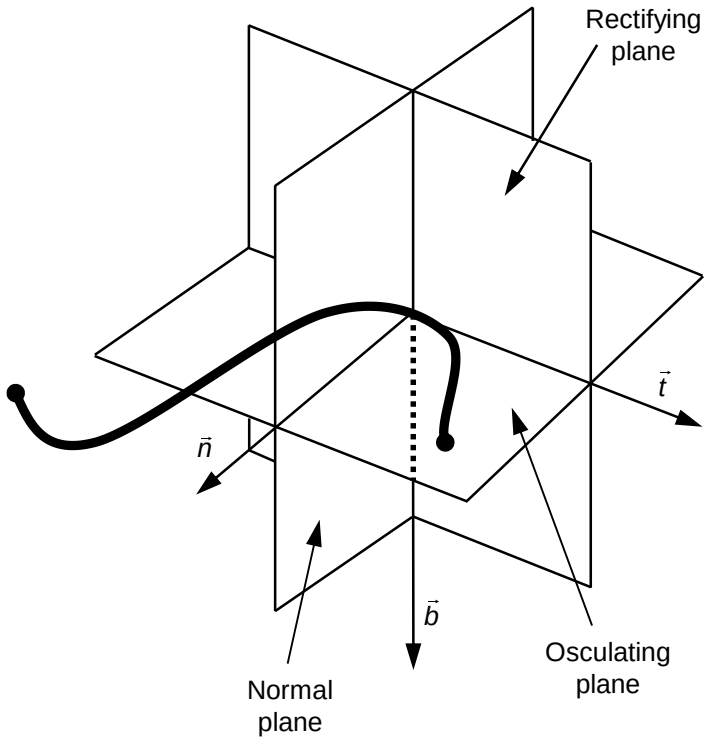

Figure 2.5: Frenet Frame of a given curve

The tangent vector **t** and the principal normal vector **n** are defined in the osculating plane. The binormal vector **b** is defined as being normal to the other two vectors, as shown in Figure 2.5. These

vectors are defined in the intersection of the normal, rectifying and osculating planes, point P, and can be written as [14]

$$\mathbf{t} = \frac{\mathbf{g}^u}{\left\|\mathbf{g}^u\right\|} \;;\; \mathbf{n} = \frac{\mathbf{k}}{\left\|\mathbf{k}\right\|} \;;\; \mathbf{b} = \tilde{\mathbf{t}}\mathbf{n} \tag{2.17}$$

where $\tilde{\mathbf{t}}\mathbf{n}$ means a cross product and the auxiliary vector $\mathbf{k}$ is given by

$$\mathbf{k} = \mathbf{g}^{uu} - \frac{\mathbf{g}^{uu^T}\mathbf{g}^u}{\left\|\mathbf{g}^u\right\|^2}\mathbf{g}^u \tag{2.18}$$

in which $\mathbf{g}^u$ and $\mathbf{g}^{uu}$ are, respectively, the first and second derivatives of the parametric curve $\mathbf{g}(u)$ with respect to the parametric variable u.

2.2.2 Prescribed Point Constraint

The curve parameter u does not ensure that the polynomial exhibits a constant velocity. For the implementation of the prescribed point constraint, it is required that the piecewise polynomial parameter u is replaced by a curve arc-length parameter L with respect to which the interpolating polynomial has a constant velocity. Consider the parametric variable u^P, corresponding to a point P, located on the k^{th} polynomial segment to which a curve length L_k^P measured from the k^{th} segment origin, is associated. The parameter u^P is obtained by [14]:

$$\int_0^{u^P} \sqrt{g_k^{u^T} g_k^u}\, du - L_k^P = 0 \tag{2.19}$$

In terms of its computer implementation, the non-linear equation (2.19) is solved in the program pre-processor, using Newton-Raphson method [16].

The prescribed point constraint is proposed to be used here as the basis for the definition of the vehicle-track interaction in the roller coaster multibody system. The wheelsets of the vehicle model move along the rails of the track and the kinematic constraint enforces each one of them to follow a given roller coaster rail. The wheel-rail contact forces of the roller coaster vehicle are not explicitly used during the dynamic analysis. It is considered that the wheelsets of the roller coaster cars are permanently in contact with the rails and follow exactly the track geometry, according with the restrictions imposed by the prescribed point constraint. That wheel-rail contact forces are related to the Lagrange multipliers associated to this constraint and are naturally obtained by using Equation (2.10).

The objective of the prescribed point constraint is to define equations that enforce a certain point, of a rigid body to follow a reference path. Consider a point P, located on rigid body i, that is constrained to follow a specified path, as depicted in Figure 2.6. The path is defined by a parametric curve $\mathbf{g}(L)$, which is controlled by a global parameter L that represent the length travelled by the point

along the curve from the origin to the current location of point P. The constraint equations that enforce point P to follow the reference path $\mathbf{g}(L)$ are written as [16]:

$$\mathbf{\Phi}^{(\text{pmc},3)} \equiv \mathbf{r}_i^P - \mathbf{g}(L) = \mathbf{0} \tag{2.20}$$

where $\mathbf{r}_i^P$ represents the coordinates of point P with respect to the global coordinate system (x, y, z), depicted in Figure 2.6.

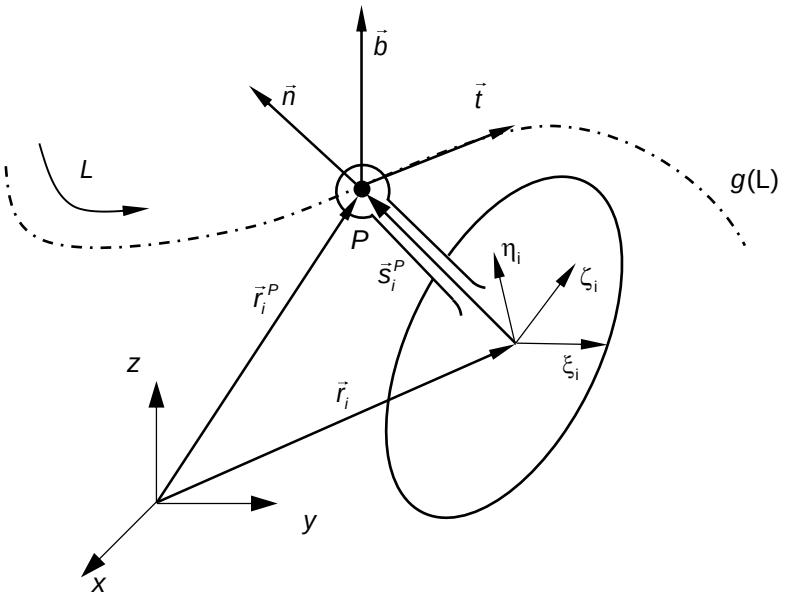

Figure 2.6: Prescribed Point Constraint

The velocity equations for the prescribed point constraint can be obtained as the time derivative of Equation (2.20), expressed as:

$$\dot{\mathbf{\Phi}}^{(pmc,3)} = \mathbf{0} \equiv \begin{bmatrix} \mathbf{I} & -\tilde{\mathbf{s}}_i^R \mathbf{A}_i & -\dfrac{d\mathbf{g}}{dL} \end{bmatrix} \begin{bmatrix} \dot{\mathbf{r}} \\ \boldsymbol{\omega}' \\ \dot{L} \end{bmatrix} = \mathbf{0} \tag{2.21}$$

where the Jacobian matrix is

$$\mathbf{\Phi}_{\mathbf{q}}^{(pmc,3)} = \begin{bmatrix} \mathbf{I} & -\tilde{\mathbf{s}}_i^R \mathbf{A}_i & -\dfrac{d\mathbf{g}}{dL} \end{bmatrix} \tag{2.22}$$

The acceleration equation is the time derivative of Equation (2.21), being written as

$$\ddot{\mathbf{\Phi}}^{(pmc,3)} = \mathbf{0} \equiv \begin{bmatrix} \mathbf{I} & -\tilde{\mathbf{s}}_i^R \mathbf{A}_i & -\dfrac{d\mathbf{g}}{dL} \end{bmatrix} \begin{bmatrix} \ddot{\mathbf{r}} \\ \dot{\boldsymbol{\omega}}' \\ \ddot{L} \end{bmatrix} = -\tilde{\boldsymbol{\omega}}_i \tilde{\boldsymbol{\omega}}_i \mathbf{A}_i \mathbf{s}_i'^P + \frac{d^2\mathbf{g}}{dL^2} \dot{L}^2 \tag{2.23}$$

where the right hand side of the acceleration equation is

$$\boldsymbol{\gamma}^{(pmc,3)} = -\tilde{\boldsymbol{\omega}}_i \tilde{\boldsymbol{\omega}}_i \mathbf{A}_i \mathbf{s}_i'^P + \frac{d^2\mathbf{g}}{dL^2} \dot{L}^2 \tag{2.24}$$

Therefore, the contribution of the prescribed point constraint to the constraint acceleration equations (2.8) is written as

$$\left[\boldsymbol{\Phi}_{\mathbf{q}}^{(pmc,3)}\right]\ddot{\mathbf{q}} = \left[\boldsymbol{\gamma}^{(pmc,3)}\right] \tag{2.25}$$

which must be assembled in the system Jacobian matrix.

2.2.3 Prescribed Cylindrical Constraint

The prescribed cylindrical constraint starts with the same formulation that the prescribed point constraint, but also restrains orientations of body i, being the body only allowed to roll about the path, i.e, the rotation around the prescribed path centreline along the longitudinal axis. The constraints equations that enforces a point in a rigid body to follow the reference path are the same, $\boldsymbol{\Phi}^{(\text{pmc},3)} \equiv \mathbf{r}_i^P - \mathbf{g}(L) = \mathbf{0}$, but in addition, there is a new local frames alignment constraint, that does not include the constraint equation that would prevent its roll. Consider a rigid body i where $\left(\mathbf{u}_\xi, \mathbf{u}_\eta, \mathbf{u}_\zeta\right)_i$ represent unit vectors associated to the body fixed coordinate system $(\xi, \eta, \zeta)_i$. Consider also that the Frenet frame of the general parametric curve $\mathbf{g}(L)$ is defined by the principal unit vectors $(\mathbf{t}, \mathbf{n}, \mathbf{b})_L$, as depicted in Figure 2.7. The relative orientation between the body vectors $\left(\mathbf{u}_\xi, \mathbf{u}_\eta, \mathbf{u}_\zeta\right)_i$ and the curve local frame $(\mathbf{t}, \mathbf{n}, \mathbf{b})_L$ is such that [22].

$$\boldsymbol{\Phi}^{(lfac,2)} = \begin{Bmatrix} \mathbf{n}^T \mathbf{A}_i \mathbf{u}_\xi \\ \mathbf{b}^T \mathbf{A}_i \mathbf{u}_\xi \end{Bmatrix} - \begin{Bmatrix} a \\ b \end{Bmatrix} = 0 \tag{2.26}$$

In which *lfac* stands for 'local frame alignment constraint', and $\{a \quad b\}^T = diag\left[\mathbf{A}_L^{0^T} \quad \mathbf{A}_i^{0^T}\right]$ are constants calculated at the initial time of the analysis, by using Eq. (2.26) with the initial conditions set by the user.

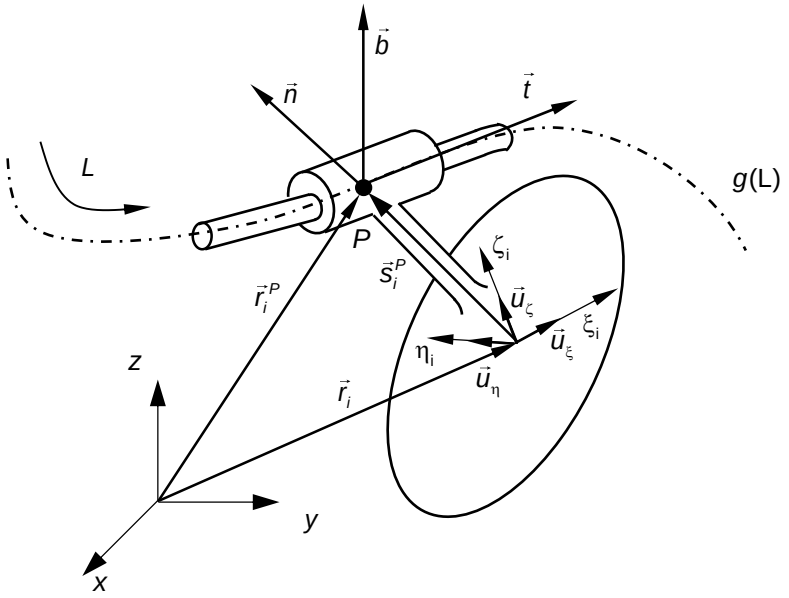

Figure 2.7: Prescribed Cylindrical Constraint

The velocity equations for this constraint can be obtained as the time derivative of Equations (2.20) and (2.26), expressed as

$$\dot{\mathbf{\Phi}}^{(pmc,3)} = \mathbf{0} \equiv \begin{bmatrix} \mathbf{I} & -\tilde{\mathbf{s}}_i^R \mathbf{A} & -\dfrac{d\mathbf{g}}{dL} \end{bmatrix} \begin{bmatrix} \dot{\mathbf{r}} \\ \boldsymbol{\omega}' \\ \dot{L} \end{bmatrix} = 0 \tag{2.27}$$

$$\dot{\mathbf{\Phi}}^{(lfac,2)} = \mathbf{0} \equiv \begin{bmatrix} \mathbf{0}^T & -\mathbf{n}^T \mathbf{A}_i \tilde{\mathbf{u}}_\xi \left(\dfrac{d\mathbf{n}}{dL}\right)^T & \mathbf{A}_i \mathbf{u}_\xi \\ \mathbf{0}^T & -\mathbf{b}^T \mathbf{A}_i \tilde{\mathbf{u}}_\xi \left(\dfrac{d\mathbf{b}}{dL}\right)^T & \mathbf{A}_i \mathbf{u}_\xi \end{bmatrix} \begin{bmatrix} \dot{\mathbf{r}} \\ \boldsymbol{\omega}' \\ \dot{L} \end{bmatrix} = 0 \tag{2.28}$$

where the Jacobian matrix associated to each part of the constraint is

$$\mathbf{\Phi}_{\mathbf{q}}^{(pmc,3)} = \begin{bmatrix} \mathbf{I} & -\tilde{\mathbf{s}}_i^R \mathbf{A} & -\dfrac{d\mathbf{g}}{dL} \end{bmatrix} \tag{2.29}$$

$$\mathbf{\Phi}_{\mathbf{q}}^{(lfac,2)} = \begin{bmatrix} \mathbf{0}^T & -\mathbf{n}^T \mathbf{A}_i \tilde{\mathbf{u}}_\xi \left(\dfrac{d\mathbf{n}}{dL}\right)^T & \mathbf{A}_i \mathbf{u}_\xi \\ \mathbf{0}^T & -\mathbf{b}^T \mathbf{A}_i \tilde{\mathbf{u}}_\xi \left(\dfrac{d\mathbf{b}}{dL}\right)^T & \mathbf{A}_i \mathbf{u}_\xi \end{bmatrix} \tag{2.30}$$

The acceleration equations are the time derivatives of Equations (2.27) and (2.28), being written as

$$\ddot{\mathbf{\Phi}}^{(pmc,3)} = \mathbf{0} \equiv \begin{bmatrix} \mathbf{I} & -\tilde{\mathbf{s}}_i^R \mathbf{A} & -\dfrac{d\mathbf{g}}{dL} \end{bmatrix} \begin{bmatrix} \ddot{\mathbf{r}} \\ \dot{\boldsymbol{\omega}}' \\ \ddot{L} \end{bmatrix} = -\tilde{\boldsymbol{\omega}}_i \tilde{\boldsymbol{\omega}}_i \mathbf{A}_i \mathbf{s}_i'^P + \frac{d^2\mathbf{g}}{dL^2} \dot{L}^2 \tag{2.31}$$

$$\ddot{\mathbf{\Phi}}^{(lfac,2)} = \mathbf{0} \equiv \begin{bmatrix} \mathbf{0}^T & -\mathbf{n}^T \mathbf{A}_i \tilde{\mathbf{u}}_\xi \left(\dfrac{d\mathbf{n}}{dL}\right)^T & \mathbf{A}_i \mathbf{u}_\xi \\ \mathbf{0}^T & -\mathbf{b}^T \mathbf{A}_i \tilde{\mathbf{u}}_\xi \left(\dfrac{d\mathbf{b}}{dL}\right)^T & \mathbf{A}_i \mathbf{u}_\xi \end{bmatrix} \begin{bmatrix} \ddot{\mathbf{r}} \\ \dot{\boldsymbol{\omega}}' \\ \ddot{L} \end{bmatrix} = \begin{Bmatrix} -\left[2\dot{L} \left(\dfrac{d\mathbf{n}}{dL}\right)^T \mathbf{A}_i \tilde{\boldsymbol{\omega}}_i' + \mathbf{n}^T \mathbf{A}_i \tilde{\boldsymbol{\omega}}_i' \tilde{\boldsymbol{\omega}}_i' + \dot{L}^2 \left(\dfrac{d^2\mathbf{n}}{dL^2}\right)^T \mathbf{A}_i \right] \mathbf{u}_\xi \\ -\left[2\dot{L} \left(\dfrac{d\mathbf{b}}{dL}\right)^T \mathbf{A}_i \tilde{\boldsymbol{\omega}}_i' + \mathbf{b}^T \mathbf{A}_i \tilde{\boldsymbol{\omega}}_i' \tilde{\boldsymbol{\omega}}_i' + \dot{L}^2 \left(\dfrac{d^2\mathbf{b}}{dL^2}\right)^T \mathbf{A}_i \right] \mathbf{u}_\xi \end{Bmatrix} \tag{2.32}$$

And the contribution of each part of the kinematic constraint to the right hand side of the acceleration equations is

$$\boldsymbol{\gamma}^{(pmc,3)} = -\tilde{\boldsymbol{\omega}}_i \tilde{\boldsymbol{\omega}}_i \mathbf{A}_i \mathbf{s}_i'^P + \frac{d^2\mathbf{g}}{dL^2} \dot{L}^2 \tag{2.33}$$

$$\boldsymbol{\gamma}^{(lfac,2)} = \begin{Bmatrix} -\left[2\dot{L} \left(\dfrac{d\mathbf{n}}{dL}\right)^T \mathbf{A}_i \tilde{\boldsymbol{\omega}}_i' + \mathbf{n}^T \mathbf{A}_i \tilde{\boldsymbol{\omega}}_i' \tilde{\boldsymbol{\omega}}_i' + \dot{L}^2 \left(\dfrac{d^2\mathbf{n}}{dL^2}\right)^T \mathbf{A}_i \right] \mathbf{u}_\xi \\ -\left[2\dot{L} \left(\dfrac{d\mathbf{b}}{dL}\right)^T \mathbf{A}_i \tilde{\boldsymbol{\omega}}_i' + \mathbf{b}^T \mathbf{A}_i \tilde{\boldsymbol{\omega}}_i' \tilde{\boldsymbol{\omega}}_i' + \dot{L}^2 \left(\dfrac{d^2\mathbf{b}}{dL^2}\right)^T \mathbf{A}_i \right] \mathbf{u}_\xi \end{Bmatrix} \tag{2.34}$$

Therefore, the contribution to the constraint acceleration equations (2.8) is written as

$$\begin{bmatrix} \mathbf{\Phi}_{\mathbf{q}}^{(pmc,3)} \\ \mathbf{\Phi}_{\mathbf{q}}^{(lfac,2)} \end{bmatrix} \ddot{\mathbf{q}} = \begin{bmatrix} \boldsymbol{\gamma}^{(pmc,3)} \\ \boldsymbol{\gamma}^{(lfac,2)} \end{bmatrix} \tag{2.35}$$

2.2.4 Prescribed Full Motion Constraint

The prescribed full motion constraint, that enforces a body to translate and rotate about a speciefied curve, is developed by Pombo and Ambrósio [14], and presented hereafter. The constraint equations that enforce point P to follow the reference path $\mathbf{g}(L)$ are written as [16]:

$$\mathbf{\Phi}^{(\text{pmc},3)} \equiv \mathbf{r}_i^P - \mathbf{g}(L) = \mathbf{0} \tag{2.36}$$

Where r_i^P represents the coordinates of point P with respect to the global coordinate system (x, y, z), depicted in Figure 2.8.

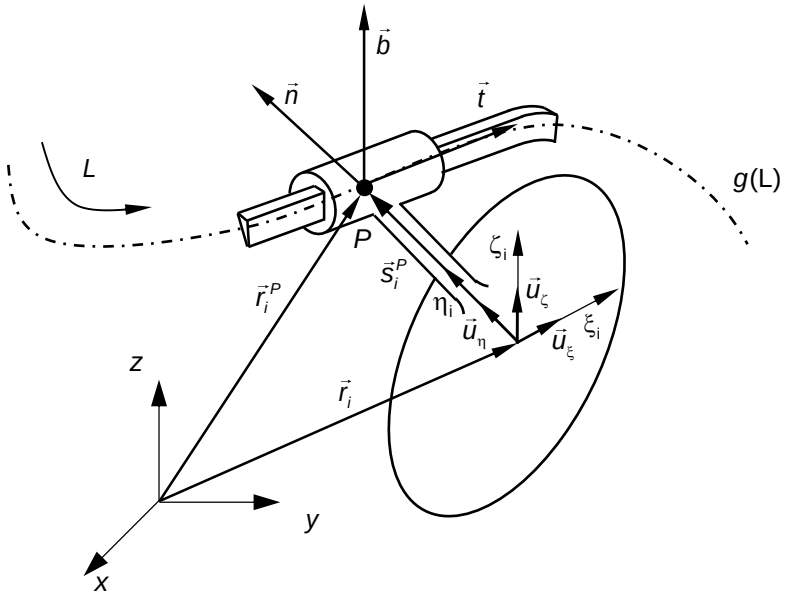

Figure 2.8: Prescribed Full Motion Constraint

The prescribed full motion constraint also ensures that the spatial orientation of body i remains unchanged with respect to the moving Frenet frame $(\mathbf{t},\mathbf{n},\mathbf{b})$ associated to the reference path curve, represented in Figure 2.8. Consider a rigid body i where $(\mathbf{u}_\xi,\mathbf{u}_\eta,\mathbf{u}_\zeta)_i$ represent unit vectors associated to the body fixed coordinate system $(\xi,\eta,\zeta)_i$. Consider also that the Frenet frame of the general parametric curve $\mathbf{g}(L)$ is defined by the principal unit vectors $(\mathbf{t},\mathbf{n},\mathbf{b})_L$, as depicted in Figure 2.8. The relative orientation between the body vectors $(\mathbf{u}_\xi,\mathbf{u}_\eta,\mathbf{u}_\zeta)_i$ and the curve local frame $(\mathbf{t},\mathbf{n},\mathbf{b})_L$ is such that [22].

$$\mathbf{\Phi}^{(lfac,3)} = \begin{Bmatrix} \mathbf{n}^T\mathbf{A}_i\mathbf{u}_\xi \\ \mathbf{b}^T\mathbf{A}_i\mathbf{u}_\xi \\ \mathbf{n}^T\mathbf{A}_i\mathbf{u}_\eta \end{Bmatrix} - \begin{Bmatrix} a \\ b \\ c \end{Bmatrix} = 0 \tag{2.37}$$

In which *lfac* stands for 'local frame alignment constraint', and $\{a \quad b \quad c\}^T = diag\left[\mathbf{A}_L^{0^T} \quad \mathbf{A}_i^{0^T}\right]$ are constants calculated ate initial time of the analysis, by using Eq. (2.37) with the initial conditions.

The velocity equations for this constraint can be obtained as the time derivative of Equations (2.36) e (2.37), expressed as

$$\dot{\mathbf{\Phi}}^{(pmc,3)} = \mathbf{0} \equiv \begin{bmatrix} \mathbf{I} & -\tilde{\mathbf{s}}_i^R \mathbf{A} & -\dfrac{d\mathbf{g}}{dL} \end{bmatrix} \begin{bmatrix} \dot{\mathbf{r}} \\ \boldsymbol{\omega}' \\ \dot{L} \end{bmatrix} = 0 \tag{2.38}$$

$$\dot{\mathbf{\Phi}}^{(lfac,3)} = \mathbf{0} \equiv \begin{bmatrix} \mathbf{0}^T & -\mathbf{n}^T \mathbf{A}_i \tilde{\mathbf{u}}_\xi \left(\dfrac{d\mathbf{n}}{dL}\right)^T & \mathbf{A}_i \mathbf{u}_\xi \\ \mathbf{0}^T & -\mathbf{b}^T \mathbf{A}_i \tilde{\mathbf{u}}_\xi \left(\dfrac{d\mathbf{n}}{dL}\right)^T & \mathbf{A}_i \mathbf{u}_\xi \\ \mathbf{0}^T & -\mathbf{n}^T \mathbf{A}_i \tilde{\mathbf{u}}_\zeta \left(\dfrac{d\mathbf{n}}{dL}\right)^T & \mathbf{A}_i \mathbf{u}_\zeta \end{bmatrix} \begin{bmatrix} \dot{\mathbf{r}} \\ \boldsymbol{\omega}' \\ \dot{L} \end{bmatrix} = 0 \tag{2.39}$$

where the Jacobian matrix associated to each part of the constraint is

$$\mathbf{\Phi}_{\mathbf{q}}^{(pmc,3)} = \begin{bmatrix} \mathbf{I} & -\tilde{\mathbf{s}}_i^R \mathbf{A} & -\dfrac{d\mathbf{g}}{dL} \end{bmatrix} \tag{2.40}$$

$$\mathbf{\Phi}_{\mathbf{q}}^{(lfac,3)} = \begin{bmatrix} \mathbf{0}^T & -\mathbf{n}^T \mathbf{A}_i \tilde{\mathbf{u}}_\xi \left(\dfrac{d\mathbf{n}}{dL}\right)^T & \mathbf{A}_i \mathbf{u}_\xi \\ \mathbf{0}^T & -\mathbf{b}^T \mathbf{A}_i \tilde{\mathbf{u}}_\xi \left(\dfrac{d\mathbf{n}}{dL}\right)^T & \mathbf{A}_i \mathbf{u}_\xi \\ \mathbf{0}^T & -\mathbf{n}^T \mathbf{A}_i \tilde{\mathbf{u}}_\zeta \left(\dfrac{d\mathbf{n}}{dL}\right)^T & \mathbf{A}_i \mathbf{u}_\zeta \end{bmatrix} \tag{2.41}$$

The acceleration equations are the time derivatives of Equations (2.38) and (2.39), and they are written as

$$\ddot{\mathbf{\Phi}}^{(pmc,3)} = \mathbf{0} \equiv \begin{bmatrix} \mathbf{I} & -\tilde{\mathbf{s}}_i^R \mathbf{A} & -\dfrac{d\mathbf{g}}{dL} \end{bmatrix} \begin{bmatrix} \ddot{\mathbf{r}} \\ \dot{\boldsymbol{\omega}}' \\ \ddot{L} \end{bmatrix} = -\tilde{\boldsymbol{\omega}}_i \tilde{\boldsymbol{\omega}}_i \mathbf{A}_i \mathbf{s}_i'^P + \frac{d^2\mathbf{g}}{dL^2} \dot{L}^2 \tag{2.42}$$

$$\ddot{\mathbf{\Phi}}^{(lfac,3)} = \mathbf{0} \equiv \begin{bmatrix} \mathbf{0}^T & -\mathbf{n}^T \mathbf{A}_i \tilde{\mathbf{u}}_\xi \left(\dfrac{d\mathbf{n}}{dL}\right)^T & \mathbf{A}_i \mathbf{u}_\xi \\ \mathbf{0}^T & -\mathbf{b}^T \mathbf{A}_i \tilde{\mathbf{u}}_\xi \left(\dfrac{d\mathbf{n}}{dL}\right)^T & \mathbf{A}_i \mathbf{u}_\xi \\ \mathbf{0}^T & -\mathbf{n}^T \mathbf{A}_i \tilde{\mathbf{u}}_\zeta \left(\dfrac{d\mathbf{n}}{dL}\right)^T & \mathbf{A}_i \mathbf{u}_\zeta \end{bmatrix} \begin{bmatrix} \ddot{\mathbf{r}} \\ \dot{\boldsymbol{\omega}}' \\ \ddot{L} \end{bmatrix} = \begin{Bmatrix} -\left[2\dot{L} \left(\dfrac{d\mathbf{n}}{dL}\right)^T \mathbf{A}_i \tilde{\boldsymbol{\omega}}_i' + \mathbf{n}^T \mathbf{A}_i \tilde{\boldsymbol{\omega}}_i' \tilde{\boldsymbol{\omega}}_i' + \dot{L}^2 \left(\dfrac{d^2\mathbf{n}}{dL^2}\right)^T \mathbf{A}_i \right] \mathbf{u}_\xi \\ -\left[2\dot{L} \left(\dfrac{d\mathbf{b}}{dL}\right)^T \mathbf{A}_i \tilde{\boldsymbol{\omega}}_i' + \mathbf{b}^T \mathbf{A}_i \tilde{\boldsymbol{\omega}}_i' \tilde{\boldsymbol{\omega}}_i' + \dot{L}^2 \left(\dfrac{d^2\mathbf{b}}{dL^2}\right)^T \mathbf{A}_i \right] \mathbf{u}_\xi \\ -\left[2\dot{L} \left(\dfrac{d\mathbf{n}}{dL}\right)^T \mathbf{A}_i \tilde{\boldsymbol{\omega}}_i' + \mathbf{n}^T \mathbf{A}_i \tilde{\boldsymbol{\omega}}_i' \tilde{\boldsymbol{\omega}}_i' + \dot{L}^2 \left(\dfrac{d^2\mathbf{n}}{dL^2}\right)^T \mathbf{A}_i \right] \mathbf{u}_\zeta \end{Bmatrix} \tag{2.43}$$

and the contribution of each part of the kinematic constraint to the right hand side of the acceleration equations is

$$\boldsymbol{\gamma}^{(pmc,3)} = -\tilde{\boldsymbol{\omega}}_i \tilde{\boldsymbol{\omega}}_i \mathbf{A}_i \mathbf{s}_i'^P + \frac{d^2\mathbf{g}}{dL^2} \dot{L}^2 \tag{2.44}$$

$$\boldsymbol{\gamma}^{(lfac,3)} = \begin{Bmatrix} -\left[2\dot{L}\left(\frac{d\mathbf{n}}{dL}\right)^T \mathbf{A}_i\tilde{\boldsymbol{\omega}}_i' + \mathbf{n}^T\mathbf{A}_i\tilde{\boldsymbol{\omega}}_i'\tilde{\boldsymbol{\omega}}_i' + \dot{L}^2\left(\frac{d^2\mathbf{n}}{dL^2}\right)^T \mathbf{A}_i \right]\mathbf{u}_\xi \\ -\left[2\dot{L}\left(\frac{d\mathbf{b}}{dL}\right)^T \mathbf{A}_i\tilde{\boldsymbol{\omega}}_i' + \mathbf{b}^T\mathbf{A}_i\tilde{\boldsymbol{\omega}}_i'\tilde{\boldsymbol{\omega}}_i' + \dot{L}^2\left(\frac{d^2\mathbf{b}}{dL^2}\right)^T \mathbf{A}_i \right]\mathbf{u}_\xi \\ -\left[2\dot{L}\left(\frac{d\mathbf{n}}{dL}\right)^T \mathbf{A}_i\tilde{\boldsymbol{\omega}}_i' + \mathbf{n}^T\mathbf{A}_i\tilde{\boldsymbol{\omega}}_i'\tilde{\boldsymbol{\omega}}_i' + \dot{L}^2\left(\frac{d^2\mathbf{n}}{dL^2}\right)^T \mathbf{A}_i \right]\mathbf{u}_\zeta \end{Bmatrix} \tag{2.45}$$

Therefore, the contribution of the prescribed motion constraint to the constraint acceleration equations (2.8) is written as

$$\begin{bmatrix} \boldsymbol{\Phi}_{\mathbf{q}}^{(pmc,3)} \\ \boldsymbol{\Phi}_{\mathbf{q}}^{(lfac,3)} \end{bmatrix} \ddot{\mathbf{q}} = \begin{bmatrix} \boldsymbol{\gamma}^{(pmc,3)} \\ \boldsymbol{\gamma}^{(lfac,3)} \end{bmatrix} \tag{2.46}$$

To understand the minimum requirements for the degree of the interpolating polynomials that can be used in the formulation of the prescribed motion constraint, the order of the derivatives used in Equations (2.20) through (2.30) must be identified. The right hand side vector in Eq. (2.43) involves $d^2\mathbf{n}/dL^2$, being $\mathbf{n} = \mathbf{k}/\|\mathbf{k}\|$, given by Eq. (2.17) and $\mathbf{k} = \mathbf{g}^{uu} - \left(\mathbf{g}^{uu^T}\mathbf{g}^u\right)\mathbf{g}^u \Big/ \left\|\mathbf{g}^u\right\|^2$ by Eq. (2.18). Therefore it is required that the fourth derivative of the interpolating polynomial is used, being a quintic polynomial the lowest odd degree polynomials that can be used to formulate the prescribed motion constraint. However, as demonstrated by Ambrósio, Antunes and Pombo [22], the errors introduced by using a cubic polynomial are naturally controlled by the Baumgarte stabilization method, during integration. Because cubic splines have a better local control, they are used here as interpolants for the curves.

2.3 Demonstrative Example

As a demonstrative example of each one of the prescribed path constraints, a simple pendulum is modelled and simulated being its position prescribed by one of the rails of a roller coaster track. This track is just a simple curve with 50 m radius used to demonstrate the differences between the kinematic constraints described here when applied to the "hinge" of the pendulum, while this travels with a constant longitudinal velocity.

As shown, in the first group of images in Figure 2.9 (a), which represents the prescribed full motion constraint, the pendulum only assumes the inclination of the track, i.e, the orientation of the pendulum is always equal to the orientation of the track. In this case, the pendulum is not allowed the tilt motion that would regulate its roll according to the centrifugal acceleration.

In the second group of images in Figure 2.9 (b), which represents the prescribed cylindrical constraint, the pendulum exceeds the torsion angle of the track, since with this kinematic constraint it is allowed to roll relative to the rail centreline and, therefore, roll according to the centrifugal forces.

In the final set of images in Figure 2.9 (c), which represents the prescribed point constraint, the pendulum has all orientations free, and it is allowed to rotate in any direction, since this kinematic constraint only enforces the hinge point to follow the rail. Besides the roll motion, similar to that of the prescribed cylindrical motion, the pendulum also exhibits yaw and pitch rotations due to changes in the velocity, orientation, that excite such motions. This constraint is proposed to be used here as the basis for the definition of the vehicle-track interaction in the roller coaster multibody system, being the only one used in this work.

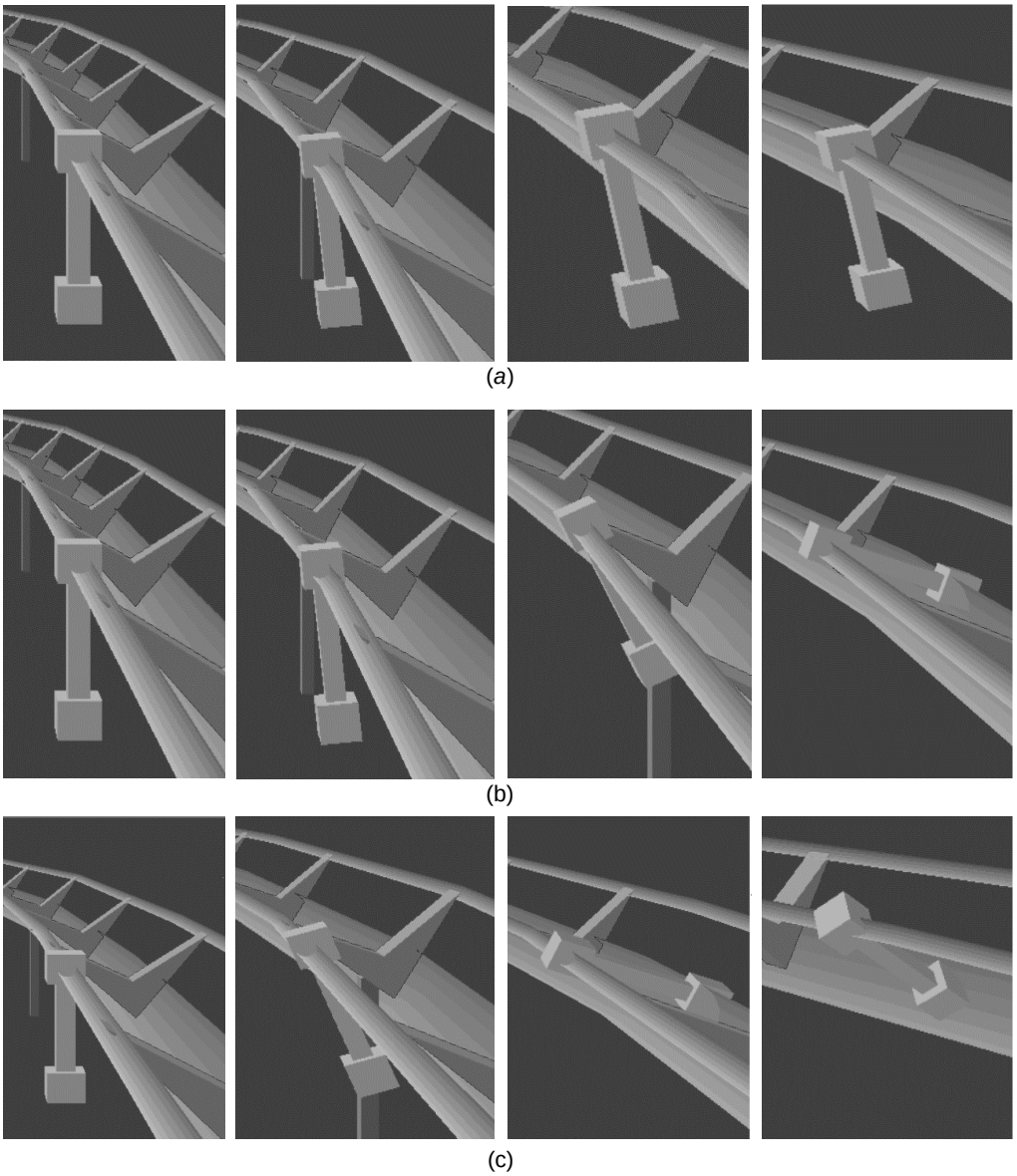

Figure 2.9: Prescribed motion constraints: (a) Full motion; (b) Cylindrical; (c) Point

In Figure 2.11 (a) it can be seen the reaction moments acting on the pendulum, which is prescribed to follow the curve at a constant velocity. In Figure 2.10 (a), it is represented the force diagram of the pendulum when in a curve with the prescribed full motion constraint. In both figures, it can be seen that this kinematic constraint applies a moment on the pendulum, about the ξ axis of the local reference

frame (ξ,η,ζ), that forces it to maintain the angle of the rail, the torsion angle. This reaction moment counteracts the centrifugal acceleration.

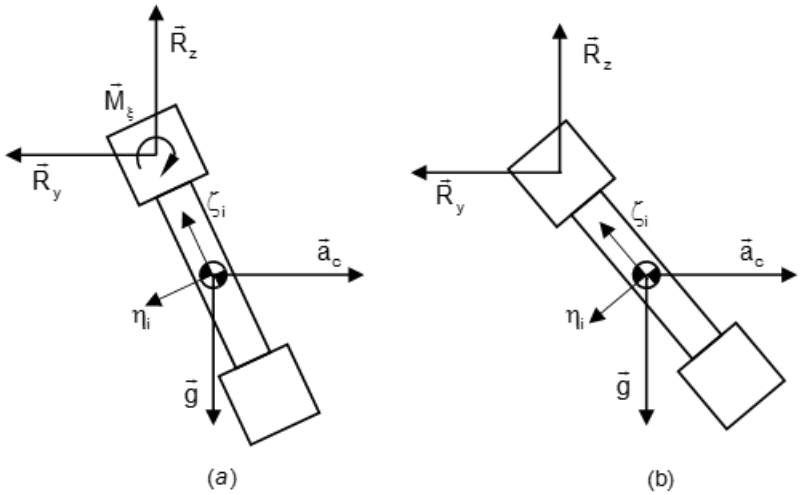

Figure 2.10: Force Diagram for the pendulum with (a) Prescribed Full Motion Constraint (b) Prescribed Cylindrical Constraint

In Figure 2.11 (a), it also can be seen the reaction moment about η, which is always zero, since the pendulum is prescribing the curve at constant velocity. In the transition between the straight line and the curve, this moment is not zero, due to the sudden transition of torsion angle between the straight line and the curve. In the straight line the torsion angle is equal to zero, and in the curve it has a constant value. In this sudden transition the kinematic constraint experiences constraints violations that are controlled with the Baumgarte Stabilization method until they stabilize when the torsion angle is constant again.

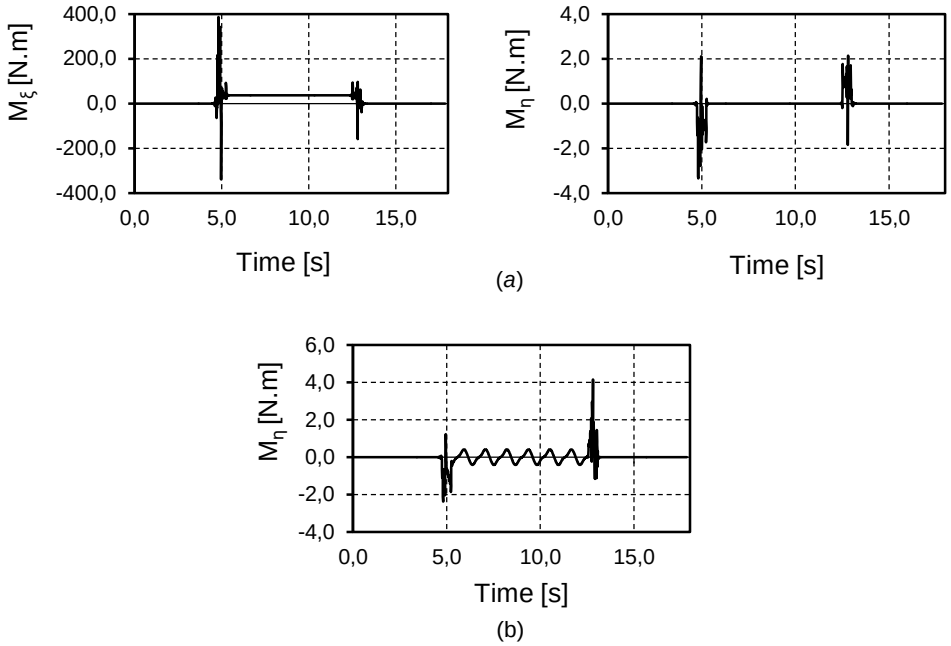

Figure 2.11: Reaction moments at the hinge of the pendulum for (a) Prescribed Full Motion Constraint (b) Prescribed Cylindrical Constraint

In Figure 2.11 (b), it is only presented the reaction moment in η direction, because with the prescribed cylindrical constraint, the pendulum is allowed to roll, so there is no reaction moment in ξ, to counteract the centrifugal acceleration, as depicted in Figure 2.10 (b). This reaction moment oscillates around zero, because, despite the roll angle is free, the other local angles, pitch and yaw, are constrained relatively to the track, and with the pendulum oscillating in the ξ direction, its reference local frame is always changing of position, and so, the kinematic constraint is always trying to stabilize the pendulum in its equilibrium position.

3 Roller Coaster

The definition of roller coaster track geometries requires an accurate geometric description of the centreline of the rails, done with the curve interpolation scheme described in chapter 2. The track is time invariant, being a pre-processor used to define the spatial geometry of the centreline of each rail. In order to achieve computational efficiency, pre-processor generates, in a tabular manner, as function of the arc length, all the track position data local vectors and other general quantities required by the path motion constraints implemented in the multibody code. The aim of this work is the dynamic analysis of the roller coaster vehicle and its occupants, so, the track parameterization presented here only defines the position and orientation of the rails. In this chapter, not only the track geometric description as used in the analysis code, is described but also a three dimensional model of the roller coaster vehicle is proposed. It consists of a collection of bodies and mechanical elements that can move along the track. Due to their high structural stiffness, all vehicle bodies and wheelsets are considered as rigid bodies.

3.1 Track Geometry

The track geometry is part of the input information in the simulations performed in this work. It is composed by two rails, which can be viewed as two side-by-side defined in a plane that sits in the track centreline spatial curve, also called as the reference path. The two rails are independent, right and left, being discretised by independent sets of nodal points. As depicted in Figure 3.1, the position of each point is defined by vector $\mathbf{r}$, being its coordinates measured with respect to the global reference frame (x, y, z), and its orientation defined by the tangent, $\mathbf{t}$, normal, $\mathbf{n}$, and binormal, $\mathbf{b}$, vectors. In Figure 3.1, presents two points, i and j, in each side of the track that represent potential locations for the vehicle wheelsets.

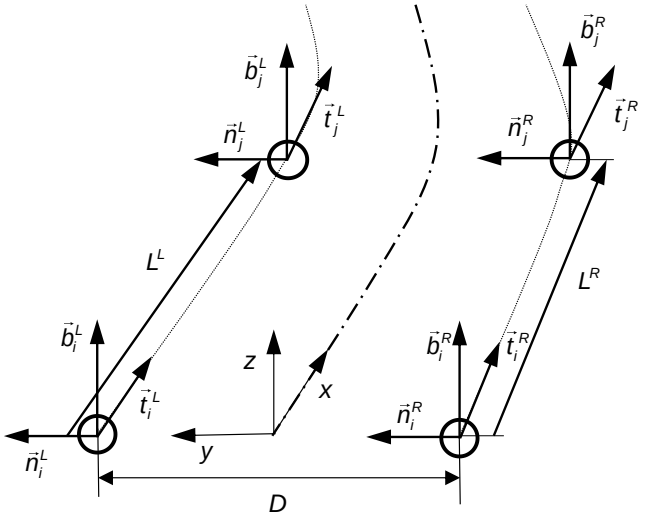

Figure 3.1: Position and orientation of the rails with their local reference frames

The three orientation vectors compose an orthogonal referential attached on the nodal points in which the rail profile is defined. To achieve the proper parameterization, it is necessary to use an appropriate modelling approach. A pre-processor, similar to that one implemented by Pombo [8], is used to define the curve parameterization. As input data to each track, it is necessary to consider the three coordinates (x, y, z), the normal and binormal vectors, $\mathbf{n}$ and $\mathbf{b}$, respectively, in each nodal point of the track centreline. Table 3.1 presents the structured input data for the pre-processor. These points are used in the interpolation procedure of the centreline, using cubic splines, being their spacing defined by the user taking into account for the accuracy required for the geometric description of the tracks.

(x, y, z)	(n_x, n_y, n_z)	(b_x, b_y, b_z)
$(x, y, z)_1$	$(n_x, n_y, n_z)_1$	$(b_x, b_y, b_z)_1$
$\vdots$	$\vdots$	$\vdots$
$(x, y, z)_k$	$(n_x, n_y, n_z)_k$	$(b_x, b_y, b_z)_k$

Table 3.1: Position of the track points and vectors defining the local frame orientation

The pre-processor evaluates the position of each rail and the orientation of its Frenet Frame using the track centreline, based on the gauge defined by D, that corresponds to the distance between the centres of the left and right rails and represented in Figure 3.1. In this work, the gauge is assumed to be $D = 1\ m$.

The length parameter step, ΔL, adopted for the database construction also has to be chosen. Then, the pre-processor constructs a table where all quantities required for the formulation of the kinematic constraint are tabulated as function of the global length parameter, L. These geometric parameters are organized in columns as function of the global length parameter, L of the rail, measured from its origin point up to the actual point in the rail. The multibody program interpolates linearly the table in order to obtain all required geometric characteristics of the track to formulate the constraints equations. If the size of the length parameter step ΔL is set to be similar to the product of the vehicle lower velocity by the average integration time step using during dynamic analysis, then only a few number of interpolations, if any, will be performed in between two successive lines of the table.

Figure 3.2 presents the structure of the roller coaster track database obtained with the pre-processor program, where the adopted step size for the track length is $\Delta L = 0.2\,\mathrm{m}$. A roller coaster track database consists of a table with 37 columns, for each rail. The first column of the database corresponds to the track length L with a step size ΔL, and the corresponding Cartesian coordinates (x, y, z) are stored in the following three columns. The next six columns are first and second derivatives of the Cartesian coordinates with respect to L, respectively, that are required for the Jacobian matrix and for the right hand side of the acceleration equations. Then, the next nine columns contain the information

about the Cartesian components of the unit tangent vector **t** and its first and second derivative with respect to L, respectively. The remaining columns contain the same information, but with respect to the unit normal and binormal vectors **n** and **b**.

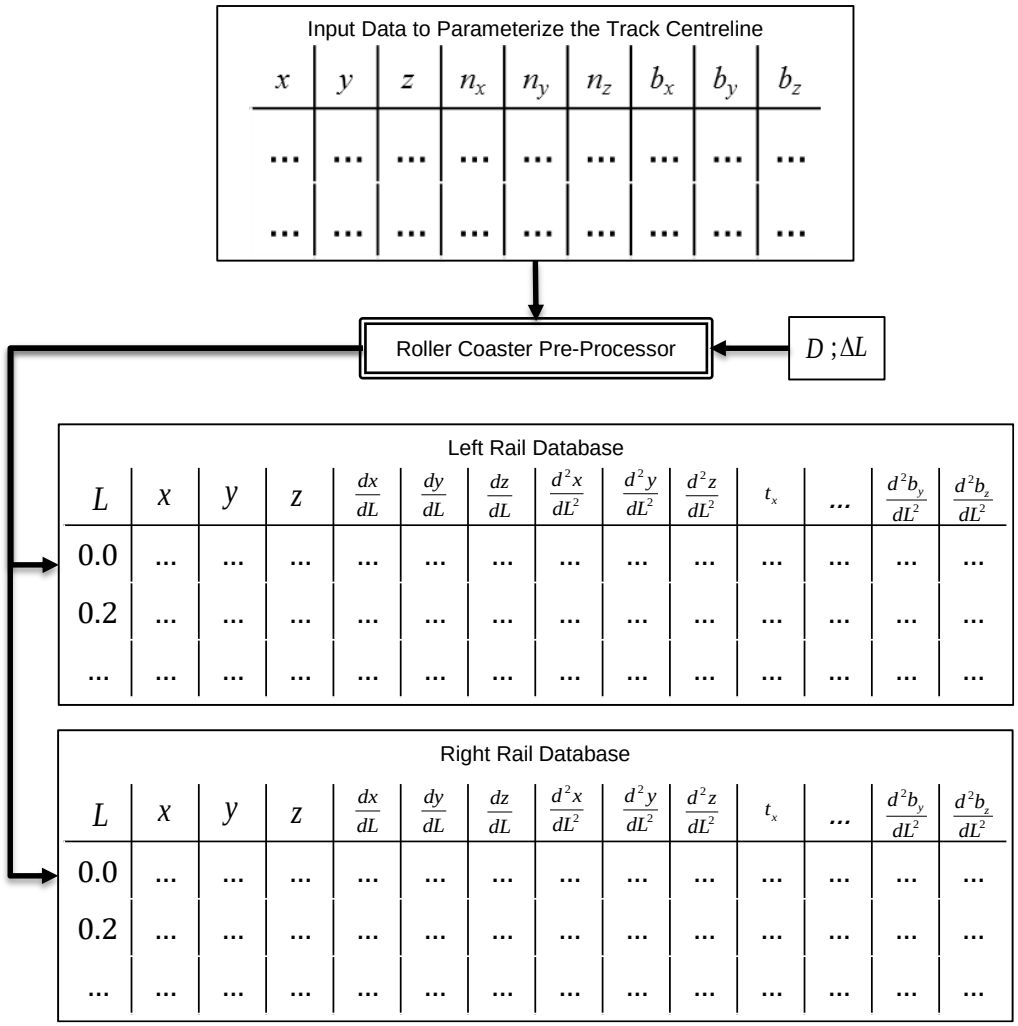

Figure 3.2: Schematic representation of the input and output data of the Roller Coaster Pre-Processor

After the roller coaster track database is built, the track model is completely defined. This is used in the multibody model of the track to roller coaster vehicle interaction during the dynamic analysis of the whole system. A three dimensional representation of two complete roller coaster tracks is displayed in Figure 3.3. It is depicted the track centreline with respective representation of the unitary vectors **n** and **b** to allow better visualization of the track torsion and of its smoothness. Figure 3.4 presents zooms of two selected sections of the tracks to show how the visualizations are used for visual inspection.

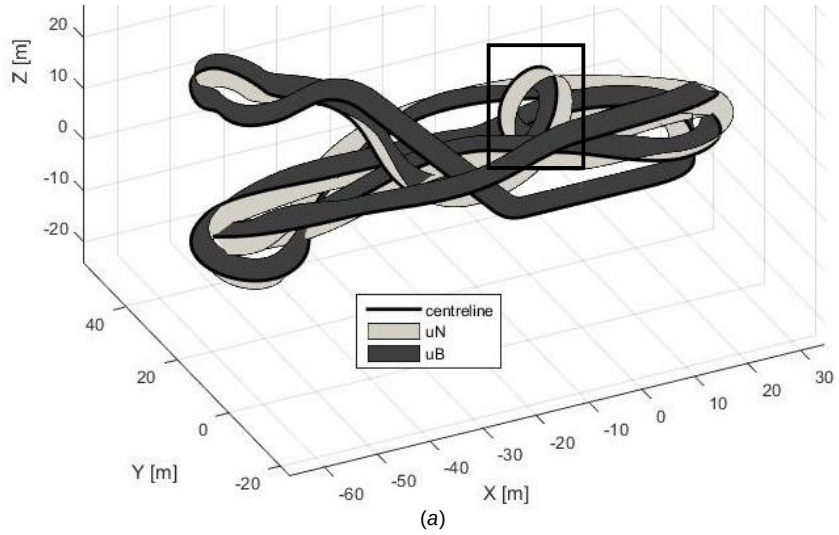

(*a*)

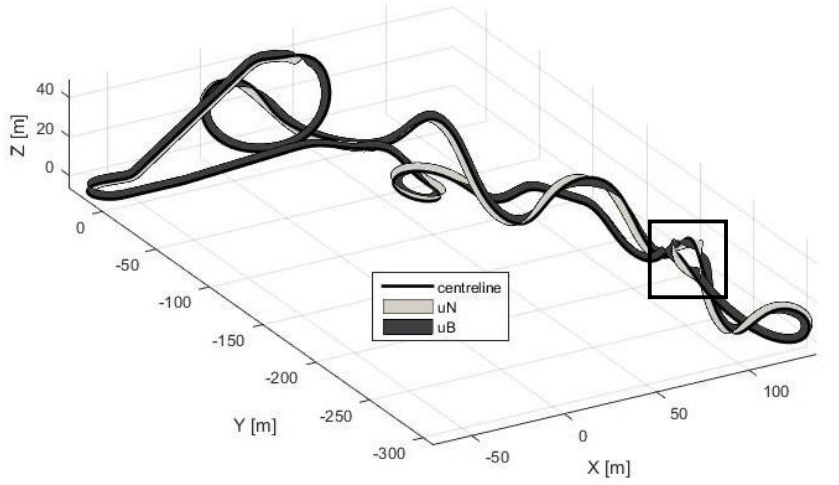

(b)

Figure 3.3: Three-dimensional representation of the track centreline and a sweep of the unitary normal and binormal vector. (a) Looping Star (b) Gate Keeper

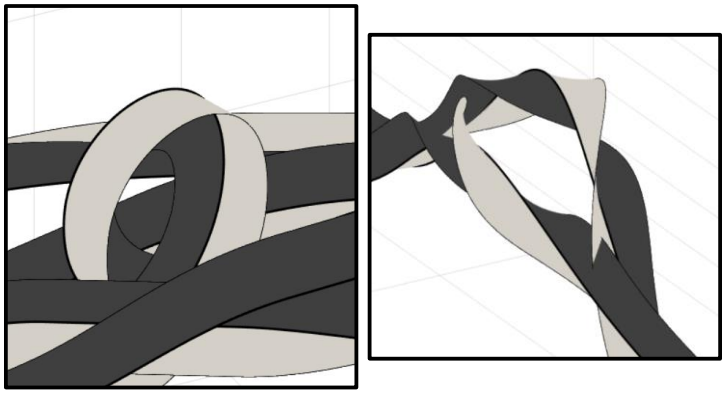

(*a*) (b)

Figure 3.4: Zoom on selected sections of the roller coaster tracks: (a) Loop in Looping Star; (b) Screw in Gate Keeper.

3.2 Vehicle Model Development

In this section, a three dimensional model of the roller coaster vehicle is developed and presented. It must be noted that not only the vehicle does not exist but also it is not intended to represent any existing roller coaster vehicle. In general, the vehicle, as the one developed and presented in Figure 3.5, consists of a collection of bodies and mechanical elements moving along the track. These bodies are connected by a set of kinematic joints and flexible links, which are responsible to passively control their relative motion. The mechanical elements and flexible links, such as springs and dampers, are used to model the vehicle primary and secondary suspensions. The information required to assemble the vehicle model includes the mass, inertia tensors, centre of mass coordinates, orientation and velocity for each rigid body. It is also necessary information to assemble the kinematic constraints, which is defined in the local reference frame of each body, located in their centres of mass. Furthermore, the suspensions elements characteristics and the location of their attachment points, with respect to the body fixed frames, are also required during the model assembling procedure.

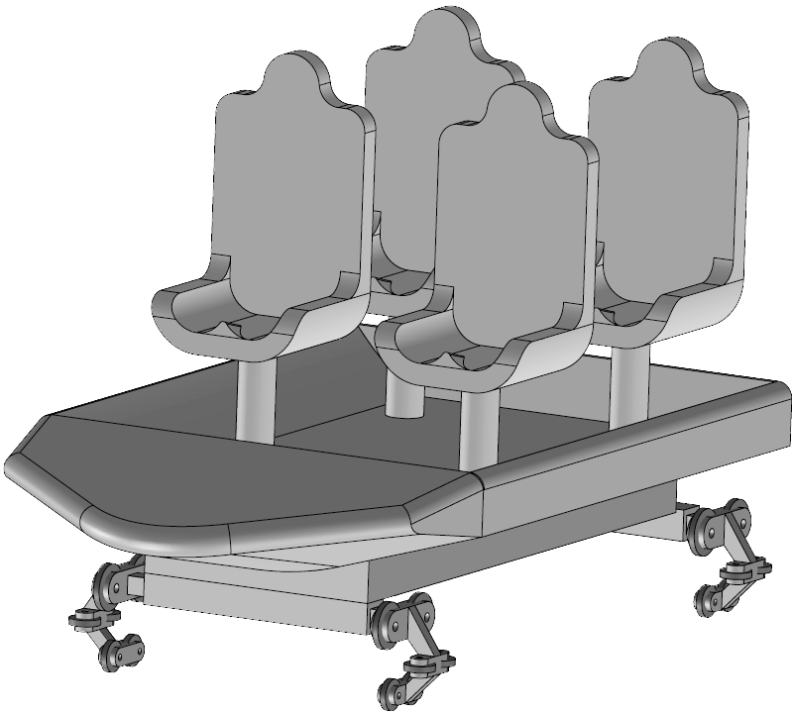

Figure 3.5: Roller Coaster Vehicle idealized and developed in this work

3.2.1 Primary Suspension Mechanism

The objective of a primary suspension mechanism is the proper running of the wheelsets on the rails and the control of any misalignments that may condition the smooth running of the vehicle along the track. In the vehicle proposed here, the primary suspension mechanism is composed by spring-

damper systems that link each wheelset to the vehicle frame, and by two types of constraint joints, prismatic and revolute joints, which are fundamental to ensure that the wheelsets fit to the rails.

In a roller coaster track, it is not always possible to ensure that four points seat in the same plane, so, in order for the four wheelsets to follow their respective rails path, it is necessary an hinge mechanism, intra-vehicle, that allows a relative rotation between the front and the rear vehicle wheelsets. The solution for fitting the wheelsets on the track, i.e, on the rails, is achieved by a revolute joint between the rear axle and the frame of the vehicle, depicted in Figure 3.6, which allows that these two bodies rotate relatively to each other. So there is only one relative degree of freedom between the front and rear of the vehicle, allowing the vehicle wheelsets to seat in different tangent planes, which is what is necessary for the vehicle to describe a curve without either the wheelsets to be out of contact with the rail or the vehicle structure to have to widstand torsion deformations. From the numerical point of view, the wheelsets being out of contact with the rail is perceived as violation of their respective path constraints. The rotation between the rear and front vehicle wheelsets is clearly depicted in Figure 3.6 with the rear view of the vehicle.

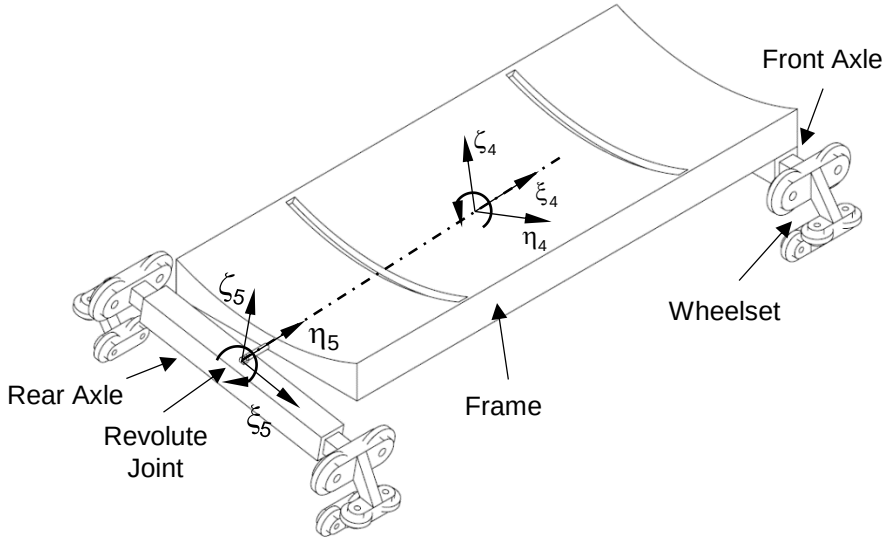

Figure 3.6: Primary Suspension System: Perspective

The wheelsets are modelled as prescribed point constraints that force the reference local frames origins, of each one of the wheelsets, to coincide with the rail path. When there are four points to be prescribed along a roller coaster track, it is necessary to have three relative degrees of freedom between the wheelsets and the rails, allowing the three relative rotations. This is because when the roller coaster vehicle enters a curve, the two front wheelsets will have a different orientation not only with respect to each other but also with respect to the rear wheelsets. It is not only necessary to allow the three relative rotations between the vehicle and the rails, so that the vehicle follow the curve without bending, but also to allow for the wheelsets in the same axis to separate or to come closer to allow a proper insertion on the curve. For example, if the prescribed cylindrical constraint, which only allows the body to roll, is

used in the system only has one relative degree of freedom, and, consequently, locks when entering a curve not being possible for the vehicle to run the complete track. The solution is to allow the separation between the wheelsets of the same axis, as seen in Figure 3.7, so that the vehicle not only is able to follow the track without locking but also is not prevented from running due to geometric defects of the track. This same mechanism also allows for the wheelsets to overcome eventual track imperfections that can be reflected in gauge variations.

The solution for the wheelsets to adjust to the local gauge of the track, i.e, distance between rails, is achieved with a prismatic joint between the wheelsets and the frame, as seen in Figure 3.7, allowing them to move along a lateral common axis. However, the prismatic constraint only assures that both bodies move along the same axis without rotating relatively to each other. Therefore, a force element that returns these two bodies to their neutral relative position is required. If there were no force element linking the two bodies, in the first curve, the wheelsets would open and no internal mechanism would close them. From the numerical point of view this situation would be perceived as the frame moving away along the wheelset axis. The spring-damper system also helps to compensate for track irregularities or gauge variations. As the right and left rails are independent from each other, being each one described by a different database, which along the simulation have different interpolations, so it is impossible to always ensure that the gauge remains constant. If the wheelsets have a fixed distance between each other, along their common axis, the smallest variation of gauge or rail irregularity, it would lead to constraints violations in the case of the numerical model or vehicle locking in the track in the case of a real prototype.

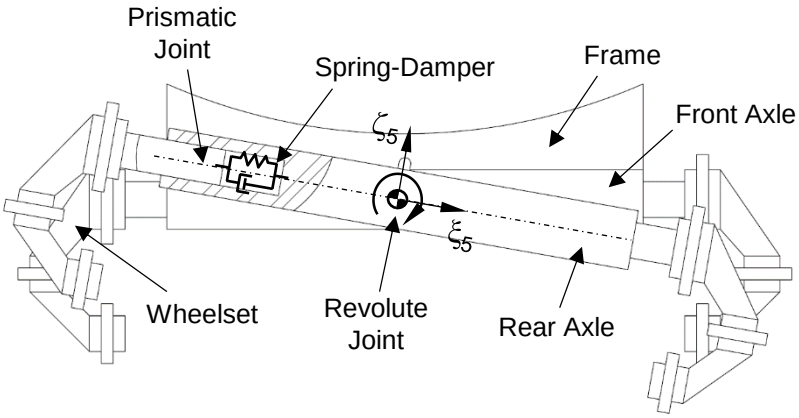

Figure 3.7: Primary Suspension System: Back View

3.2.2 Secondary Suspension Mechanism

A vehicle moving along a circular curve is subjected to an inertial centrifugal acceleration, which is perceived by the passenger as lateral acceleration. This lateral acceleration is not only felt by the passengers as an uncomfortable sensation, but it presents some level of physiological danger for the

roller coaster user that, if not kept inside healthy limits eventually leading to the need to stop the roller coaster operations. The acceleration perceived by a passenger is generally referred to us as g-forces, being their different components, in the passenger local reference frame, depicted in Figure 3.8. The human body has different level of tolerance to different directions of the g-forces.

The secondary suspension mechanism or passive tilting mechanism, has the objective of reducing the uncomfortable sensation, or even motion sickness, that can occurs to a passenger when the roller coaster vehicle is moving along a circular curve. Usually, the curves have torsion angle that is adjusted to the vehicle travel speed. But either because the operation speed differs from the design speed for other reasons such torsion may be deficient. The parameter used to assess the level of discomfort of the passengers is the non-compensated lateral acceleration, NCA [36]. As it can be seen in Figure 3.8, the objective of the secondary suspension system allow controlling, eventually to compensate at least in part, the effects of the lateral accelerations acting on the roller coaster occupant by using a passive tilting mechanisms.

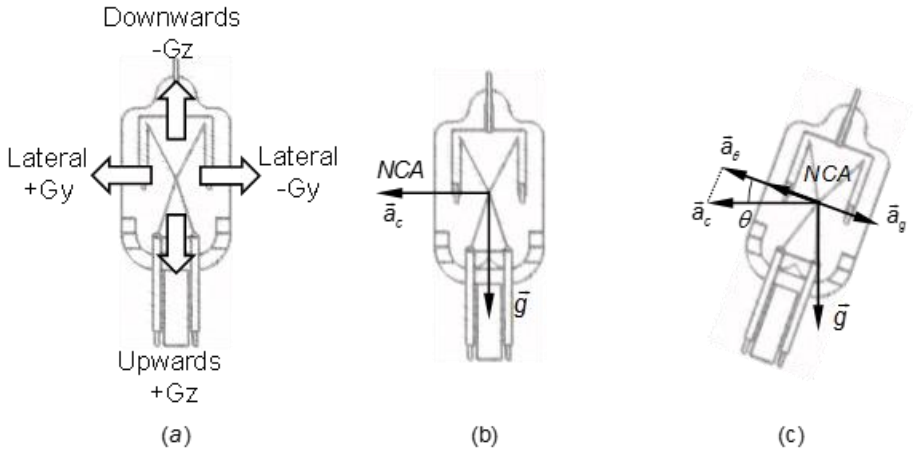

Figure 3.8: Acceleration on the human body in a curve: (a) Nomenclature for acceleration components; (b) acceleration on occupant of vehicle without tilting; (c) acceleration on occupant of vehicle with tilting.

Traditionally, roller coaster vehicles are configured such that the passenger compartment is rigidly mounted to the chassis, which follows the roller coaster path. While this provides a well-known experience that is relatively predictable to the passenger, the lateral forces resultant from such rigid mounting can be uncomfortable, especially when over-the shoulder restraints are used to secure passengers within the passenger compartment [37]. The secondary suspension system provides the passengers compartment, carbody, a roll degree of freedom. The carbody is attached to the roller coaster track via a chassis, in such way that the carbody has a roll degree of freedom relative to the chassis, as seen in Figure 3.9.

This roll degree of freedom is achieved computationally with a revolute joint between the carbody and the chassis. To materialize this concept, although it is a passive tilting mechanism, it is necessary to impose a limited range of roll variation, so the carbody does not rotate freely. The control of lateral

accelerations is achieved by allowing the passenger platform of the carbody, to roll, within a limited range. These limits are achieved physically by using joint stops, which only allow a specified roll variation. The passive control of roll motions is also achieved with a spring-damper arrangements, as depicted in Figure 3.9. Such force elements not only smooth the tilting within its limited range, but also damp the vibrations.

The passive tilting mechanism with a revolute joint between the occupant compartment and the frame is a model that is materialized by a radial mount between the carbody and the chassis. In any case, the relative center of rotation between the passenger platform and the frame of the chassis, modeled as a revolute joint, is located above the assembly center of mass, as depicted in Figure 3.9 and Figure 3.10.

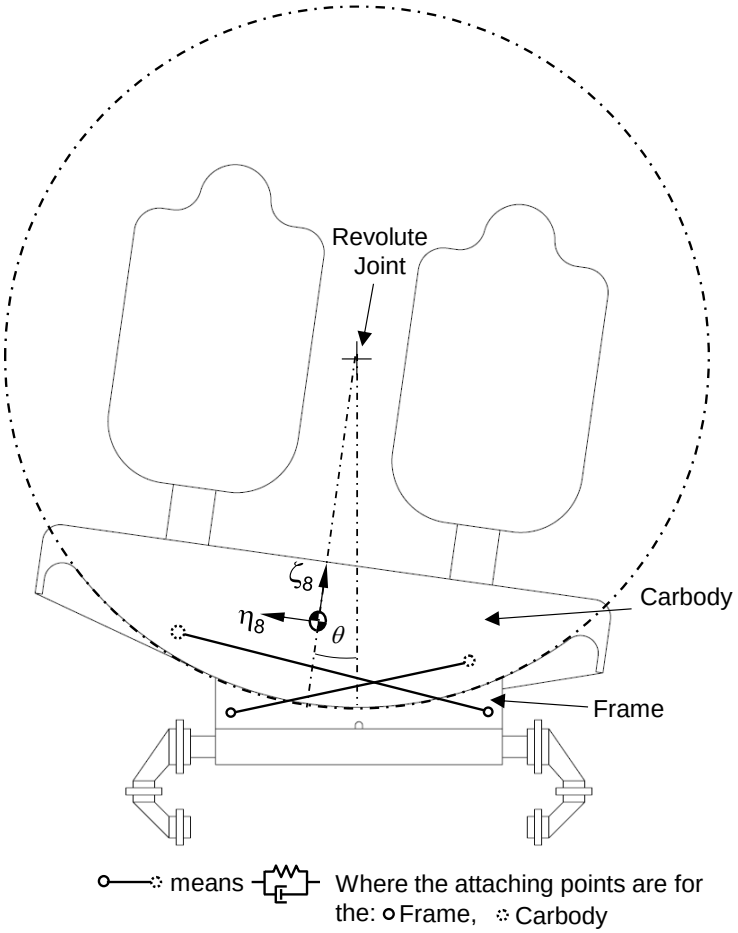

Figure 3.9: Secondary Suspension System

3.2.3 Non-compensated Acceleration

As the non-compensated acceleration reduction plays an important role in the vehicle secondary suspension design, its characterization is important at this stage. The NCA is defined by a relation between the centrifugal and gravitational accelerations applied on the carbody in its local lateral direction. The NCA, depicted in Figure 3.10, is obtained by:

$$NCA = a_c \cos(\varphi + \theta) - g \sin(\varphi + \theta) = a_{\varphi+\theta} - a_{\mathbf{g}} \tag{3.1}$$

where $a_{\varphi+\theta}$ is the local lateral acceleration of the carbody due to the centrifugal acceleration a_c, φ is the torsion angle, θ is the roll angle between the carbody and the chassis, due to the passive tilting mechanism, as depicted in Figure 3.10 and g is the gravitational acceleration. Notice that the centrifugal acceleration can be estimated using the relation $a_c = v^2/R$, where v is the velocity of the vehicle and R is the radius of the curve.

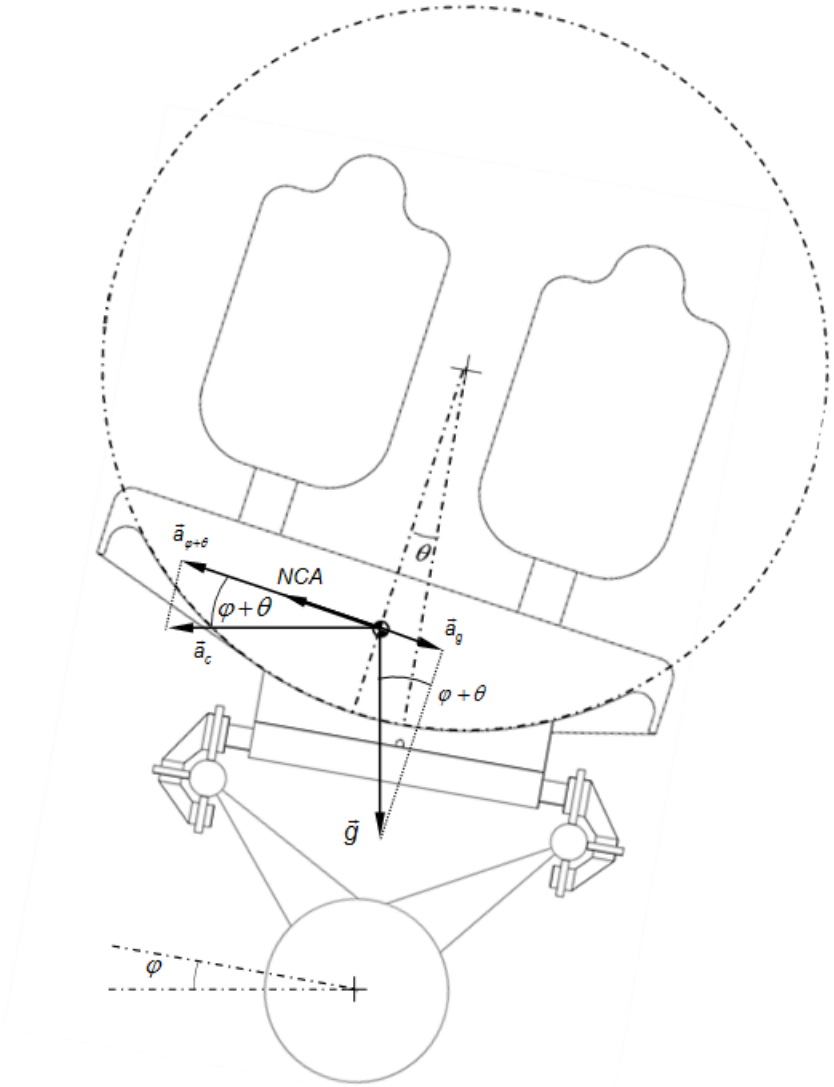

Figure 3.10: Graphical scheme to show the non-compensated acceleration (NCA)

For the vehicle running in the roller coaster track depicted in Figure 3.3(a), the NCA is displayed in Figure 3.11 for a vehicle with the passive tilting mechanism and a traditional vehicle with the passengers compartment rigidly mounted to the chassis. The Figure 3.11 shows a slight reduction of the NCA acting on the roller coaster vehicle, equipped with the tilting mechanism. A large difference can be seen, for example, between the 32s and 33s, approximately, where there is a reduction of 30% of the NCA experienced by the occupants.

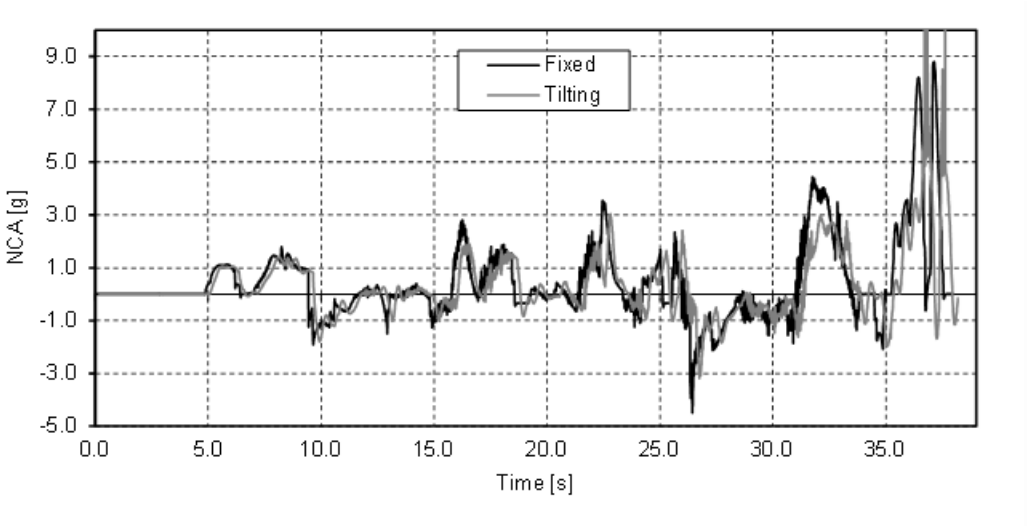

Figure 3.11: Non-Compensated Acceleration (NCA)

This reduction happens in longer curves with smaller radius, where guest compartment has time to stabilize after entering the curve. It is for this type of curves that the tilting mechanism is more important, since it is when the lateral accelerations on the passenger exists for larger time periods. In the majority of the curves, the graph reveals a smaller reduction of the NCA, not so significant, because there are curves with smaller length, and eventually with a balanced torsion, in which the mechanism has no time to stabilize and do its job. Certainly a fine tuning of the spring-damper characteristics of the suspension can contribute to a better dynamic response.

The passive tilting mechanism also reduces, slightly, the velocity of the vehicle. With the wheelsets trajectory being prescribed by a kinematic constraint, and the carbody, or passenger compartment, rigidly attached to the chassis, the primary suspension system is the only mechanism that dissipates some energy. With the secondary suspension system, some extra energy is dissipated, what causes the vehicle to slow down when compared with a vehicle without secondary suspension.

In the final seconds of the simulation, it can be seen that the NCA has two peaks, much higher for the vehicle with the tilting mechanism. This happens because the final two curves of the roller coaster have not sufficient torsion angle, for the small radius of the curve and for the velocity that the vehicle arrives to these curves, so the joint stops are reached. This means that the roll rotation limited range of the occupant compartment is reached, and stops the relative rotation immediately. This sudden stop causes the peak of lateral accelerations. These peaks are expected, because in real roller coasters, this final part of the tracks is traveled at a much lower speed by acting brakes that slow down the vehicle, so the vehicle reaches the final part of the track progressively reducing its velocity until it stops at the arrival/departure station.

It must be mentioned that in loops for which the resulting accelerations on the passenger platform are downwars, this is, –Gz according to the convention in Figure 3.8, the secondary suspension must be locked to prevent the platform inversion. Such locking mechanism is not studied here.

3.2.4 Vehicle Construction

The multibody model of the roller coaster vehicle is assembled using eight rigid bodies, identified, in Figure 3.12 and Figure 3.13, with the numbers 1 to 8, and their local reference frames.

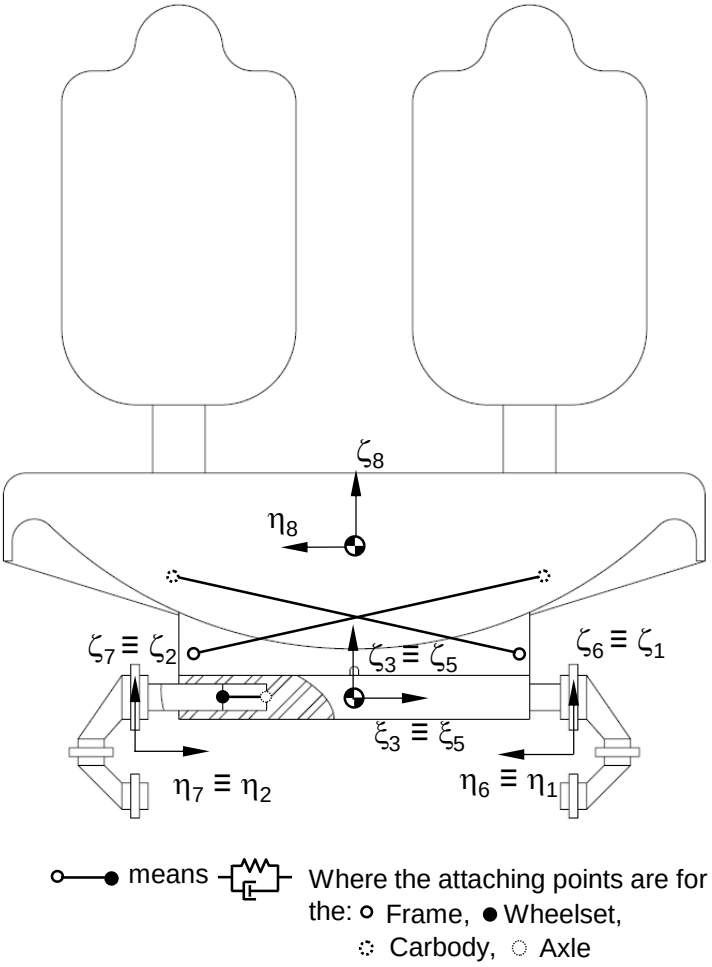

Figure 3.12: Rear view of the multibody model

The vehicle is set in such a way that the wheelsets reference local frames are coincident with the path that each rail describes, so, the reference local frame origin of each wheelset is the point to be prescribed. In the prescribed constraint, this point is the basis for the definition of the vehicle-track interaction. The prescribed point constraint enforces this point, the wheelset reference local frame origin, to move along the rail path, therefore, there are four prescribed point constraints, each one applied to a wheelset. It is considered that the wheelsets of the roller coaster vehicle are permanently in rigid contact with the rails and follow exactly the track geometry, according with the restrictions imposed by the

prescribed point constraint. The wheel-rail contact forces are related to the Lagrange multipliers associated to the prescribed point constraint and are obtained by post-processing the dynamic analysis response of the vehicle.

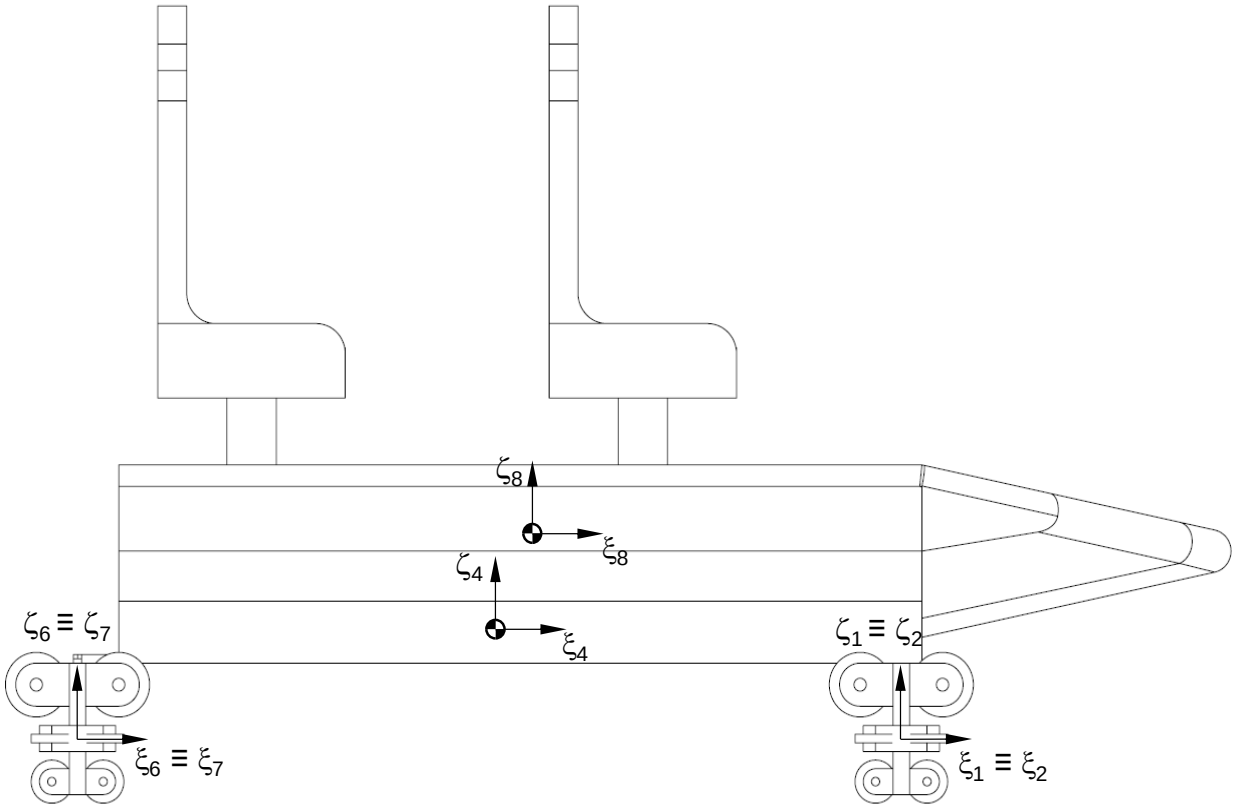

Figure 3.13: Side view of the multibody model

A local reference frame (ξ,η,ζ) is rigidly attached to the centre of mass (CM) of each body. The spatial orientations of the local reference frames are such that they are aligned with the principal inertia directions of the respective rigid body. The mass and the inertia properties, with respect to the three principal local axes, of each body are presented in Table 3.2. In the first column of the table, the ID numbers identify the rigid bodies in the vehicle model presented in Figure 3.12 and Figure 3.13. The mass and inertia properties have been estimated based on the geometry of each body with the help of the software *SOLIDWORKS* [38].

The geometric representation of each body and of its body fixed frames is shown in Figure 3.14. In this figure, it is not possible to see the wheelset that correspond to the body number 7, in Table 3.2, since it is covered by the carbody.

ID	Rigid Bodies	Mass (Kg)	Inertia Properties $(Kg.m^2)$		
			$I_{\xi\xi}$	$I_{\eta\eta}$	$I_{\zeta\zeta}$
1	Wheelset Front Left	10.1	0.14115	0.13446	0.93322
2	Wheelset Front Right	10.1	0.14115	0.13446	0.93322
3	Front Axle	51.5	0.097884	2.3432	2.34232
4	Frame	245	13.0706	77.8762	90.9305
5	Rear Axle	51.5	0.097884	2.3432	2.34232
6	Wheelset Rear Left	10.1	0.14115	0.13446	0.93322
7	Wheelset Rear Right	10.1	0.14115	0.13446	0.93322
8	Carbody	280	30.7503	127.8009	145.6759

Table 3.2: Physical properties of each body

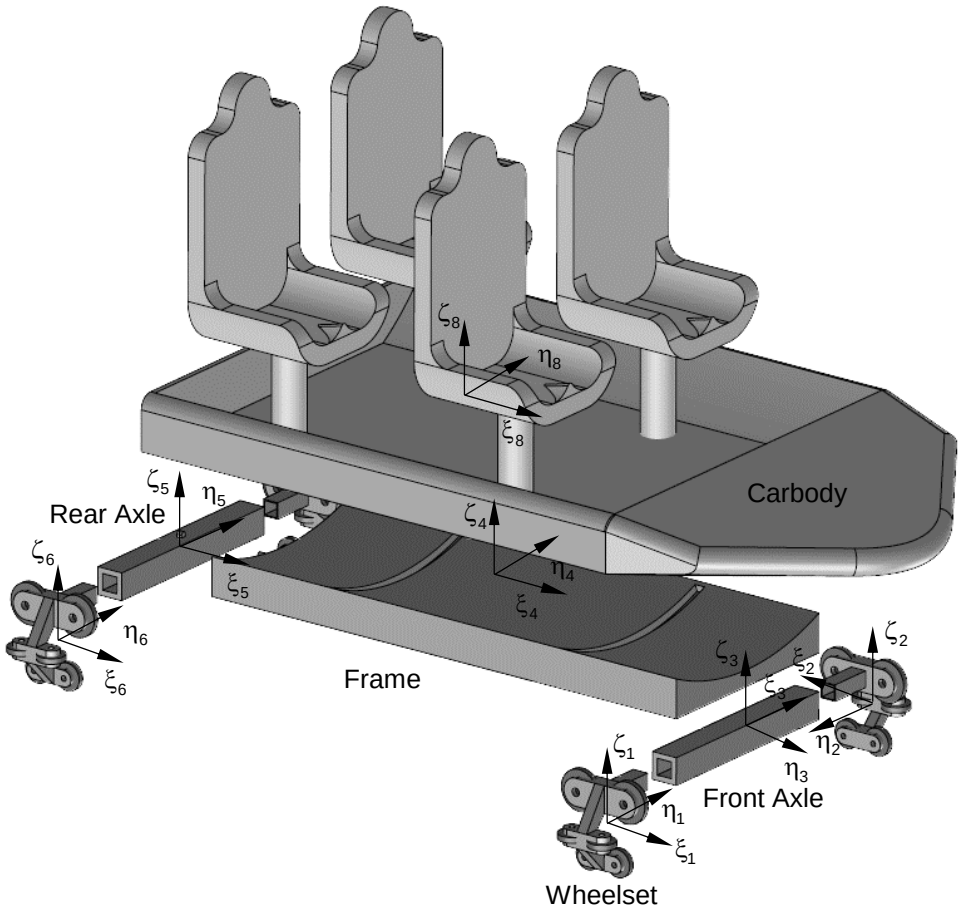

Figure 3.14: Geometric representation of body fixed frame for each individual body in the vehicle

The initial positions, orientations and velocities of each body are presented in Table 3.3. The initial position of each rigid body is given by the location of its body fixed frame origin, coincident with its centre of mass, with respect to the global reference frame (x, y, z).

ID	Initial Position (m)			Orientation			Velocity (m/s)		
	x_0	y_0	z_0	e_1	e_2	e_3	v_{x_0}	v_{y_0}	v_{z_0}
1	-2.1	0.5	0	0	*0*	*1*	-26	0	0
2	-2.1	-0.5	0	0	*0*	*0*	-26	0	0
3	-2.1	0	0.125	0	0	-0.7071	-26	0	0
4	-1.1	0	0.185	0	0	1	-26	0	0
5	-0.1	0	0.125	0	0	-0.7071	-26	0	0
6	-0.1	0.5	0	0	0	1	-26	0	0
7	-0.1	-0.5	0	0	0	0	-26	0	0
8	-1.175	0	0.48	0	0	1	-26	0	0

Table 3.3: Initial positions, orientations and velocities

Note that the initial velocity of 26 m/s is used to take the vehicle to the top of the highest point of the roller coaster track, so that if reaches such point at an almost null velocity. In reality, such guidance is achieved with other type of control, not modelled in this work.

ID	Kinematic Constraint	Bodies		Attachment Points Local Coordinates (m)			
		i	j	$s_P^{'i}$	$s_Q^{'i}$	$s_P^{'j}$	$s_Q^{'j}$
1	Prescribed Point	1	Rail	[0;0;0]	-	-	-
2	Prescribed Point	2	Rail	[0;0;0]	-	-	-
3	Prescribed Point	6	Rail	[0;0;0]	-	-	-
4	Prescribed Point	7	Rail	[0;0;0]	-	-	-
5	Prismatic	3	1	[0.1;0;0]	[0.2;0;0]	[0;0.1;0.125]	[0;0.2;0.125]
6	Prismatic	3	2	[-0.1;0;0]	[-0.2;0;0]	[0;0.1;0.125]	[0;0.2;0.125]
7	Prismatic	5	6	[-0.1;0;0]	[-0.2;0;0]	[0;0.1;0.125]	[0;0.2;0.125]
8	Prismatic	5	7	[0.1;0;0]	[0.2;0;0]	[0;0.1;0.125]	[0;0.2;0.125]
9	Revolute	4	5	[-1;0;0]	[-1.1;0;0]	[0;0;0.06]	[0;0.1;0.06]
10	Revolute	4	8	[1.05;0;1.05]	[1.075;0;1.05]	[0.975;0;0.755]	[0.95;0;0.755]
11	Rigid	3	4	[0;0;0]	-	[0;0;0]	-

Table 3.4: Kinematic Joints

In the roller coaster vehicle model, four prescribed point constraints are used to guide each wheelset on a rail path. These kinematic constraints are defined between the vehicle wheelsets and the rails centerlines, in order to enforce the wheelsets to move along the roller coaster, with their spatial position prescribed according to the track geometry. The remaining kinematic constraints are used to assemble the roller coaster vehicle model, all kinematic constraint data is presented in Table 3.4, which includes the number of the bodies connected and the local coordinates of the attached points.

The suspension of the roller coaster vehicle consists of a group of flexible links that ensure the transmission of forces between the wheelsets and the carbody with the frame, as shown in Figure 3.12. In fact, the primary suspension system links the wheelset with the axles, front and rear. But as these

ones are constrained with the frame by rigid joints, it can be said that the three bodies, front and rear axle and frame are equivalent to a bogie in a railway application.

ID	$K\ (N/m)$	$c\ (N.s/m)$	l_0 (m)	Bodies		Attachment Points Local Coordinates (m)	
				i	j	$s_P^{'i}$	$s_P^{'j}$
1	8×10^5	4×10^4	0.1	3	1	[0.2;0;0]	[0;0.2;0]
2	8×10^5	4×10^4	0.1	3	2	[-0.2;0;0]	[0;0.2;0]
3	8×10^5	4×10^4	0.1	5	6	[-0.2;0;0]	[0;0.2;0]
4	8×10^5	4×10^4	0.1	5	7	[0.2;0;0]	[0;0.2;0]
5	2×10^4	1×10^3	0.7577	3	1	[-0.9;0.35;0]	[-0.975;-0.35;0.00505]
6	2×10^4	1×10^3	0.7577	3	2	[-0.9;-0.35;0]	[-0.975;-0.35;-0.00505]

Table 3.5: Characteristics of the spring-damper systems

The flexible links, or force elements, correspond to spring-damper systems, and all their characteristics, bodies connected and local coordinates of the attachment points are presented in Table 3.5. The spring-damper system is characterized by three parameters, the stiffness k , the unformed length l_0 and the damping coefficient c. The bodies that are connected and the coordinates of the spring-damper system attached points are also depicted in Table 3.5.

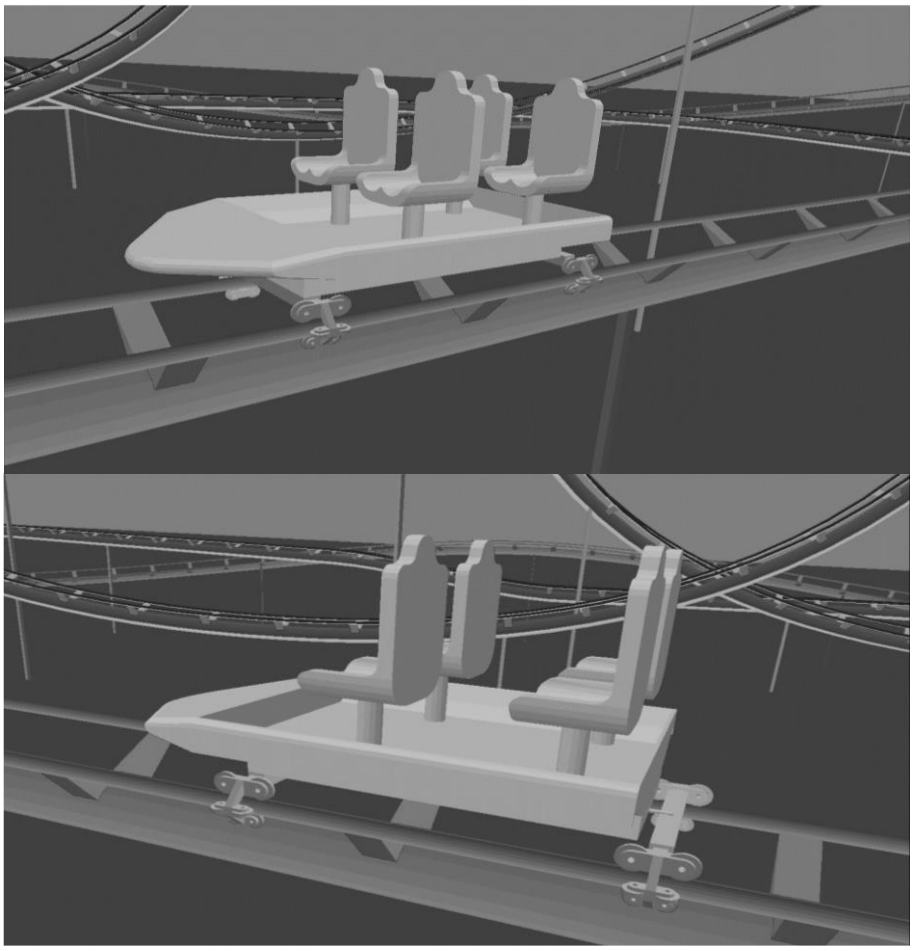

Figure 3.15: Demonstration Vehicle on the track

It must be noted, at this point, the mechanical properties of the suspension elements are defined only for the feasibility studies, presented hereafter. A fine tuning of these properties is crucial for the safe running of the roller coaster vehicle.

A demonstration of the roller coaster vehicle, developed in this work, is shown in Figure 3.15. After the dynamic analysis of the roller coaster, the SAGA [39] program is used for the visualization and animation of the mechanical system. This program receives an input file that contains the history of positions and orientations of the rigid bodies of the roller coaster vehicle and displays the system components in their actual positions and orientations, thus providing an animated output of the motion. Selected frames of these animations are displayed throughout this work.

4 Biomechanical Model of Occupant

The use of biomechanical models to describe, from the mathematical point of view, the human body in terms of its anthropometry, physiology and topology, has been developed, with different purposes and with different approaches, depending on the nature of the research and the objectives of the analysis. There are two type of mathematical approaches that are used to construct and describe biomechanical models, multibody formulations and finite element methods. In this work, it is used the multibody approach, usually applied in simulation cases where gross-motions are involved and when complex interactions with the surrounding environment are to be modelled and analysed [26].

In many situations, these "gross-motion " simulators [40] are preferred to the more expensive finite element based models because the dynamic responses that need to be measured can be predicted with equal accuracy by any of the approaches. In the "gross-motion" simulators the different segments of the human body are typically represented within the framework of multibody systems by a set of rigid bodies connected by different types of joints and flexible links with a varying degree of complexity [28]. In a roller coaster the posture of the human occupant can be considered as a typical case of passive human motion case, making sense to use a multibody approach with an anthropometric model of the occupant. In order to have more reliable measures of the human exposure to roller coaster induced forces and vibrations, the use of a biomechanical model of the occupant seated in the vehicle seat is required in this work.

4.1 The Anthropometric Model

The anthropometric model is considered to be a representation of the static body geometry, in which relevant dimensions and physical properties are described [41]. These relevant dimensions and physical properties include, among others, the body size, shape and proportion as well as the mass, inertia and centres of mass location of its principal anatomical segments. The anthropometric model used here is based on the one presented in the computer simulation code SOMLA [26], regarding the uniform mass distribution and body size of the 50^{th} percentile dummy. The model considers the human body divided in sixteen anatomical segments, presented in Figure 4.1, being briefly described in Table 4.1.

4.2 Occupant Model

The occupant model is used in the complete roller coaster model as a subsystem. In this section, the relevant anthropometric characteristics, required for the construction of the biomechanical model are presented based on the work by Silva and Ambrósio [28]. The model is described using 16 rigid

bodies, shown in Figure 4.2, which represent independent anatomical segments, interconnected by 15 kinematic joints, which represent anatomical joints.

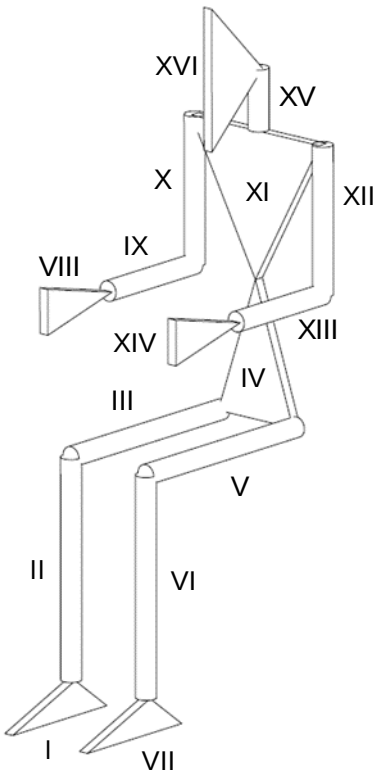

Figure 4.1: Human body divided in sixteen anatomical segments

ID	Name	Description
I	Right Foot	From ankle to toe
II	Right Lower Leg	From knee to ankle
III	Right Upper Leg	From hip to knee
IV	Lower Torso	From the first lumbar vertebrae to the bony pelvis
V	Left Upper Leg	From hip to knee
VI	Left Lower Leg	From knee to ankle
VII	Left Foot	From ankle to toe
VIII	Right Hand	From wrist to finger tips
IX	Right Lower Arm	From elbow to wrist
X	Right Upper Arm	From shoulder to elbow
XI	Upper Torso	From the first thoracic joint to the twelfth
XII	Left Upper Arm	From shoulder to elbow
XIII	Left Lower Arm	From elbow to wrist
XIV	Left Hand	From wrist to finger tips
XV	Neck	From the first cervical vertebrae to the seventh
XVI	Head	Cranium, upper and lower jaws

Table 4.1: Description of the anatomical segments of the anthropometric model [25]

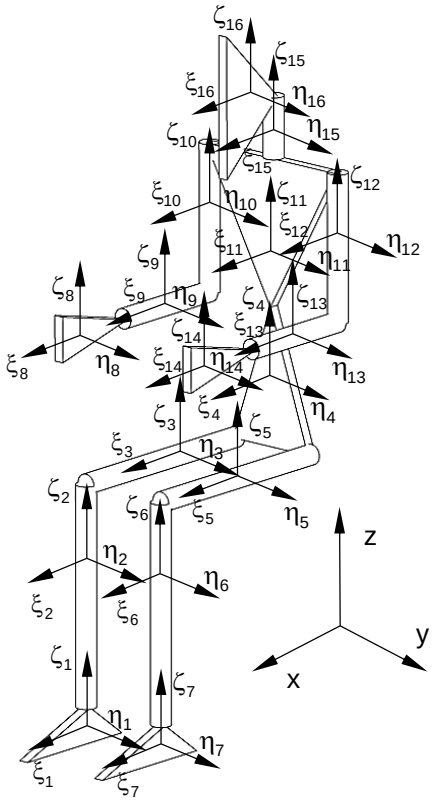

Figure 4.2: Global and local reference frames.

A local reference frame is rigidly attached to the centre of mass of each body, as shown in Figure 4.2. The principal characteristics of the 16 rigid bodies are related to the description of the anatomical segments in Table 4.1. The physical properties of each rigid body are presented in Table 4.2, and indude the masses and the moments of inertia with respect to the three principal axes of each rigid body.

In Table 4.3, the initial positions, orientations and velocities of each body, for a seated occupant, are presented. The initial positions and velocities are consistent with the vehicle and track subsystems, which means that the global reference frame is unique to all subsystems, and the positions, orientations and velocities of the occupant model are compatible with the others subsystems. The spatial orientation of the local reference frames is given in such a way that the moments of inertia required in the definition of each body are all principal moments.

The joints used in the biomechanical model are of three types, revolute, spherical and universal joints, being that the universal joint is only used between the lower and upper torso. Spherical joints, with three degrees of freedom, are used to model the hip or shoulder, and revolute joints, with only one degree of freedom, used to model anatomical segments that only flex and extend, as the knee and the elbow.

ID	Rigid Bodies	Mass (Kg)	Inertia Properties $(10^{-2} Kg.m^2)$		
			$I_{\xi\xi}$	$I_{\eta\eta}$	$I_{\zeta\zeta}$
1	Right Foot	1.182	0.1289	0.128	2.569
2	Right Lower Leg	3.626	1.086	3.83	3.14
3	Right Upper Leg	9.843	1.435	15.94	3.14
4	Lower Torso	14.2	26.22	13.45	26.22
5	Left Upper Leg	9.843	1.435	15.94	3.14
6	Left Lower Leg	3.626	1.086	3.83	3.14
7	Left Foot	1.182	0.1289	0.128	2.569
8	Right Hand	0.489	0.067	0.146	0.148
9	Right Lower Arm	1.402	0.124	0.964	0.298
10	Right Upper Arm	1.991	1.492	1.356	2.487
11	Upper Torso	24.948	8.625	21.198	13.638
12	Left Upper Arm	1.991	1.492	1.356	2.487
13	Left Lower Arm	1.402	0.124	0.964	0.298
14	Left Hand	0.489	0.067	0.146	0.148
15	Neck	1.061	0.268	0.215	0.215
16	Head	4.241	2.453	2.2249	2.034

Table 4.2: Physical properties of each body (from Silva and Ambrósio [28])

ID	Initial Position (m)			Orientation			Velocity (m/s)		
	x_0	y_0	z_0	e_1	e_2	e_3	v_{x_0}	v_{y_0}	v_{z_0}
1	-1.809	-0.306	0.469	0	0	1	-26	0	0
2	-1.809	-0.306	0.792	0	0	1	-26	0	0
3	-1.59	-0.306	0.943	0	0	1	-26	0	0
4	-1.375	-0.4	1.007	0	0	1	-26	0	0
5	-1.59	-0.494	0.943	0	0	1	-26	0	0
6	-1.809	-0.494	0.792	0	0	1	-26	0	0
7	-1.809	-0.494	0.469	0	0	1	-26	0	0
8	-1.7056	-0.3278	1.217	0	0	-0.9914	-26	0	0
9	-1.4931	-0.2708	1.217	0	0	-0.9914	-26	0	0
10	-1.375	-0.239	1.359	0	0	-0.9914	-26	0	0
11	-1.375	-0.4	1.319	0	0	1	-26	0	0
12	-1.375	-0.561	1.359	0	0	0.9914	-26	0	0
13	-1.4931	-0.5291	1.217	0	0	0.9914	-26	0	0
14	-1.7056	-0.4722	1.217	0	0	0.9914	-26	0	0
15	-1.375	-0.4	1.573	0	0	1	-26	0	0
16	-1.426	-0.4	1.654	0	0	1	-26	0	0

Table 4.3: Initial positions, orientations and velocities for the biomechanical model of the seated roller coaster vehicle occupant

ID	Kinematic Constraint	Bodies		Attachment Points Local Coordinates (m)			
		i	*j*	$s_P^{'i}$	$s_Q^{'i}$	$s_P^{'j}$	$s_Q^{'j}$
1	Spherical	1	2	[0;0;0.035]	-	[0;0;-0.288]	-
2	Revolute	2	3	[0;0;0.151]	[0;0,1;0.151]	[0.219;0;0]	[0.219;-0.1;0]
3	Spherical	3	4	[-0.215;0;0]	-	[0;-0.094;-0.064]	-
4	Spherical	4	5	[0;0.094;-0.064]	-	[-0.215;0;0]	-
5	Revolute	5	6	[0.219;0;0]	[0.219;-0.1;0]	[0;0;0.151]	[0;0.1;0.151]
6	Spherical	6	7	[0;0;-0.288]	-	[0;0;0.035]	-
7	Spherical	8	9	[-0.093;0;0]	-	[0.127;0;0]	-
8	Revolute	9	10	[-0.123;0;0]	[0;-0.1;-0.142]	[0;0;-0.142]	[0;-0.1;-0.142]
9	Spherical	10	11	[0;0;0.153]	-	[0;-0.161;0.193]	-
10	Spherical	11	12	[0;0.161;0.193]	-	[0;0;0.153]	-
11	Revolute	12	13	[0;0;-0.142]	[0;-0.1;-0.142]	[-0.123;0;0]	[0;-0.1;-0.142]
12	Spherical	13	14	[0.127;0;0]	-	[-0.093;0;0]	-
13	Universal	4	11	[0;0;0.211]	[0;0.1;0.211]	[0;0;-0.101]	[0.1;0;-0.101]
14	Spherical	11	15	[0;0;0.193]	-	[0;0;-0.061]	-
15	Revolute	15	16	[0;0;0.061]	[0;0.1;0.061]	[-0.051;0;-0.02]	[-0.051;0.1;-0.02]

Table 4.4: Kinematic Joints used in the biomechanical model

In a real roller coaster vehicle the occupant is restrained to the seat by a varied number of safety systems that effectively prevent its gross motions with respect to the seat. Generally the arms and legs are free to move, although through muscle actions such relative motions have resistance.

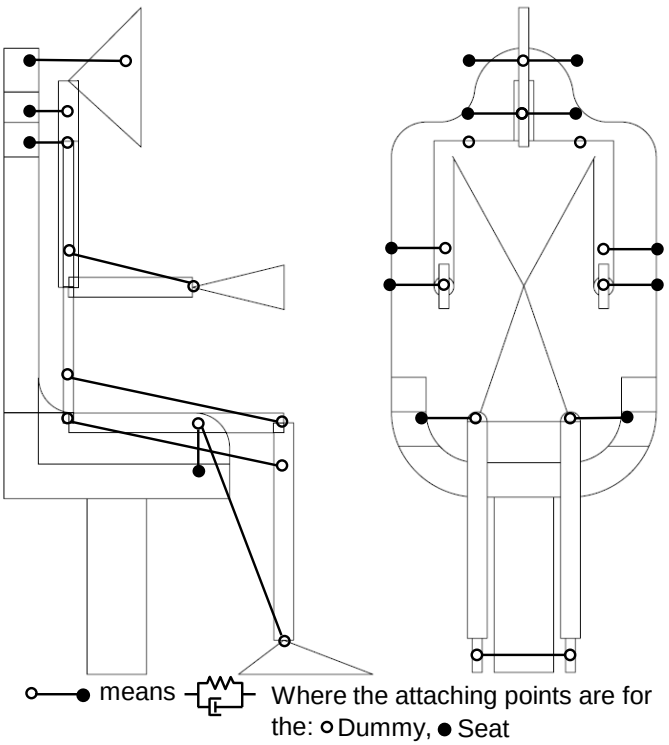

Figure 4.3: Biomechanical model seated

In this work a very sophisticated model of the seat restraints or muscle bracing actions is out of its scope. So, alternative forms of modelling the relative kinematics between seat and occupant, and between its anatomical segments is devised.

The objective here is to maintain the biomechanical model seated and slightly stuck to the seat, only allowing small movements, as for a roller coaster vehicle occupant that is restrained to the seat. The objective is to represent the natural resistance of the relative motion between anatomical segments as an occupant of a roller coaster, by using spring-damper restraints, as shown in Figure 4.3.

ID	$K\ (N/m)$	$c\ (N.s/m)$	l_0 (m)	Bodies		Attachment Points Local Coordinates (m)	
				i	j	$s_P^{'i}$	$s_P^{'j}$
1	1×10^4	5×10^3	0.06	Seat	11	[0.14;0.3195;1.032]	[0;-0.805;0.193]
2	1×10^4	5×10^3	0.06	Seat	11	[0.14;0.4805;1.032]	[0;0.805;0.193]
3	1×10^4	5×10^2	0.0805	Seat	11	[0.275;0.3195;1.032]	[0;0;0]
4	1×10^4	5×10^2	0.0805	Seat	11	[0.275;0.4805;1.032]	[0;0;0]
5	5×10^4	5×10^3	0.083	Seat	3	[0.5;0.306;0.38]	[0.085;0;0]
6	5×10^4	5×10^3	0.103	Seat	3	[0.5;0.203;0.463]	[0.085;0;0]
7	5×10^4	5×10^3	0.083	Seat	5	[0.5;0.494;0.38]	[0.085;0;0]
8	5×10^4	5×10^3	0.103	Seat	5	[0.5;0.597;0.463]	[0.085;0;0]
9	5×10^4	5×10^3	0.103	Seat	2	[0.634;0.203;0.024]	[0;0;-0.288]
10	5×10^4	5×10^3	0.103	Seat	6	[0.634;0.597;0.024]	[0;0;-0.2881]
11	1×10^5	5×10^4	0.106	Seat	10	[0.2;0.133;0.832]	[0;0;-0.047]
12	1×10^5	5×10^3	0.06	Seat	10	[0.14;0.239;0.832]	[0;0;-0.047]
13	1×10^5	5×10^3	0.106	Seat	12	[0.2;0.667;0.832]	[0;0;-0.047]
14	1×10^5	5×10^3	0.06	Seat	12	[0.14;0.561;0.832]	[0;0;-0.047]
15	5×10^4	5×10^3	0.1378	Seat	9	[0323;0.133;0.737]	[0;0;0]
16	5×10^4	5×10^3	0.1378	Seat	13	[0323;0.667;0.737]	[0;0;0]
17	1×10^4	5×10^2	0.459	2	3	[0;0;-0.288]	[0.085;0;0]
18	1×10^4	5×10^2	0.459	6	5	[0;0;-0.288]	[0.085;0;0]
19	7.5×10^3	7.5×10^2	0.0805	15	11	[0;0;0.061]	[-0.0805;0;0.315]
20	7.5×10^3	7.5×10^2	0.0805	15	11	[0;0;0.061]	[0;-0.0805;0.315]
21	7.5×10^3	7.5×10^2	0.0805	15	11	[0;0;0.061]	[0;0.0805;0.315]
22	1×10^4	1×10^3	0.0805	16	11	[0;0;0]	[0.051;-0.0805;0.335]
23	1×10^4	1×10^3	0.0805	16	11	[0;0;0]	[0.051;0.0805;0.335]
24	1×10^4	1×10^3	0.0805	16	11	[0;0;0]	[0.051;0;0.2545]
25	1×10^4	1×10^3	0.075	8	14	[0.092;0;0]	[0.092;0;0]
26	1×10^4	1×10^2	0.2674	9	10	[0.127;0;0]	[0;0;-0.047]
27	1×10^4	1×10^2	0.2674	13	12	[0.127;0;0]	[0;0;-0.047]
28	1×10^4	1×10^3	0.188	2	6	[0;0;-0.288]	[0;0;-0.288]
29	1×10^4	1×10^3	0.188	3	5	[0.085;0;0]	[0.085;0;0]

Table 4.5: Characteristics of the spring-damper systems of the biomechanical model

It is assumed that for the passenger safety system there are shoulder restraints applied. To represent such restrictions, the lower torso is fixed to the seat by a kinematic rigid joint. The other links between the biomechanical model and the seat are all simulated by spring-damper systems. Spring-damper systems also represent the passive resistance of the biomechanical joints due stiffening that results from muscles resistance, because of muscle bracing. The spring-damper systems, their

characteristics, bodies connected and local coordinates of the attachment points are presented in Table 4.5.

4.3 Injury Biomechanics

Injury biomechanics uses the mechanical description of the human body, in particular via its mechanical principles, kinematics and dynamics, to provide relations that can be associated to observed human physical trauma. Injury occurs if the individual loading is so severe that the biological system is loaded beyond a recoverable limit, resulting in damage to anatomical structures and alteration of its the normal function.

Numerical methods and models are important tools since they allow to assess the human biomechanical response in a large range of scenarios. In this work, the 50^{th} anthropomorphic dummy, described in Section 4.2 is used. Note that for a thorough study on the human exposure to injury in roller coasters it is necessary to consider that there are different sizes and gender of human bodies, with different characteristics, that affect the human response and tolerance. The mass, height or even the age are factors to take into account in the human models and numerical methods development for injury assessment. In fact, in the biomechanical response analysis it is not only important to understand and quantify injury mechanisms, but also to define injury thresholds for each type of injury criterion.

Some relevant injury criteria for users of roller coasters are overviewed here. These criteria provide information regarding the severity of the injuries produced in specific anatomical segments of the biomechanical model, as a consequence of the exposure of the body to external actions. This work focus the exposure of the head and other body parts and on their tolerance to g-forces. Common effects on the human body, related with extreme ride, such blackout or loss of consciousness or overload of the blood vessels are associated to g-forces [23].

An injury criterion can be defined as a biomechanical response index of exposure that quantifies the magnitude of a determined injury caused by impact or large accelerations. These qualifications of a criteria can be regarded as a quantification of human response to a given level of injury resulting from an external action. Injury criteria result from the interpretation of data collected by several experiments or numeric simulations done using different kinds human beings, animals or models and then correlation with injuries effectively observed by medical doctors. They are, in fact, the engineering measures of injury that can be used a roller coaster track design or vehicle improvement, among many other fields of application.

The understanding of the injury mechanisms is of great importance for passive safety improvement. The existence of some injury scales such as AIS (Abbreviated Injury Scale) [42], Table 4.6, together with loading conditions during this external actions are important qualification that the result from medical observation of real life injuries that complement the injury criteria classification and

fill the information bridge between engineers and medical doctors. The injury criteria implemented in this work are:

- Head Injury Criterion (HIC);
- Result Head Acceleration (3ms);
- G-force induced loss of consciousness (GLOC).

Although initially applied to aerospace and automotive crashworthiness cases, these indicators can also be applied in other areas of activity, such as the one presented in the current work as a roller coaster analysis. Notice that other injury measures may be considered, but the literature is inexistent for this type of application to roller coaster rides.

AIS	Injury Category
1	Minor
2	Moderate
3	Serious
4	Severe
5	Critical
6	Survival not sure

Table 4.6: Abbreviated Injury Scale [29]

4.3.1 Head Injury Criterion (HIC)

The Head Injury Criterion (HIC) is based on the Wayne State Tolerance Curve (WSTC), and establishes a relationship between the average acceleration and the time duration in which this average acceleration occurs. The resulting tolerance curve, illustrated in Figure 4.4, indicates the potential for a given acceleration to cause severe head injuries, when above the tolerance curve, or to be within the human tolerance levels, if below the tolerance curve.

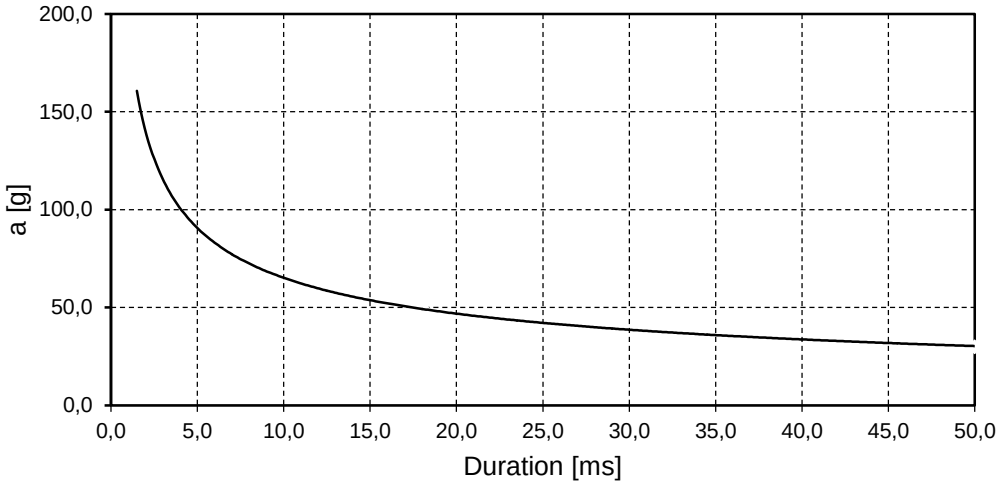

Figure 4.4: The Wayne State Tolerance Curve (Adapted from Walz [7])

The Head Injury Criteria (HIC) is the most frequently used criterion to quantify head injury potential in all commonly application areas. The HIC is computed as [7]:

$$HIC = \max\left\{\left[\frac{1}{t_2 - t_1}\int_{t_1}^{t_2} a(t)\,dt\right]^{2.5}(t_2 - t_1)\right\} \tag{4.1}$$

where t_1 and t_2 are the time limits of the acceleration pulse, measured in $[\text{sec}]$, and $a(t)$ is the resultant head acceleration, measured in the center of mass of the head in multiples of the gravity acceleration $[g]$. It is considered that the maximum allowable time interval that produces suitable HIC values is 36 ms for accelerations pulses not involving direct head impact, although the interval of 15 ms is also used in some fields. A tolerance level of 1000 is used in this criterion as the threshold for permanent head injuries for the 50th percentile male. In Figure 4.5, it can be seen the relation between the HIC and the AIS.

Although, there are some limitations in this criterion, since that only considers linear acceleration which is not a limited representation of reality as angular motion may play a role on head injuries. Despite this, HIC is the most used criterion in crashworthiness research and considered to be an appropriate discriminator between contact and non-contact impact responses. Because many of current developments of passive safety are based on this criteria, industry and regulations are not inclined to change it.

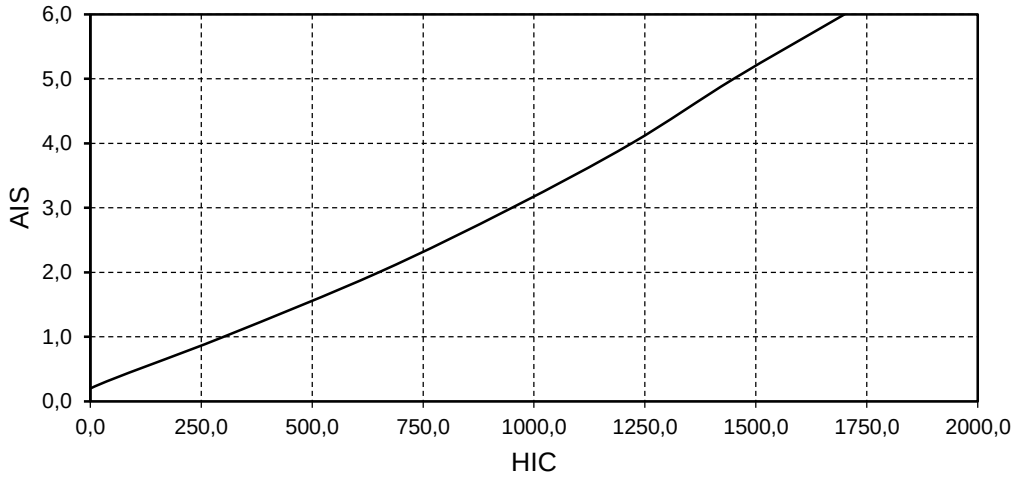

Figure 4.5: Relation between HIC and AIS(Adapted from Shojaati [29])

4.3.2 Result Head Acceleration (3ms)

The 3ms criterion is also based on the WSTC [7]. It is defined as the acceleration level exceeded for a duration of 3 ms and should not exceed 80g. Generally, large accelerations acting more than 60 ms are called sustained accelerations, while those below 60 ms are called transitory accelerations, or impact [43]. This criterion is an essential element to assess non-contact injuries of the head.

4.3.3 Human Tolerance to G-Force

The human body is considered to be a fluid-filled, hydraulic system responding to changes in acceleration fields, and limiting human tolerance. Acceleration takes place when the velocity of a body changes either in magnitude or direction. The human body has different tolerances and reactions to different directions. The acceleration applied to the human body should be considered with respect with its direction and magnitude. In Figure 4.6, the common nomenclature for directional accelerations is shown.

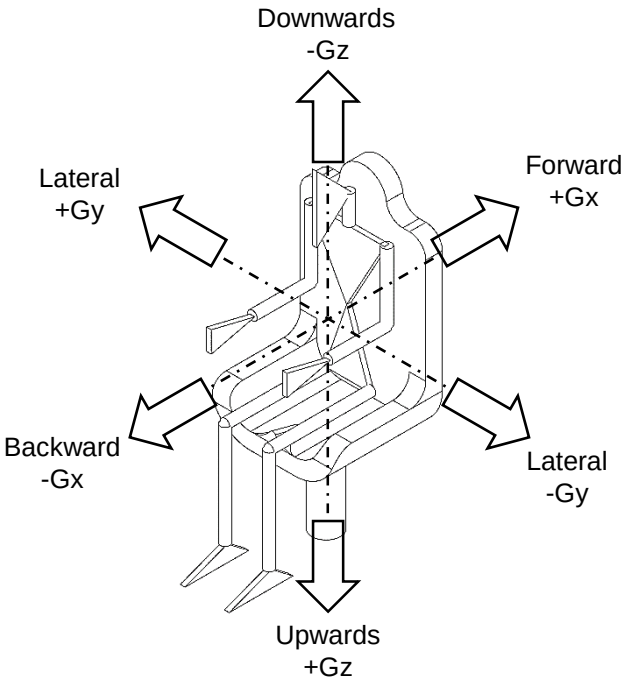

Figure 4.6: Nomenclature for acceleration components

4.3.3.1 Upwards +Gz

The effects of upward acceleration are primarily due to hydrostatic pressure changes in the cardiovascular system. The effects of +Gz are limited by visual symptoms and loss of consciousness, it drives blood downward to the feet of a seated or standing person. When an occupant of a vehicle is exposed to an increase in +Gz, the pressure required to perfuse the eyes and the brain increases and blood begins to pool in the capacity blood vessels of the lower limbs. With increased acceleration levels, the perfusion pressure requirements increase and the volume of blood returning to the heart decreases further. The eyes and the brain receive an ever-decreasing amount of oxygenated blood, eventually leading to a G-force induced loss of conscience (GLOC) The common symptoms due to +Gz are listed below , in Table 4.7 [43]:

+1 Gz	Erect/seated terrestrial posture;
+2 Gz	Increase in weight; Movement against acceleration is difficult;
+3 to 4 Gz	Difficult to raise arms and legs; Dimming of vision after 3-4s; progressive tunnelling of vision; arterial oxygen saturation falls to 93%;
+4.5 to 6 Gz	Progressive blackout after 5s; hearing and then G-induced loss of consciousness (GLOC) if continued;

Table 4.7: Upwards +Gz [43]

The loss of consciousness has different effects depending on the aggression to the central nervous system. These effects depend mainly on the time duration and magnitude of +Gz, its repetition and on the individual tolerance to +Gz. If the exposure to +Gz is high and/or repeated enough, it can cause other injuries such as hernias or cardiac dysrhythmias. To long durations of exposure to +Gz, symptoms will manifest by loss of peripheral vision, proceed to total loss of vision, if the acceleration is high and long enough. With the increase of acceleration, the passenger will lose consciousness, and so, loss of postural control. The passenger would regain consciousness once the acceleration level is below the human threshold tolerance to +Gz, which will higher than normal due to activation of cardiac compensation mechanisms. One of the concerns of the GLOC with respect to a roller coaster is the lack of postural control due to loss of consciousness, which might result in an injury.

4.3.3.2 Downwards –Gz

Tolerance to downwards –Gz, which drives blood to the head is lower when compared to +Gz. Initially during –Gz acceleration, the arterio-venous oxygen difference is maintained, but increasing loads, increased carotid sinus pressure causes bradycardia and fall in arterial pressure, while venous pressure is still maintained. This results in fall of arterio-venous oxygen difference, leading to the tolerance limiting symptoms such as confusion and unconsciousness.

-1 Gz	Sense of pressure and fullness in the head
-2 to -3 Gz	Throbbing headache; Red out, blood laden lower eyelid being pulled into the field of vision;
-4 to -6 Gz	Seldom tolerated beyond 6 seconds; causes mental confusion and unconsciousness;

Table 4.8: Downwards –Gz [43]

4.3.3.3 Forward +Gx

Forward acceleration +Gx is primarily limited by respiratory problems, although minimal hydrostatic effects persist. In general, human tolerance to g-forces in this direction are much higher than other axes. The human body is better to tolerate g-forces perpendicular to the spine.

+1 Gx	Slight increase in abdominal pressure; respiratory rate increases;
+2 to 3 Gx	Difficulty in spatial orientation; +2 Gx tolerable up to 24 hours
+3 to 6 Gx	Progressive tightness of chest; Difficulty in breathing; Blurring of vision; Cardiac rhythm disturbances;
+6 to 9 Gx	Head cannot move at +9 Gx; Blurring and tunnelling of vision; Arterial oxygen saturation falls below 85%;
+9 to 12 Gx	Reduced peripheral vision and dimness of central vision; Ventilation-perfusion inequalities in the lungs increase further;
> +12 Gx	Breathing extremely difficult, Pain in the chest; Loss of vision;

Table 4.9: Forward +Gx [43]

4.3.3.4 Backward –Gx

The response to backward acceleration are similar to +Gx, but the respiratory problems are less severe. The hydrostatic effects that occur in +Gx are reversed. Although, the human body has higher tolerance to forward +Gx than to backward –Gx, since blood vessels in the retina appear more sensitive in the latter direction.

-6 Gx	No deterioration of lung vital capacity; blurring of vision, probably due to mechanical effects;
-8 Gx	Cardiac arrhythmias; abundant lacrimation; restraint of human body difficult;

Table 4.10: Backward –Gx [43]

4.3.3.5 Lateral –Gy and +Gy

The information on the human tolerance to lateral +/-Gy is limited. It is known that haemorrhages in the dependent limbs can occur around +/-5 Gy. These lateral accelerations can cause an uncomfortable sensation or even motion sickness in the roller coaster passenger. The measure of this level of discomfort is the non-compensated lateral acceleration, NCA , described in Section 3.2.2.

4.3.3.6 General Thresholds for Tolerance to G-forces

The simple observation of the graphs acceleration vs time does not allow a clear understanding of the thresholds of the human tolerance to g-forces. As the human body tolerance to g-forces varies with direction, magnitude and time durations, a post-processor in MATLAB [44] is developed. The input is the acceleration of the whole body center of mass. The output consists in the g-forces, for the different directions shown in Figure 4.6, and their durations. The objective is to obtain graphs of g-forces vs time duration, in order to compare the g-forces measured in the simulation with the human

tolerances to g-forces, depicted in Figure 4.7, reproduced from Brulle [4] and commonly used in aerospace engineering.

All these different tolerances and reactions to g-forces in different directions vary with the axis of acceleration, magnitude of accelerations and time duration. Figure 4.7 depicts the limits of human tolerance for almost every directions for different time intervals and durations. For each time interval, there is a magnitude of g-force threshold that is tolerable for the average human being. In Figure 4.7, it can be understood the nomenclature used in the accelerations components, already depicted in Figure 4.6. It is a semilog graph, because only the time durations are in log scale.

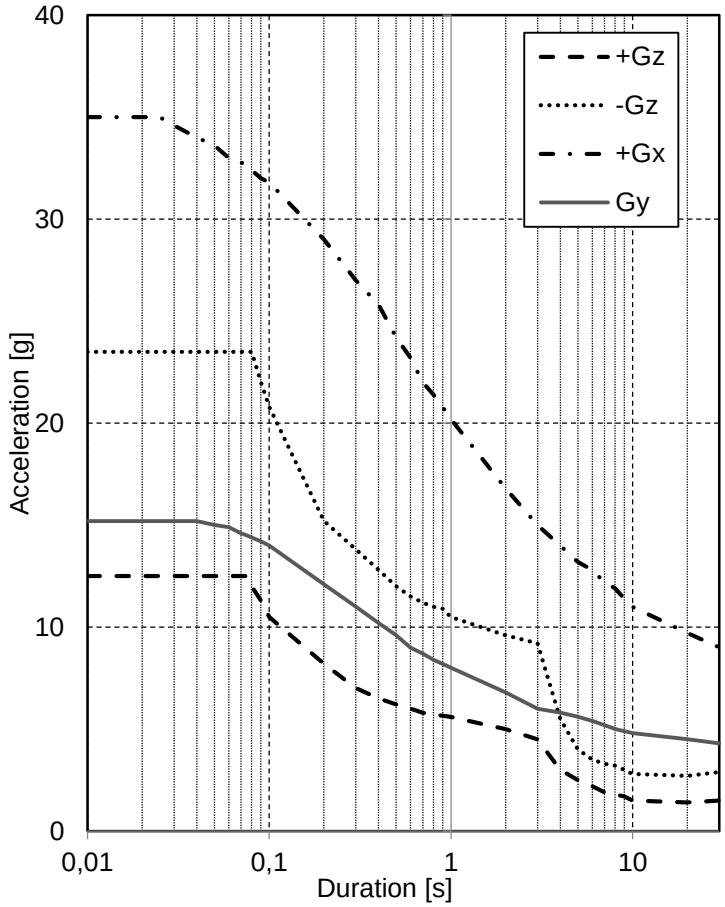

Figure 4.7: Thresholds of human tolerance for sustained g-forces, with respect to duration. (Adapted from Brulle [4])

Besides the thresholds shown in Figure 4.7, developed for fighter jet pilots [4], there are equivalent thresholds for human injury resulting from studies by Eiband [5]. Figure 4.8 and Figure 4.9

depict the Eiband thresholds for traumatic injury that result from experiments with human volunteers and animals.

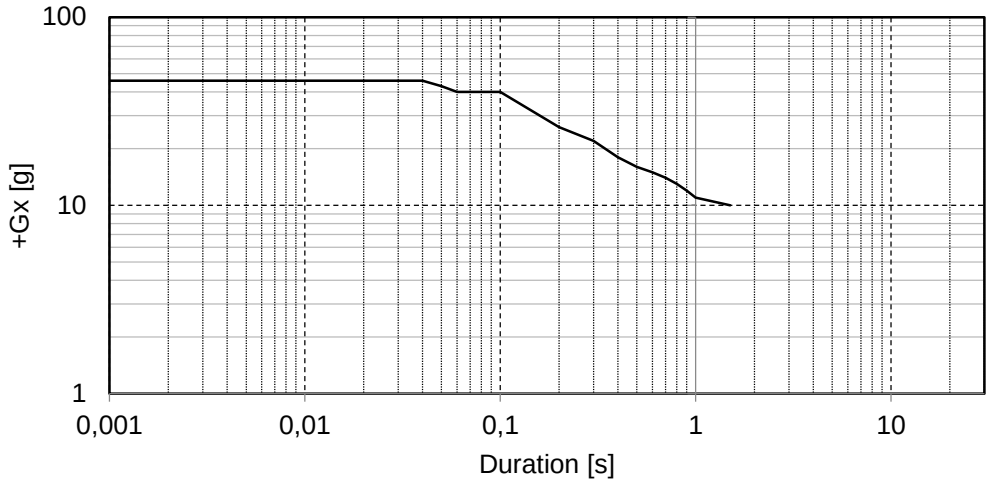

Figure 4.8: Eiband Curve for +Gx (Adapted from Shanahan [5])

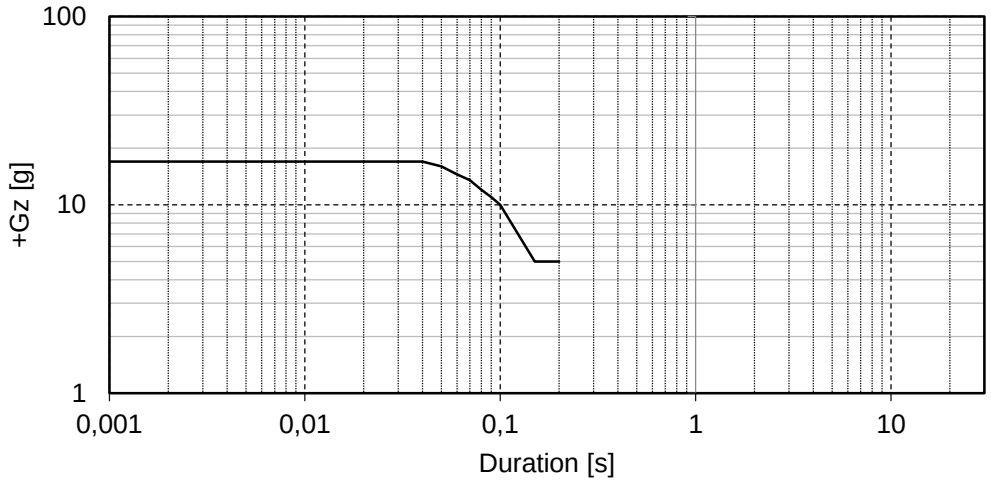

Figure 4.9: Eiband Curve for +Gz (Adapted from Shanahan [5])

Due to the fact that roller coaster human exposure has more similarity to fighter pilots exposure, the thresholds of Figure 4.7 are used. However, the flattens in Figure 4.7, for short duration g-forces are used in the definition of the thresholds to mimic the observations by Eiband [5]. Certainly in further studies a more detailed look at these injury thresholds is required as no further information was possible to be obtained at this stage.

5 Application to the Analysis of Roller Coaster Rides

In this chapter, two case studies involving two different roller coaster tracks are presented. The first is a conceptual design, while the second is based on an existing roller coaster in operation. The tracks geometry are obtain in the site https://nolimits-exchange.com/, which is a forum to exchange roller coaster tracks with the purpose to be used in the roller coaster game simulator *No Limits 2 – Roller Coaster Simulation.*

5.1 Roller Coaster Tracks

The first roller coaster track, designated by Looping Star, has its geometry depicted in Figure 5.1. In Figure 5.1, it can be seen the global reference frame of the simulation, i.e, all subsystems of the simulation, track, vehicle and biomechanical model, have a unique global reference frame, which is the one depicted in Figure 5.1. The simulation begins in the negative direction x , and it is given an initial velocity to the roller coaster vehicle only enough to reach the highest point of the roller coaster track. Thereafter, it is only the conservation of energy that makes the vehicle move, i.e, the potential energy is transformed in kinetic energy and vice-versa, maintaining its sum basically constant. So, from the highest point of the track, the roller coaster vehicle travels without using any additional power source or force, other than the gravitational force. The Looping Star has a maximum height of 32 m and a total length of, approximately, 765 m, having a single loop and seven curves.

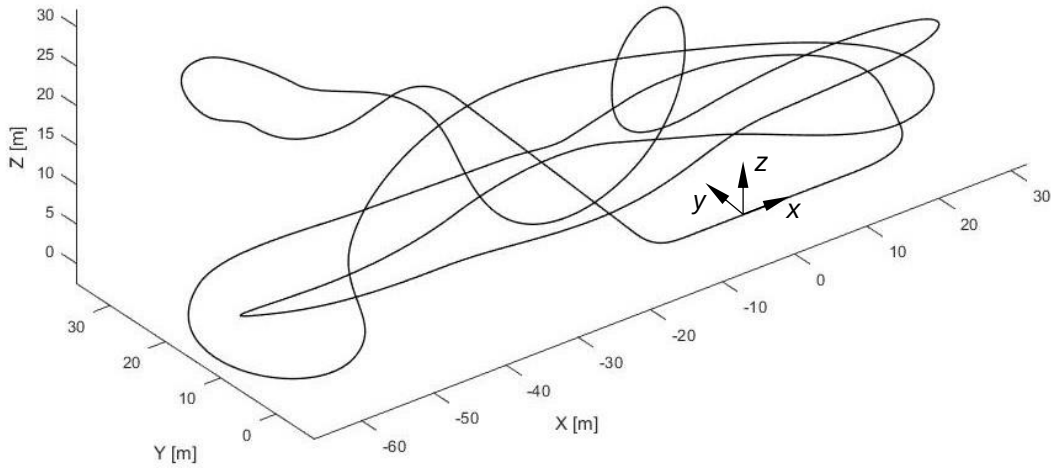

Figure 5.1: Looping Star roller coaster geometry

The second roller coaster is the Gate Keeper shown in Figure 5.2 and in Figure 5.3 as a screenshot of the computer model implemented in this work. This is an existing roller coaster in operation in the Cedar Point Amusement Park, in the USA. Although, this is based on a real roller coaster, its geometry

is also obtained in the internet forum https://nolimits-exchange.com/, to support the game simulator *No Limits 2 – Roller Coaster Simulation*. Although the source for the geometry is not necessarily reliable, it is assumed in this work its realism.

Figure 5.2: Gate Keeper Conceptual design by Jeremy Thompson/WikiCommons

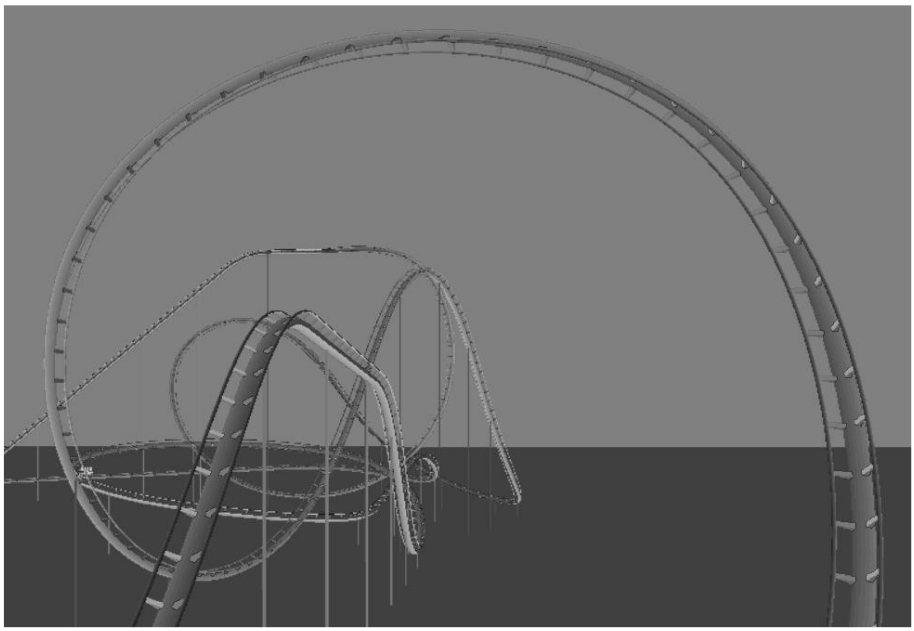

Figure 5.3: Gate Keeper roller coaster computational implementation

The roller coaster track geometry is depicted in Figure 5.4, where it can be seen its global reference frame, which is unique for all subsystems of the simulation. The simulation of the roller coaster

vehicle also begins in the negative direction x. An initial velocity to the roller coaster vehicle is set to be only enough to reach the highest point of the track, which is in the top of the first ramp. The dynamic response measured until the vehicle reaches the highest point are ignored, because the first curve and hill were designed so the vehicle manoeuvres them at a much slower speed than on the simulation. The Gate Keeper has a maximum height of 45 m and a total length of, approximately, 1315 m, accounting for various corkscrews, better seen in Figure 3.3, and a loop.

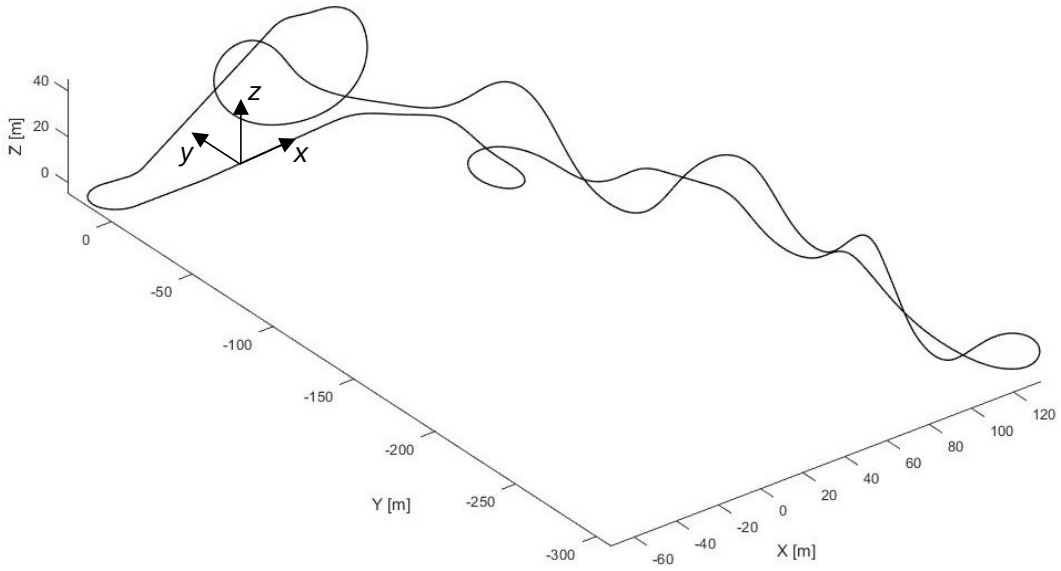

Figure 5.4: Gate Keeper track geometry

5.2 Analysis of Scenario 1: Looping Star

The motion resulting from the simulation of the roller coaster Looping Star, observed from a frontal point of view, is depicted by several screenshots and can be seen in Figure 5.5. The figure is supposed to be visualized top to bottom, first by the left column and then by the right column of images.

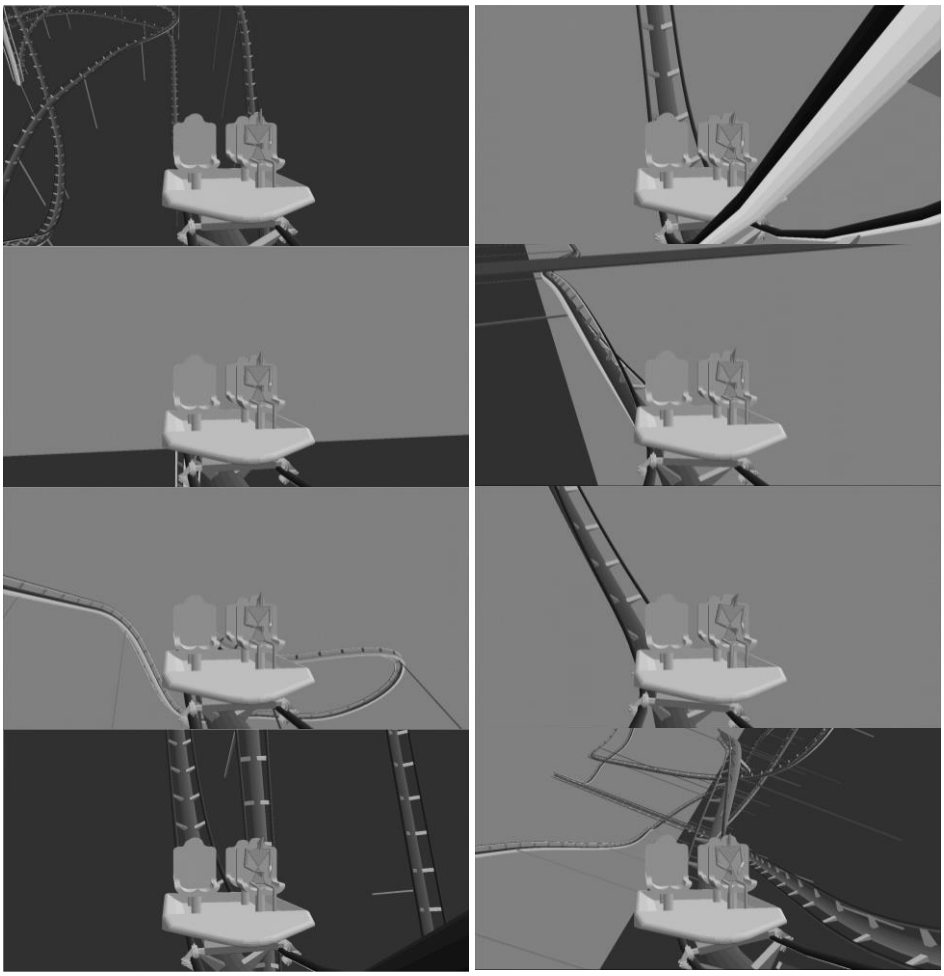

Figure 5.5: Screenshot of roller coaster motion resulting from the simulation of the Looping star roller coaster (sequence is top to bottom in the left followed by top to bottom on right column).

In some of the images, and in the animations of the system, it is possible to see the actions of the passive tilting mechanism, i.e, the secondary suspension system, by observing that the passenger compartment has a different inclination from the rest of the vehicle and track. This system is better understood by looking at the Figure 5.6, where is displayed the difference between the roll angle of the passenger compartment and the torsion angle, of the roller coaster track. It is perceivable that the passive tilting mechanism works better in longer curves, where the torsion angle of the track does not change suddenly. In the final part of the simulation, it can be seen that torsion angle of the track is zero, despite that there are still two curves before the arrival gate. This final part of the track is to be traveled at a much lower speed than that in current analysis, by acting brakes that slow down the vehicle. So the vehicle should reach the final part of the track progressively reducing its velocity until it stops at the departure station. In the current analysis this braking is not applied and, consequently, the dynamic response of the roller coaster, for the final two curves of the track must be disregarded.

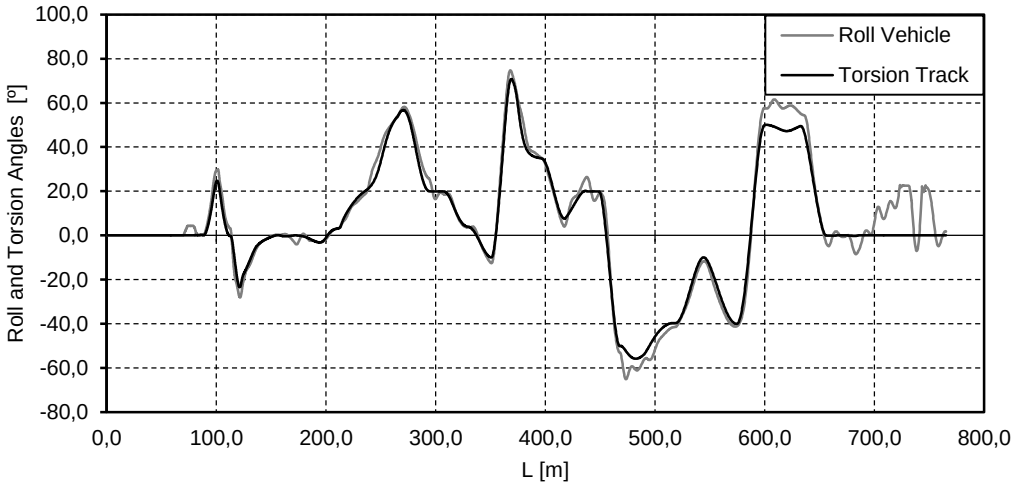

Figure 5.6: Difference between roll angle of passenger compartment and torsion angle of the roller coaster track

Figure 5.7 shows the resultant velocity along the roller coaster track length. This graph clearly shows the conservation of energy in the roller coaster system. The simulation finishes, approximately, with the same velocity that it begins, because the model only dissipates energy in the suspension systems. It can be seen that this dissipation is minimal, since there is only a reduction of 4% of the final velocity of the vehicle relative to the starting velocity. The minimum velocity of the vehicle happens in the top of the highest hill, where it is 6.6 m/s. For a more realistic simulation of the roller coaster, this velocity should be minimized to be almost null as it reaches the highest point on the track. Also, the final part of the track should be traveled at a much lower velocity so that the vehicle gradually slows down until it stops ate the arrival/departure station.

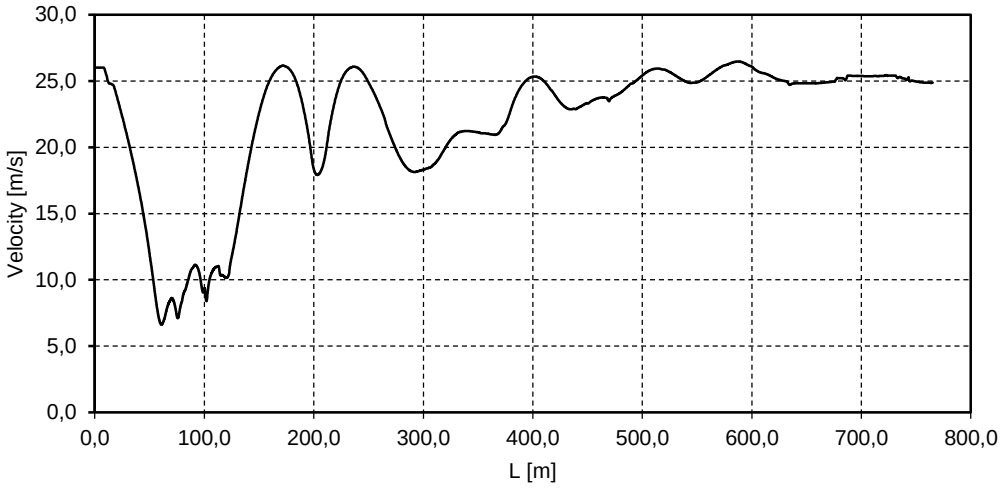

Figure 5.7: Resultant Velocity of the roller coaster vehicle

For the Looping Star roller coaster track, the longitudinal acceleration, i.e, local ξ direction, is presented in Figure 5.8. In Figure 5.9 and Figure 5.10 the lateral and vertical accelerations, η and ζ directions, are also presented. These accelerations are taken in the center of mass of the upper torso of the biomechanical model on its local reference frame.

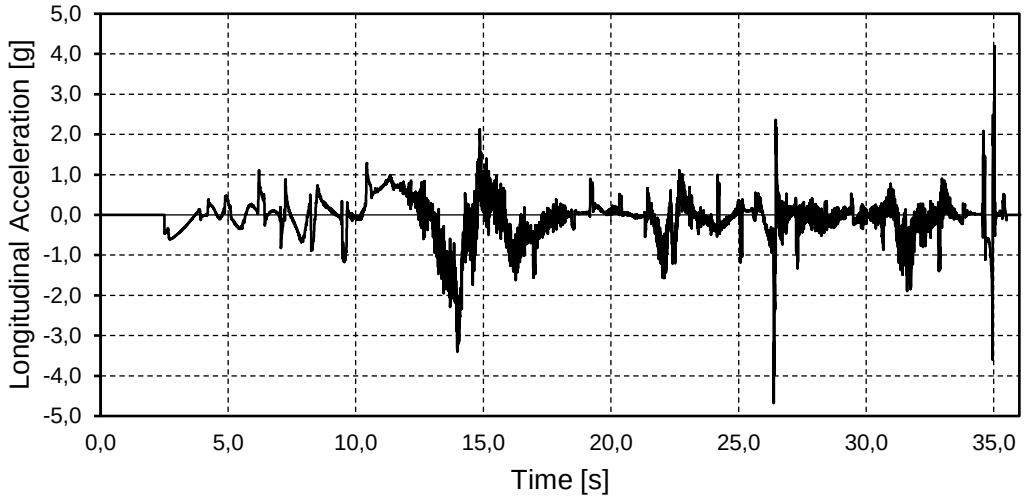

Figure 5.8: Longitudinal Acceleration measured in the center of mass of the occupant upper torso

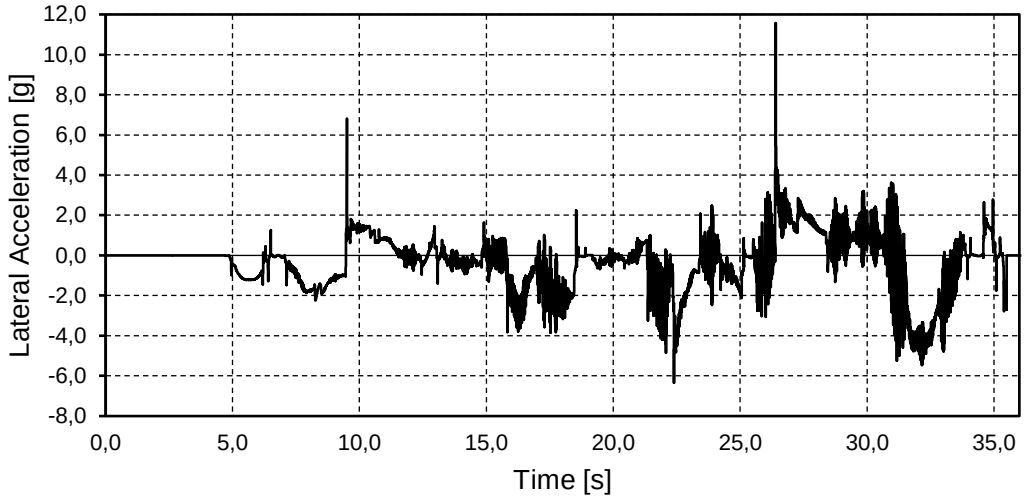

Figure 5.9: Lateral Acceleration measured in the center of mass of the occupant upper torso

The simulation results of the final curve of the roller coaster are not here presented, because in the current simulation, the roller coaster vehicle arrives to this curve in a much higher velocity than would arrive in reality. Therefore, in that section of the track the results of the analysis lack realism.

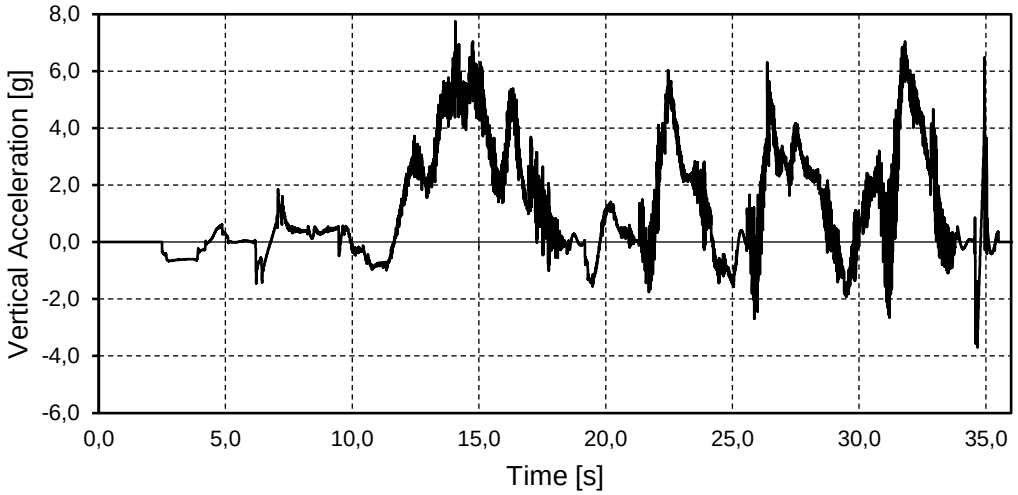

Figure 5.10: Vertical Acceleration measured in the center of mass of the occupant upper torso

The comparison between the human tolerance to g-forces in forward +Gx direction and the magnitudes of g-forces measured for several time durations on the roller coaster passenger can be seen in Figure 5.11. It can be seen that the g-forces acting on the passenger in the forward +Gx direction are far below the tolerance to this direction, thus suggesting a safe ride.

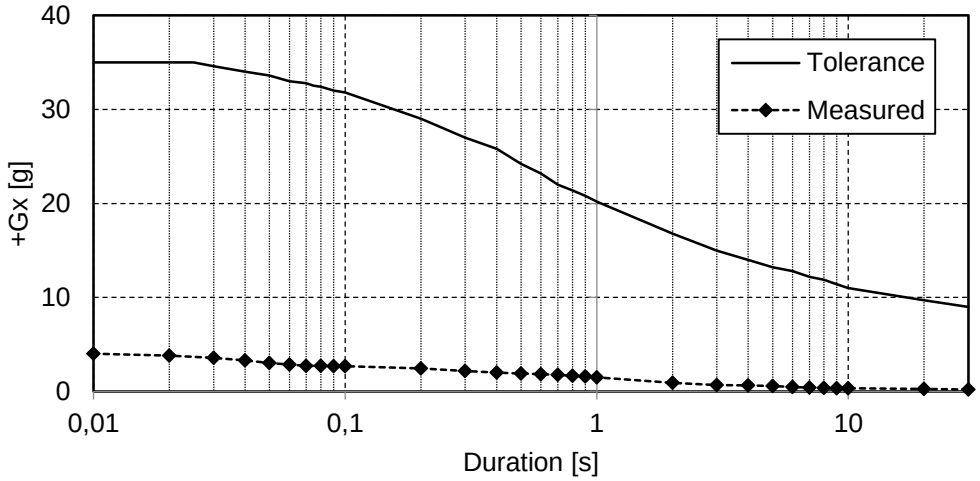

Figure 5.11: Forward G-force +Gx acting on passenger

In the lateral Gy g-force graph, presented in Figure 5.12, it can be seen that for the time duration $\Delta t = 0.01s$, the g-force acting on the roller coaster passenger is the highest. This probably happens due the peak of accelerations that can be seen in Figure 5.9, around the 26 s, which has a value of acceleration way above the rest. For the complete time durations, the g-forces measured present healthy values, below

the human tolerance. These results suggest that the geometry of the track about the point at which the response is closer to the threshold can be revised for a safer ride.

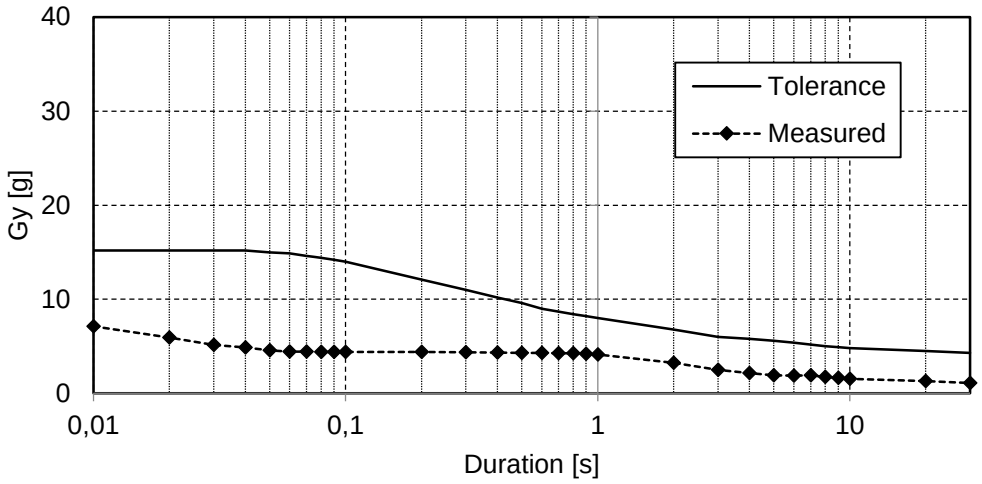

Figure 5.12: Lateral G-force Gy acting on passenger

In the upwards and downwards g-force directions, Figure 5.13 and Figure 5.14, there are no values above the human tolerance. In the upwards +Gz direction there two values of g-force that approach more the limit, in the first two time intervals measured. The downwards –Gz direction the tolerance, the time intervals presents a good response, with results below the human tolerance.

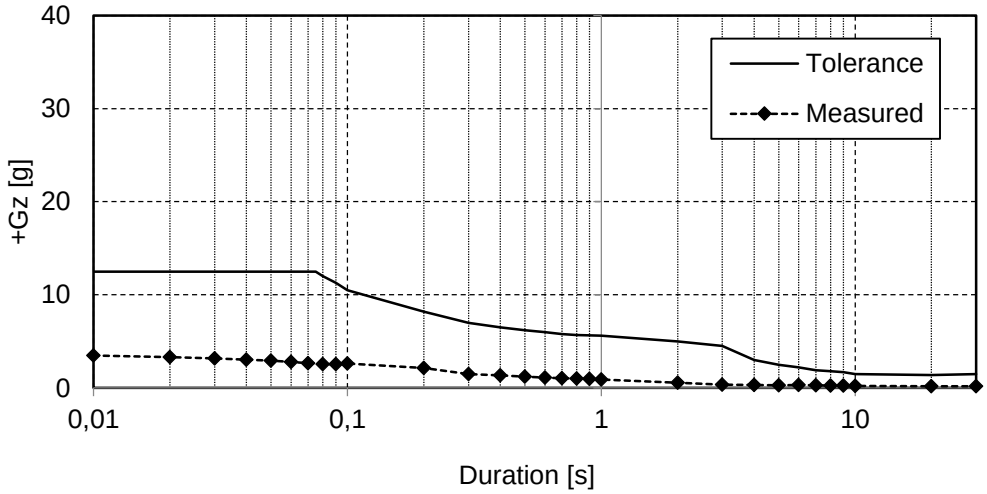

Figure 5.13: Upwards G-force +Gz acting on passenger

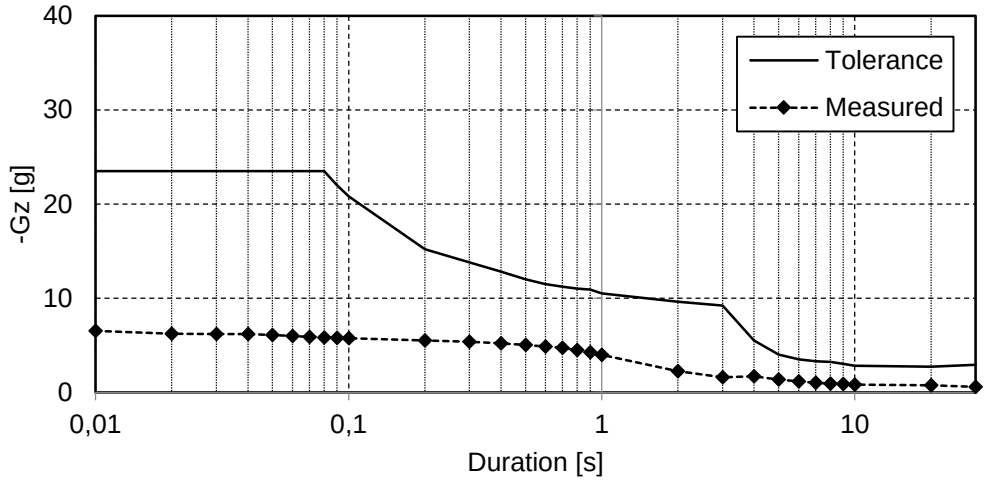

Figure 5.14: Downwards G-force -Gz acting on passenger

In the graphs in Figure 5.11 through Figure 5.14, the values of g-forces never exceed the human tolerance. Furthermore, the characteristics of the suspension of the vehicle can be tuned for improved performance and the model of contact between the biomechanical model and seat restraints can be revised for improved analysis.

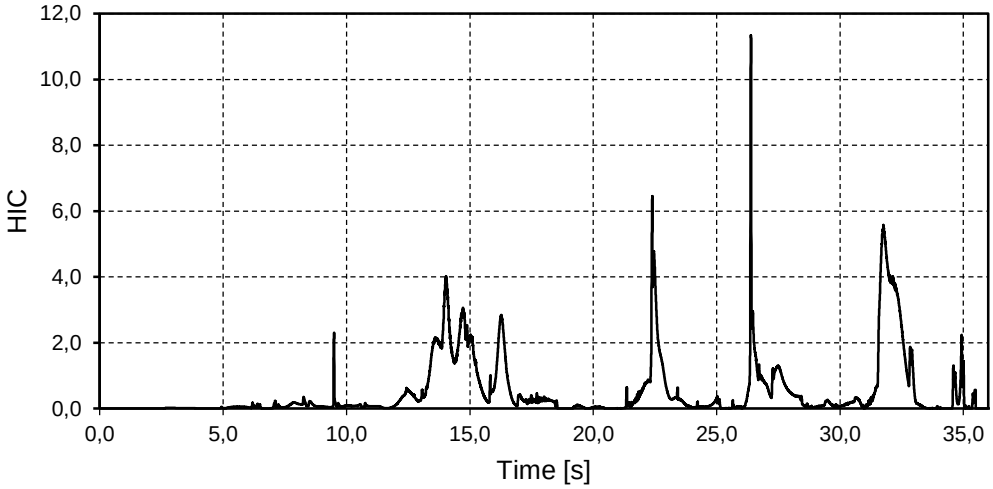

Figure 5.15: HIC for the Looping Star

The human response to accelerations is also evaluated using the Head Injury Criteria (HIC) and the Result Head Acceleration (3ms). In Figure 5.15, it can be seen the evolution of the HIC over time, during the roller coaster simulation, which produces a maximum value of 11.34. The maximum value appears around the 26 s, and it is far from being a concern, according to the Figure 4.5 and to the AIS code.

For the Head Acceleration, shown in Figure 5.16, the same behavior is observed as the maximum value is clearly below the 80g threshold. The maximum acceleration measured in a time interval of 3 ms is 21.27g, also around the 26s. In any case, the peaks observed for the head acceleration criteria provide indications on which region of the roller coaster track can be improved for human protection against its exposure to harmful accelerations.

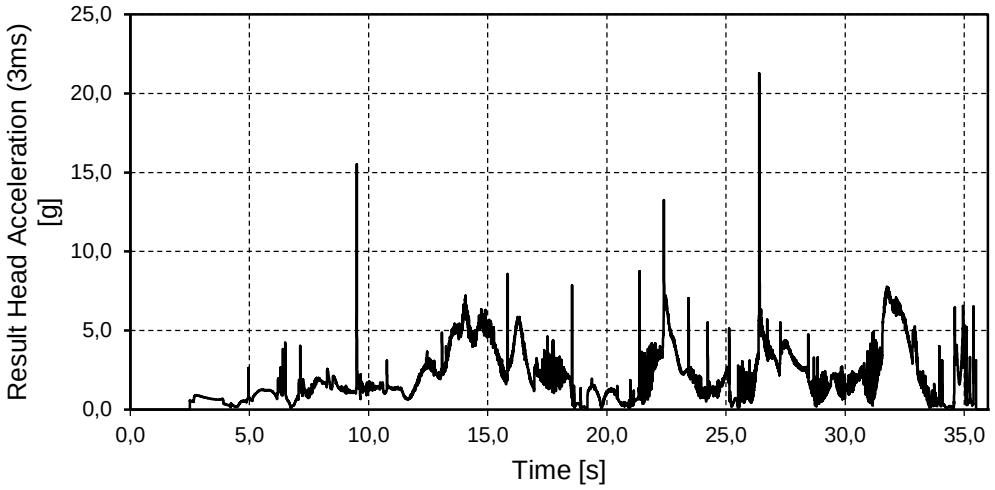

Figure 5.16: Resultant Head Acceleration (3ms) for the Looping Star

The graph of the Non-Compensated Acceleration (NCA) for the Looping Star roller coaster track is showed and discussed, in Figure 3.11, of the Chapter 3, to demonstrate the utility of the passive tilting mechanism, or secondary suspension system. The conclusions expressed at that point are still valid in this discussion.

5.3 Analysis of Scenario 2: Gate Keeper

In roller coaster Gate Keeper, the difference between the roll angle of the passenger compartment and the torsion angle of the track is less evident because there are no curves where its torsion angle remains constant for a long period, as it is always changing as shown in Figure 5.17. Even so, and with the help of the Figure 5.18, where the non-compensated acceleration (NCA) is displayed along the track length, just before reaching 1200 m of track length, a reduction of the NCA is felt by the passenger. This is caused by the passive tilting mechanism. When looking back to Figure 5.17, it is confirmed that the secondary suspension mechanism helps to minimize the lateral accelerations felt by the roller coaster passenger, by passively tilting the passenger compartment.

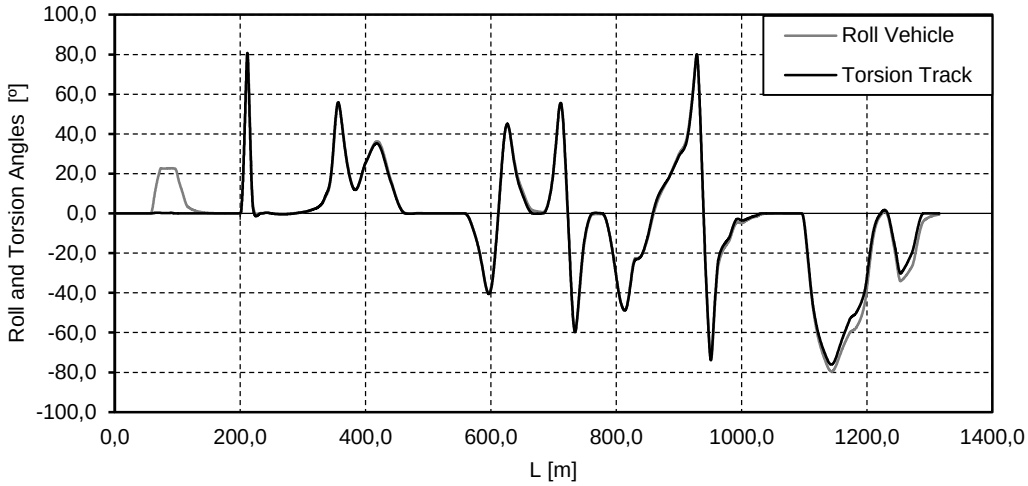

Figure 5.17: Difference between the roll angle of the passenger compartment and the torsion angle of the track

The information shown in Figure 5.17 , Figure 5.18 and depicted in Figure 5.19 reveal that the torsion angle for the roller coaster curves of the Gate Keeper is well adjusted to the velocity of the vehicle, hardly needing the compensation provided by the passive tilting mechanism.

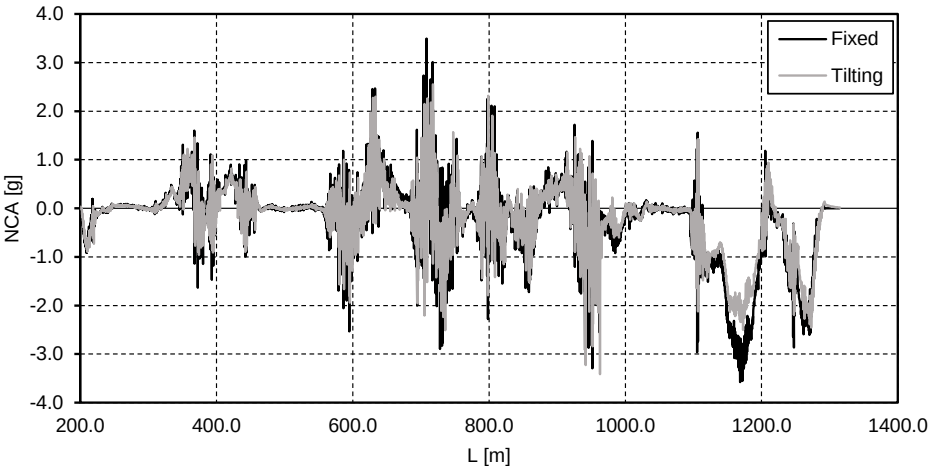

Figure 5.18: Non-Compensated Acceleration (NCA)

The resultant velocity along the roller coaster track graph, in Figure 5.20, shows that there is a conservation of energy, only with a small dissipation due to the suspension of the vehicle systems.

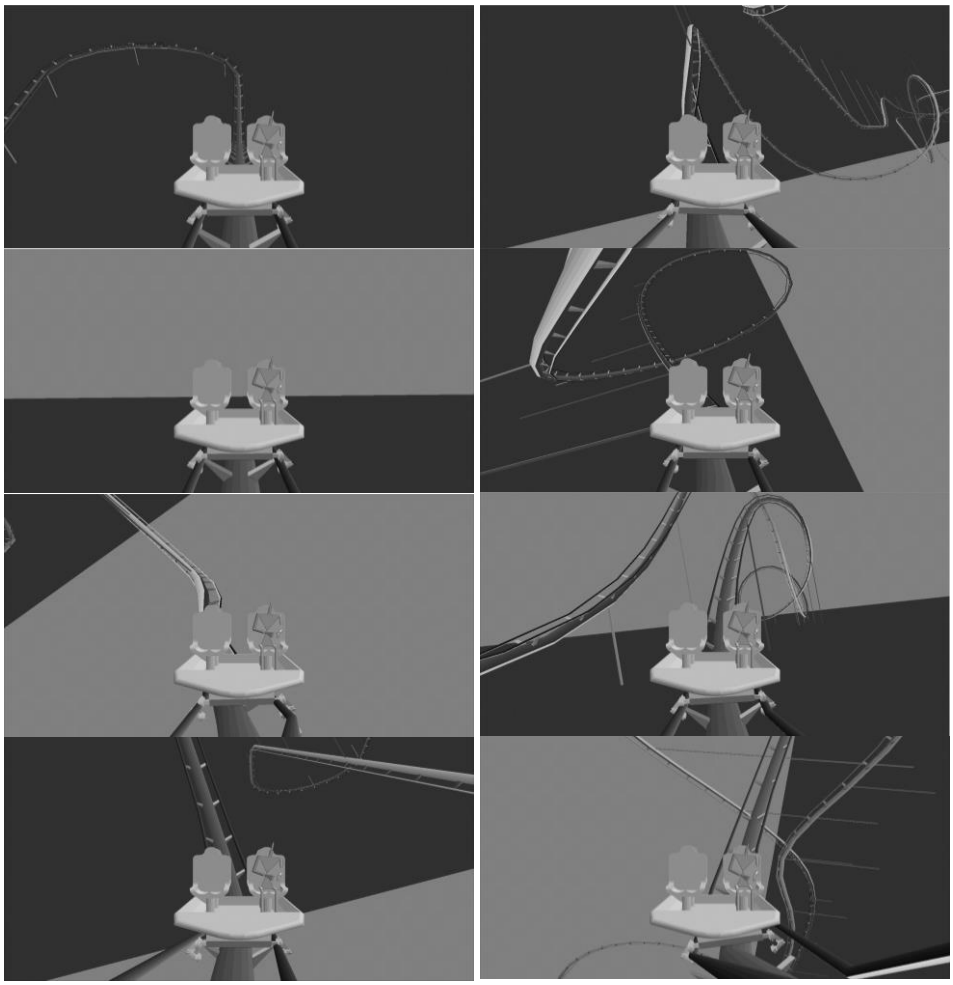

Figure 5.19: Screenshot of roller coaster motion resulting from the simulation of the Looping star roller coaster (sequence is top to bottom in the left followed by top to bottom on right column).

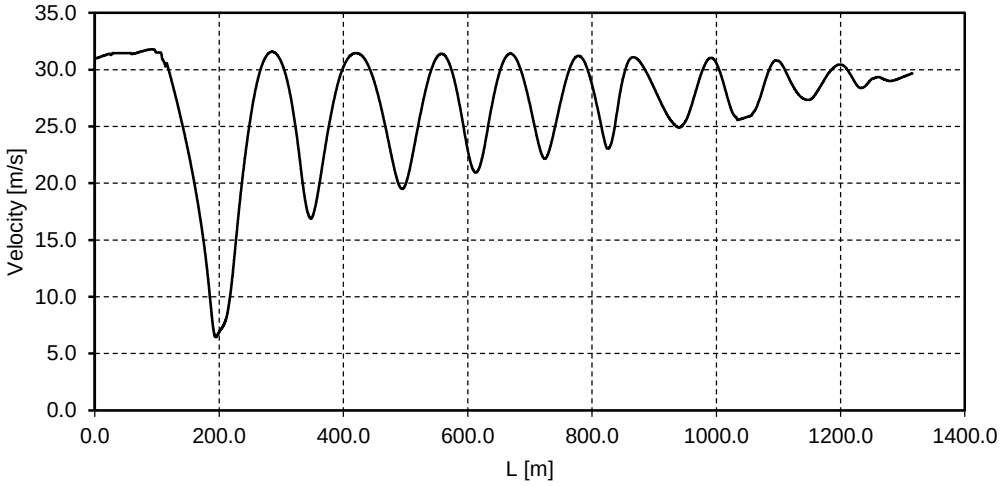

Figure 5.20: Resultant Velocity of the Roller Coaster Vehicle

The acceleration components of the upper torso of the occupant biomechanical model are depicted in Figure 5.21, Figure 5.22 and Figure 5.23, along the longitudinal direction ξ, the lateral direction η, in y direction, and the vertical direction ζ, being all depicted in the occupant body fixed frame.

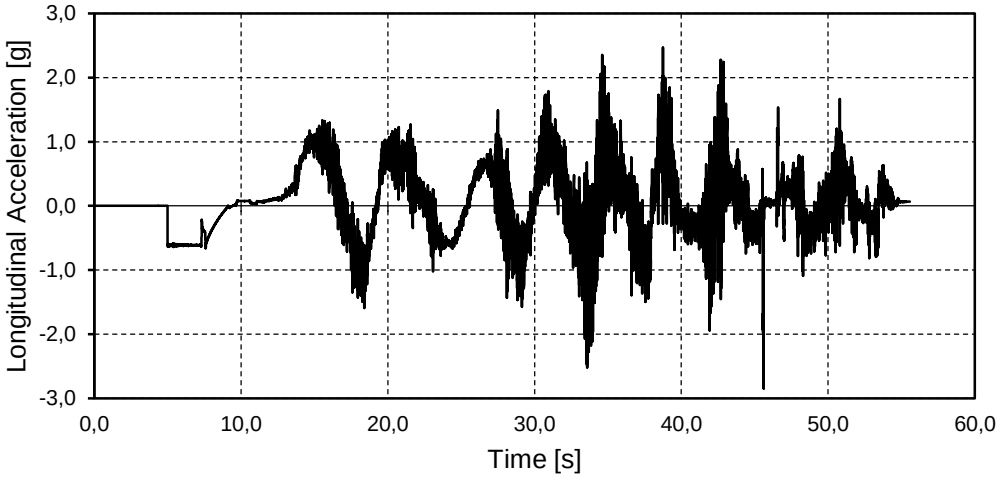

Figure 5.21: Longitudinal Acceleration on the center of mass of the upper torso of the occupant, in the local coordinate system

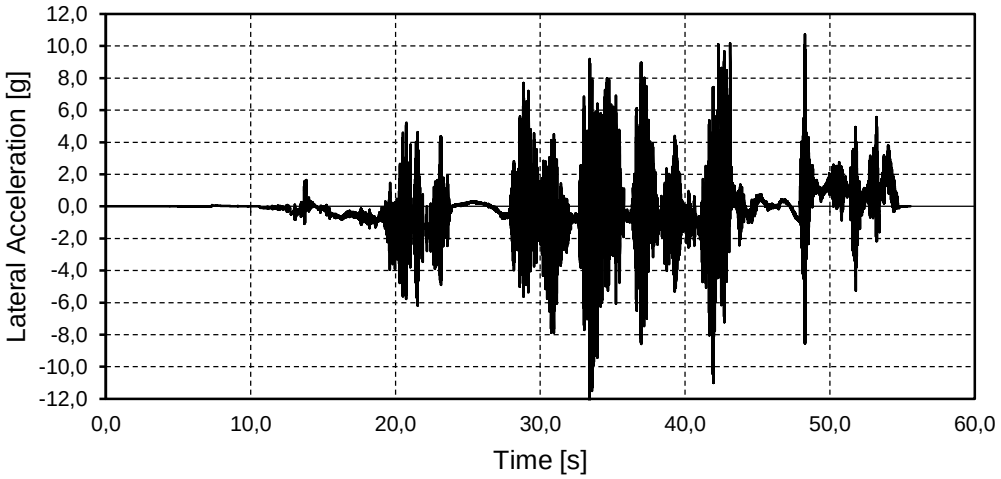

Figure 5.22: Lateral Acceleration on the center of mass of the upper torso of the occupant, in the local coordinate system

Similarly to what is observed for the Looping Star roller coaster, the acceleration graphs continue to present an oscillatory behaviour. Probably due to irregularities of the track geometry or the lack of calibration in the suspension systems of the vehicle or that links the biomechanical model to the seat.

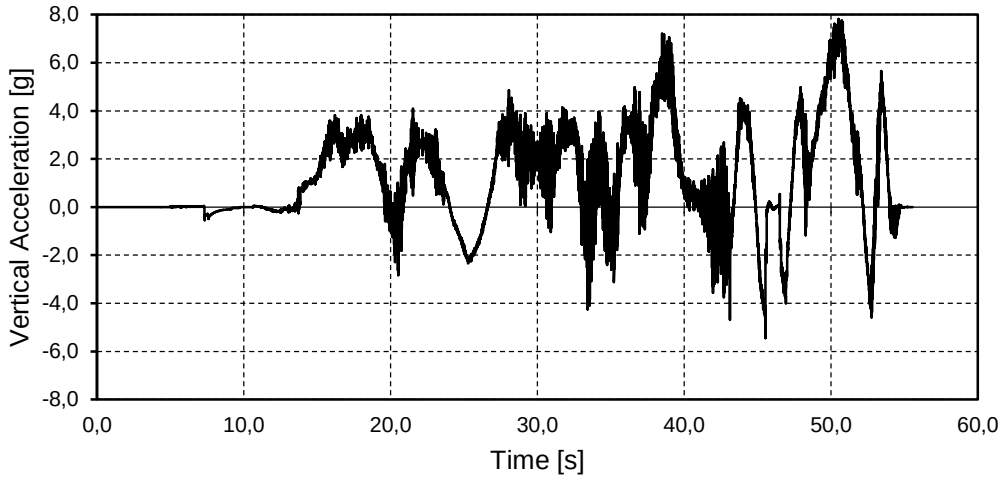

Figure 5.23: Vertical Acceleration on the center of mass of the upper torso of the occupant, in the local coordinate system

The g-forces measured in the center of mass of the upper torso in forward +Gx direction are far below the human tolerance to this direction, as shown in Figure 5.24. But as it can be seen, the human tolerance in this direction is higher than in the remaining directions. In Figure 5.25, the lateral Gy g-force graph is presented. For the complete ride, the g-forces measured in the center of mass of the upper torso of the biomechanical model are below the human tolerance, thus suggesting a safe ride.

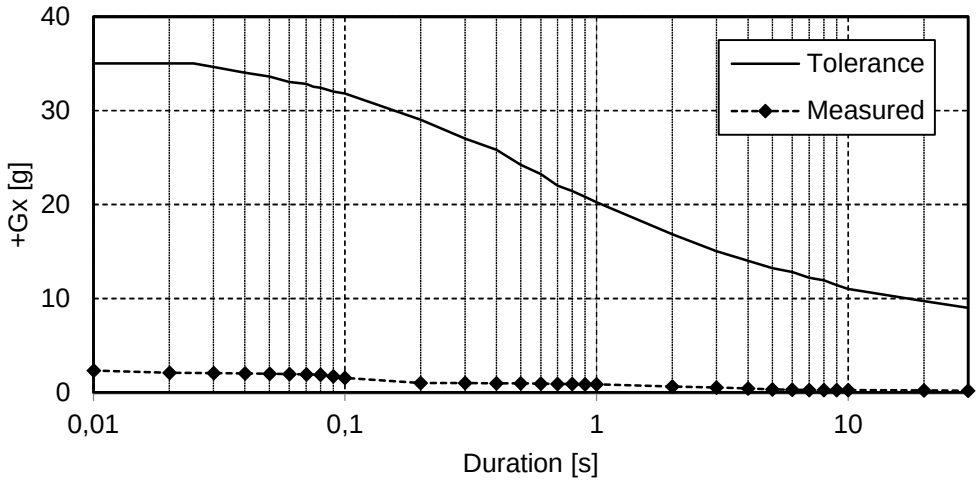

Figure 5.24: Forward G-force +Gx acting on passenger

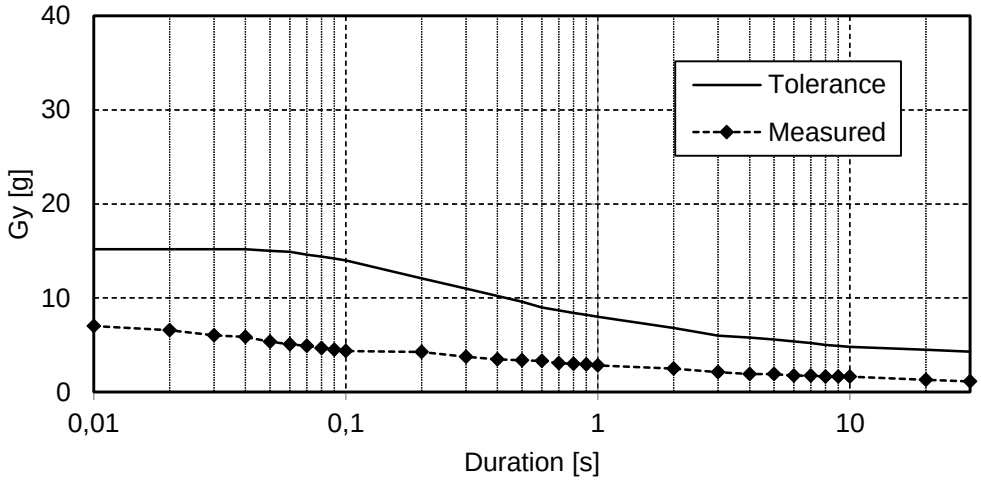

Figure 5.25: Lateral G-force Gy acting on passenger

The upwards +Gz direction is the direction that shows less tolerance to g-forces. However the ride is still safe according to this threshold. The oscillatory behavior that the accelerations graph present can be minimized with the improvement of the model, with proper track geometries and the calibration of the suspension systems. As before, the worst situations caused by accelerations in this direction, happens for longer time intervals, such as 5 s, and for these, the model presents a good behavior, below the human tolerance.

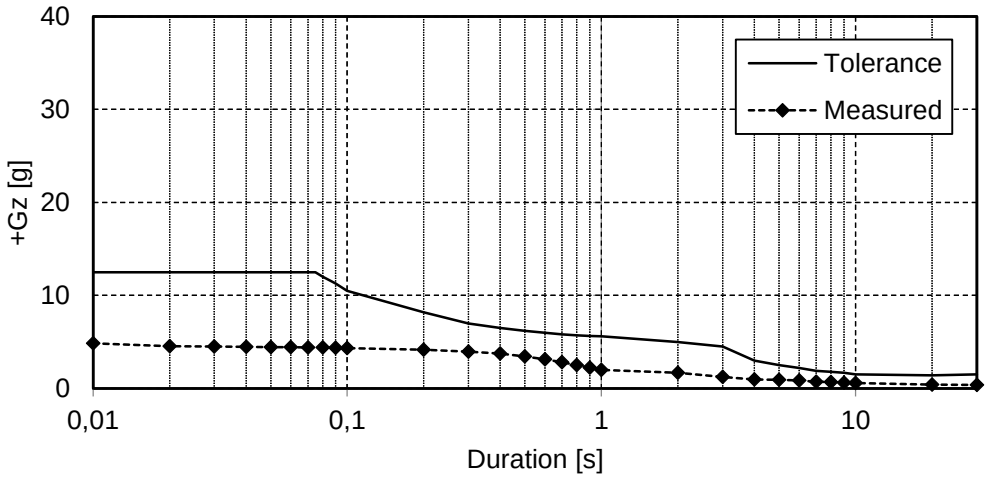

Figure 5.26: Upwards G-force +Gz acting on passenger

In Figure 5.27, it is presented the magnitude values of g-force in the downwards –Gz direction, that shows the same behavior as the remaining graphs.

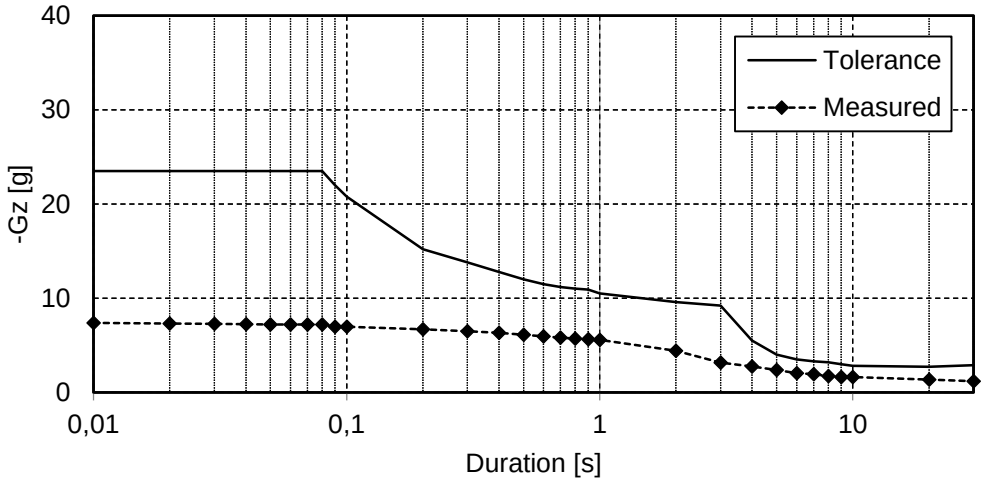

Figure 5.27: Downwards G-force -Gz acting on passenger

The Head Injury Criteria (HIC) and Result Head Acceleration (3ms) show results suggest no issues regarding the roller coaster passenger safety. In Figure 5.28, it can be seen the evolution of the HIC during the roller coaster simulation, which produces a maximum value of 4.9 around the 51 s.

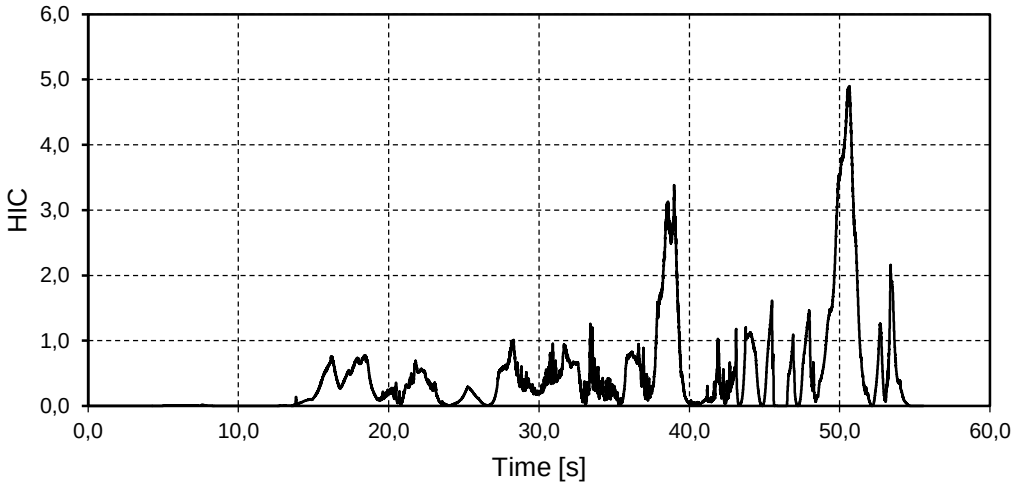

Figure 5.28: HIC

The Result Head Acceleration (3ms) that produces a maximum value of 7.4g, is also below the maximum tolerable by the human body, 80g. This value also reaches the value 51 s, as seen in Figure 5.29.

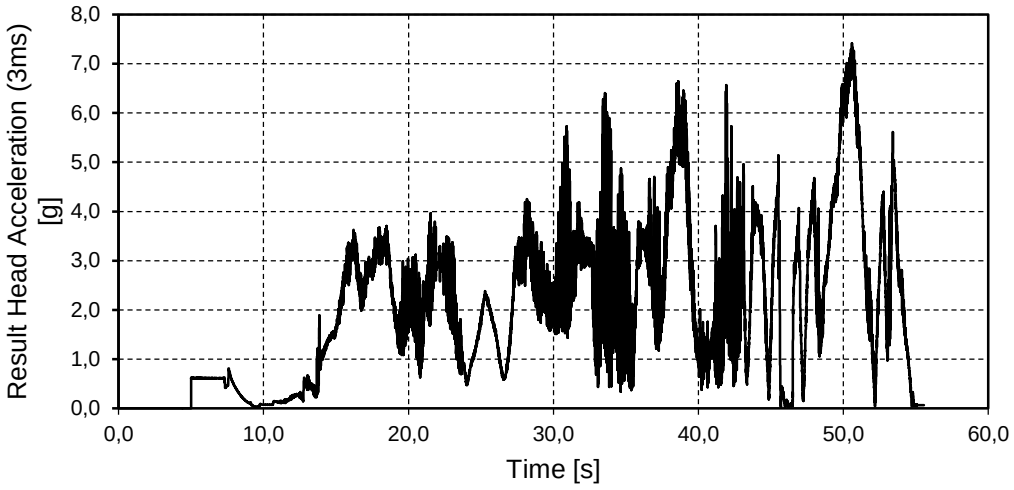

Figure 5.29: Result Head Acceleration (3ms)

6 Conclusion and Future Developments

6.1 Conclusions

A roller coaster vehicle model based on a multibody methodology was developed. The multibody model uses a new prescribed path kinematic constraint, developed in this work, necessary to improve the roller coaster analysis. The vehicle model developed has four wheelsets being prescribed independently around the roller coaster track, and it is able to control track misalignments, to ensure the fit of the wheelsets in the rails, to allow separation between wheelsets and to compensate track irregularities or gauge variations. It was also implemented a passive tilting mechanism, in order to compensate the effects of lateral accelerations, felt by the passengers as an uncomfortable sensation. A biomechanical model of the roller coaster passenger is restrained to the seat, in order to represent the natural resistance of a roller coaster occupant, and to obtain reliable measures of the human exposure to roller coaster induced g-forces.

Two different roller coaster tracks were analysed, and both present g-forces far below the human tolerance thresholds. The injury criterions analysed are also extremely low, proving that roller coaster riding is associated with a very low injury risk, and resulting head motion fall within the range of normal activities and far below human tolerance thresholds for normal individuals.

6.2 Future Developments

The objective of this work was to present a tool to be used to assess potential injury risks by riding roller coasters. So, this work was not focused in the precise modelling of any existing roller coaster. The source of the roller coaster track geometries used is not the most reliable, so, obtaining reliable and accurate track geometries or even a tool to build them can be a future development

It is necessary time to tune and calibrate the suspension systems of the roller coaster vehicle and to make it adjusted to the roller coaster track. By using optimization tools the best characteristics for the springs and dampers of the suspension systems, for each particular roller coaster track can be identified, thus leading to better rides.

The method to restrain the biomechanical model of the roller coaster passenger implemented here lack the physical significance associated to the roller coaster vehicle restraints and human muscle bracing. It is necessary to develop a model of contact between the biomechanical model and the seat, and to develop realistic models for the vehicle over the head restraints. Also the use of different percentile dummies, in different positions of the vehicle are required to represent the diversity of the roller coaster users. The simulations presented in this work, only involved one biomechanical model and one vehicle, which is not what happens in reality. So, it is also important to develop the analysis with a

train of roller coaster vehicles, linked between them, having several of its seats occupied by diverse biomechanical models.

In this work, it was used a kinematic constraint to simulate the interaction between the wheels and the track. In order to perceive track irregularities and induced vibrations, a model of contact between the wheels and the rails can be devised. Such model would allow considering conditions as the wear of the wheels and rails, or even flexible tracks.

With these and other approaches, this work proves to have the necessary tools for model validation, to assess several types of injury in the human body. With access to experimental data, this task must be accomplished by comparing the computational response of the roller coaster models to the experimental measurements of real roller coasters. Not being complete, from this point of view this work provides all the basic tools for a comprehensive analysis of roller coaster rides.

References

[1] E. Heiden and S. McGonegal, "2001-2002 Fixed-Site Amusement Ride Injury Survey Analysis," *Injury Insights*, 2003.

[2] D. H. Smith and D. F. Meaney, "Roller coasters, g forces, and brain trauma: on the wrong track?," *Journal of neurotrauma*, vol. 19, pp. 1117-1120, 2002.

[3] B. J. Pfister, L. Chickola, and D. H. Smith, "Head motions while riding roller coasters: implications for brain injury," *The American journal of forensic medicine and pathology*, vol. 30, p. 339, 2009.

[4] R. V. Brulle, *Engineering the Space Age: A Rocket Scientist Remembers*: DIANE Publishing, 2009.

[5] D. F. Shanahan, "Human tolerance and crash survivability," *Pathological Aspects and Associate Biodynamics in Aircraft Accident Investigation*, 2004.

[6] T. M. Fraser, *Human response to sustained acceleration: a literature review* vol. 103: Scientific and Technical Information Division, National Aeronautics and Space Administration:[for sale by the Superintentdent of Documents, US Govt. Print. Off.], 1966.

[7] K.-U. Schmitt, P. F. N. E. Zürich, M. H. Muser, and F. Walz, *Trauma biomechanics: Introduction to accidental injury*: Springer Science & Business Media, 2013.

[8] J. Pombo, "A Multibody Methodology for Railway Dynamics Applications," PhD Dissertation, IDMEC/Department of Mechanical Engineering, Instituto Superior Técnico, Lisbon, Portugal, 2004.

[9] A. A. Shabana, *Dynamics of Multibody Systems*, 2nd Edition ed. Cambridge, United Kingdom: Cambridge University Press, 1998.

[10] J. Baumgarte, "Stabilization of Constraints and Integrals of Motion in Dynamical Systems," *Computer Methods in Apllied Mechanics and Engineering*, vol. 1, pp. pp. 1-16, 1972.

[11] J. Ambrósio and A. Neto, "Stabilization Methods for the Integration of DAE in the Presence of Redundant Constraints," *Multibody Systems Dynamics*, vol. 10, pp. pp. 81-105, 2003.

[12] J. Pombo and J. Ambrósio, "Modelos Computacionais para Aplicação em Dinâmica Ferroviária (Computational Models for Railway Dynamics Applications)," IDMEC - Institute of Mechanical Engineering, Instituto Superior Técnico, Lisbon, Portugal, Technical Report IDMEC/CPM/98/0051998.

[13] J. Pombo and J. Ambrósio, "Development of a Roller Coaster Model," in *Proceedings of the Métodos Numéricos en Ingeniería V*, Madrid, Spain, 2002.

[14] J. Pombo and J. Ambrósio, "General Spatial Curve Joint for Rail Guided Vehicles: Kinematics and Dynamics," *Multibody Systems Dynamics*, vol. 9, pp. pp. 237-264, 2003.

[15] J. Pombo and J. Ambrósio, "A General Track Model for Rail Guided Vehicles Dynamics," in *Proceedings of the VII Congresso de Mecânica Aplicada e Computacional*, Évora, Portugal, 2003, pp. pp. 47-56.

[16] P. E. Nikravesh, *Computer-Aided Analysis of Mechanical Systems*. Englewood Cliffs, New Jersey: Prentice-Hall, 1988.

[17] F. Frenet, "Sur les courbes à double courbure," *Journal des mathématiques pures et appliquées*, vol. 17, pp. 437-447, 1852.

[18] c. J. L. Lagrange, J. A. Serret, and G. Darboux, *Oeuvres [de Lagrange]: Publiées par les soins de JA Serret*: Gauthier-Villars, 1889.

[19] M. Tandl and A. Kecskemethy, "Singularity-free trajectory tracking with Frenet frames," in *Proceedings of the 1st conference EuCoMeS. Obergurgl, Austria*, 2006.

[20] M. Tändl, *Dynamic simulation and design of roller coaster motion*: VDI Verlag, 2009.

[21] J. A. Serret, *Cours de calcul différentiel et intégral par J.-A. Serret: Calcul différentiel. 1*: Gauthier-Villars, 1868.

[22] J. Ambrósio, P. Antunes, and J. Pombo, "On the Requirements of Interpolating Polynomials for Path Motion Constraints," in *Interdisciplinary Applications of Kinematics: Proceedings of the International Conference, Lima, Peru, September 9-11, 2013*, A. Kecskeméthy and F. Geu Flores, Eds., ed Cham: Springer International Publishing, 2015, pp. 179-197.

[23] T. Wayne, *Roller Coaster Physics - An Educational Guide to Roller Coaster Design and Analysis for Teachers and Students*. Charlottesville, Virginia, 1998.

[24] B. M. Nigg and W. Herzog, *Biomechanics of the musculo-skeletal system*: John Wiley & Sons, 2007.
[25] M. P. Silva and J. Ambrósio, "Kinematic data consistency in the inverse dynamic analysis of biomechanical systems," *Multibody System Dynamics,* vol. 8, pp. 219-239, 2002.
[26] D. H. Laananen, A. O. Bolukbasi, and J. W. Coltman, "Computer Simulation of an Aircraft Seat and Occupant in a Crash Environment. Volume 1. Technical Report," DTIC Document1983.
[27] D. H. Laananen, "Computer simulation of an Aircraft Seat and Occupant (s) in a Crash Environment-Program SOM-LA/SOM-TA (User Manual)," DTIC Document1991.
[28] M. Silva and J. Ambrósio, "Biomechanical Model with Joint Resistance for Impact Simulation," *Multibody Systems Dynamics,* vol. 1, pp. pp. 65-84, 1997.
[29] M. Shojaati, "Correlation between injury risk and impact severity index ASI," in *Proceedings of the 3rd Swiss Transport Research Conference Monte Verita/Ascona*, 2003.
[30] J. E. Whinnery and A. M. Whinnery, "Acceleration-induced loss of consciousness: a review of 500 episodes," *Archives of Neurology,* vol. 47, pp. 764-776, 1990.
[31] T. Whinnery and E. M. Forster, "The+ Gz-induced loss of consciousness curve," *Extreme Physiology & Medicine,* vol. 2, p. 1, 2013.
[32] T. Fraser, "Sustained linear acceleration," 1973.
[33] R. Burton, S. Leverett Jr, and E. Michaelson, "Man at high sustained+ Gz acceleration: a review," *Aerospace medicine,* vol. 45, pp. 1115-1136, 1974.
[34] R. R. Burton and J. E. Whinnery, "Biodynamics: sustained acceleration," *Fundamentals of aerospace medicine,* vol. 3, pp. 201-260, 1996.
[35] C. De Boor, *A Practical Guide to Splines*. New York, New York: Springer-Verlag, 1978.
[36] J. Pombo, "Application of a Computational Tool to Study the Influence of Worn Wheels on Railway Vehicle Dynamics," *Journal of Software Engineering and Applications,* vol. 5, pp. 51-61, 2012.
[37] D. Howard, "Roller Coaster Vehicle," ed: Google Patents, 2011.
[38] U. s. G. SolidWorks, "Dassault Systemes SolidWorks Corp," *Concord, Massachusetts,* 2012.
[39] J. Milho and J. Ambrósio, "System Animation for Graphical Analysis - SAGA User's Guide VS 1.0," Institute of Mechanical Engineering, Instituto Superior Técnico, Lisbon, Portugal, Technical Report IDMEC/CPM - 95/0291995.
[40] P. Prasad, "An overview of major occupant simulation models," SAE Technical Paper 0148-7191, 1984.
[41] K. H. Kroemer, S. H. Snook, S. K. Meadows, and S. Deutsch, "Ergonomic models of anthropometry, human biomechanics and operator-equipment interfaces," 1988.
[42] C. P. Carroll, J. A. Cochran, J. P. Price, C. E. Guse, and M. C. Wang, "The AIS-2005 Revision in Severe Traumatic Brain Injury: Mission Accomplished or Problems for Future Research?," *Ann Adv Automot Med,* vol. 54, pp. 233-8, Jan 2010.
[43] K. V. Kumar and W. T. Norfleet, "Issues on human acceleration tolerance after long-duration space flights," 1992.
[44] M. U. s. Guide, "The mathworks," *Inc., Natick, MA,* vol. 5, p. 333, 1998.